The Evaluation and Improvement of the Maximum Entropy Production (MEP) Evapotranspiration method at graduated spatial scales – Point, Catchment and Continental scales

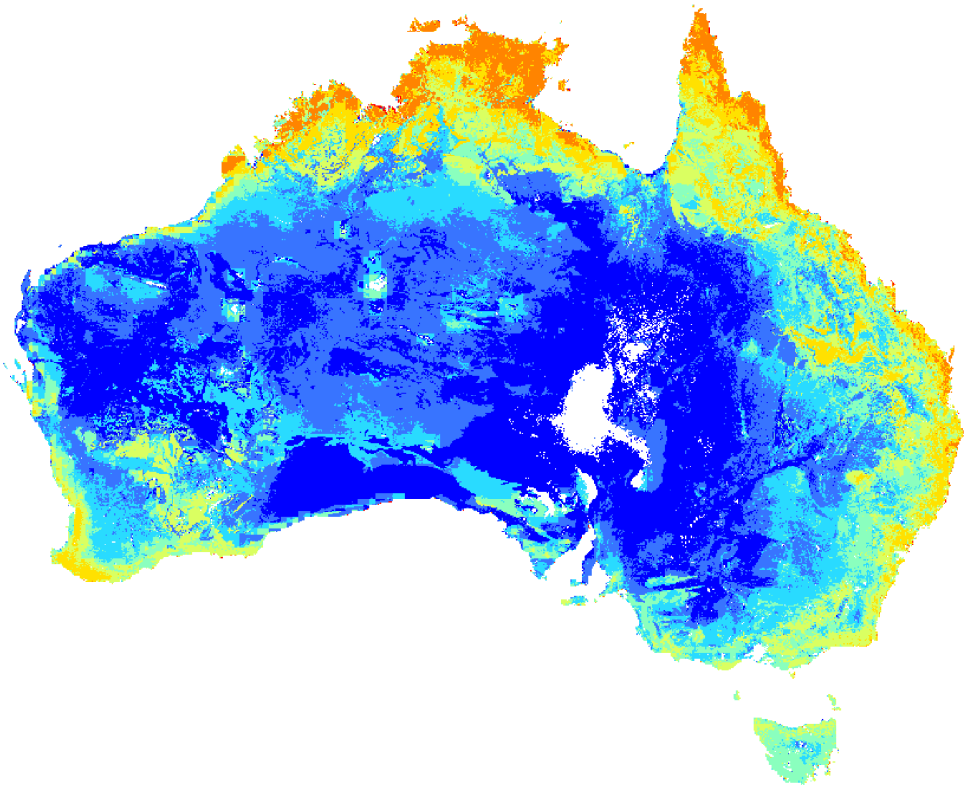

Olanrewaju O. Abiodun

B. Eng, M.Sc

A thesis submitted in fulfilment of the requirements for the degree of Doctor of Philosophy

In the

College of Science and Engineering

Flinders University, South Australia

December 2019

Declaration

I certify that this thesis does not incorporate without acknowledgment any material previously submitted for a degree or diploma in any other university; and that to the best of my knowledge and belief it does not contain any material previously published or written by another person except where due reference is made in the text.

Olanrewaju O. Abiodun

Declaration of Co-authorship

Olanrewaju Abiodun is the primary author and lead researcher of the manuscripts presented in this thesis. On the published and submitted manuscripts, my supervisors and co-authors provided guidance and intellectual support. Their contributions are acknowledged. I also acknowledge the support of the Australian Government Research Training Program Scholarship in sponsoring me to complete this doctoral study.

Acknowledgements

First of all, I would like to give all the glory to my Heavenly Father, my Saviour Jesus Christ and the Holy Spirit for the inspiration, wisdom and strength to pursue this course. I knew I would complete this endeavour just because you said it.

I would like to appreciate my foundational principal supervisor Vincent Post who believed in me, and whom I consider a faithful friend. To my principal supervisor Okke Batelaan, who often functioned in the dual role of supervisor and father to keep me on the straight and narrow path to completion while providing much needed financial support, I am forever grateful. I truly cannot appreciate you enough. To my associate supervisor Huade Guan, it was your guidance and sound knowledge of the science that supported me and saw me through many confusing equations and ecohydrological concepts. Thank you for your open door policy, you were always happy to answer my questions and point me in the right direction, thank you. I am indebted to my unofficial supervisor Jingfeng Wang who developed the MEP method and delighted in teaching and guiding me through every step of the modelling. I cannot express my gratitude enough; you played a part in my completing this PhD that I cannot underestimate. Thank you

To my colleagues Karina and Ankit whom we've grown to become friends thank you for making the journey worthwhile.

And now to my family, the RCCG Living Spring Parish, for all your prayers and support, I am eternally grateful. To David's mighty men, this is just the beginning, don't stop pushing, there is glory ahead!

To my mum and dad, I truly love you and want to say thank you for all your sacrifices over my life. You always wanted me to do this. I hope you're proud of the son you raised. To Bros T, my brother and true friend, thank you for always being there. To my sister Jola, how I love your beautiful heart. To my brother Sola and my sister Ronke, I am proud to have you as siblings along with your mighty strides in life. To my second mum (my mother in law), thank you for your prayers, they strengthened me in difficult moments.

Now to my beloved daughter Rehoboth in whom I am well pleased, thank you for your love, kindness and understanding through the difficult times, you have a heart of gold, I will forever love you. To my son Joshua, daddy loves you deeply, greater works than this, you will do.

Finally to my loving wife, the incubator of this vision, the talented encourager, a pillar of strength, true Proverbs 31 woman and my express gift from God on this journey of life. You've been all I asked God for and more. We'll finish well together in Jesus name. I will love you for minimum of one life time. This thesis is for you. Now we can move on to greater things! I am excited for our next season!

Table of Contents

Contents

List of Tables

Table of Figures

1.1 Literature

Evapotranspiration (ET) is a major component of the hydrologic system and it even exceeds rainfall in some environments (Brown et al., 2014). ET is strongly coupled to the type of natural environment, anthropogenic activities and changes in the soil-water-atmosphere system. Changes in ET can have therefore far reaching impacts on the environment, agriculture, water availability and climate. Due to these facts ET has been widely and extensively studied in the past century with several researchers developing methods for estimation. However, some pertinent challenges still plagues the science of evapotranspiration; (1) the cost of high temporal resolution measurements at point/field scale is still exorbitant; (2) the understanding of drivers of ET at high to low temporal resolutions to determine optimal temporal resolution of specific ET products across different climate and environmental conditions; (3) scale issues still abound - determination of optimal spatial resolution for ET measurements when using remote sensing data still requires qualitative analysis; (4) the currently available high spatial resolution ET products covering regional to continental scales have been determined to be inaccurate by several studies (Ramoelo et al., 2014, Di et al., 2015, Hu et al., 2015a, Du and Song, 2018) across various land covers, environmental conditions and/or climate; (5) the need for the development of separate evaporation (E) and transpiration (T) products tested across catchment and regional scales to understand the contributions of E and T to the total ET in the environment. While, it has been discussed that ET is perhaps the most complex hydrological component to fully understand in a hydrological system (Fisher et al., 2005), the need to confront the above challenges remain. In this thesis, I aim via the setup of a practical experimental field site to contribute to the science of ET regarding challenges 1 and 2 above, while an attempt to contribute to solving challenges 3, 4 and 5 will be made as well.

The dynamism of ET has seen the science approached from different conceptual methods, such as the mass transport method (Valipour, 2014), energy balance method (Bastiaanssen et al., 1998c), empirical method (Choudhury, 1999), and physical methods (Tyagi et al., 2000) amongst others. These methods have been successful to varying degrees. Several reviews of evapotranspiration methods have been undertaken (Dickinson et al., 1991, Rana and Katerji, 2000, Drexler et al., 2004a, Kalma et al., 2008, Wang and Dickinson, 2012) to improve our understanding of the strengths and weaknesses of these methods, which has led to the realization that the majority of the methods are not viable beyond a narrow range of topography, environmental condition (e.g. irrigation), climate and/or vegetation type. While some methods are only viable under certain conditions others can be improved or integrated in models for wider use.

Evapotranspiration over Australia has been of particular interest in recent years due to its net effect on total global ET (Jung et al., 2010). It was observed by Jung et al. (2010) that the global decline in ET was driven significantly by the decline in ET over Australia. The drought over Australia termed the "millennium drought" which occurred between the years 2000 – 2010 contributed immensely to the global decline in ET. Hence, the need to accurately estimate ET over the dynamic Australian landscape at point, catchment and regional scales.

Within the Australian context, several methods have been applied to measure ET at the point, catchment and regional scales. Lysimeters, and sap flow methods have been used at point or tree scale measurements. Although lysimeters, which function by measuring water percolation through a controlled experimental soil column over a period of time have been determined to be very accurate, they can be quite expensive to set up and often impractical to set up over large areas and for trees (Howell et al., 1991). The sap flow method on the other hand, which involves the injection of small heat into the stem of a plant or tree is very useful in studies focused on the transpiration component of ET (Glenn et al., 2011). The sap flow method is however inadequate where the total ET is the goal of the measurement.

On the catchment scale, several ET estimation methods have been developed over the years. The methods can be broadly categorised into the Temperature-Vegetation Index methods (T-VI), Surface energy balance methods (SEB) and the water balance method. Some of other methods have been developed on the back of existing methods such as the Penman-Monteith and Priestley-Taylor methods. These methods principally exploit the advent of remote sensing data to estimate ET on catchment to regional scales. The science behind T-VI methods involves the understanding of the relationship between the spatio-temporal variations in land surface temperature and the vegetation index to partition the net radiation into the latent and sensible heat components (Price, 1990, Carlson et al., 1995, Nishida et al., 2003). While the T-VI method has the advantage of requiring few meteorological data to estimate ET, the relationship derived between T and VI over an area may not be valid across other land covers and climatic conditions.

Developed SEB models are further divided into single-source (SSEB) and two-source (TSEB) energy balance models. SSEB models calculate ET as a residual of the energy balance and sensible heat from a heat transfer model equation. The SSEB models lump the evaporation and transpiration components of ET together as the thermodynamic system at the land surface is viewed as a single layer, while the TSEB models parameterise and estimate the evaporation and transpiration components of the ET separately. Several variations of the SSEB models have been developed, with the Surface Energy Balance for Land (SEBAL) (Bastiaanssen et al., 1998a)

as one of the earliest SSEB models applicable on catchment scale. Many TSEB models have also been developed with the Two-Source Model (TSM) developed by Norman et al. (1995) as one of the earliest TSEB models. The SSEB and TSEB models have been widely used in ET estimation on catchment scales but their significant reliance on the accuracy of land surface temperature and air temperature in parameterisation is a major challenge of the methods (Zhang et al., 2016).

The water balance method is premised on the water balance equation, $P - ET - R - \Delta S = 0$. ET is calculated as a residual of the equation where P is precipitation, R is the runoff and ΔS is change in storage. The water balance method is simple to use, however obtaining accurate values for the parameters can be challenging. In recent years, the advances in remote sensing has made the method more accessible with different precipitation products available globally. Although the Gravity Recovery and Climate Experiment (GRACE) is the only widely known and freely available global change in storage product, with runoff also mostly available locally. While the water balance method is simple and easy to apply, errors in the precipitation component significantly impacts the ET estimation. Another major disadvantage of the method is the spatio-temporal coarseness of the estimation grid due to the grid size of the change in storage product. Hence the water balance method is mostly suitable for regional scale ET estimation.

Few ET methods have been very successful such as the acclaimed eddy covariance (EC) method and the Penman-Monteith (P-M) equation, which many ET models are built on, but not without extensive improvements by several research works and re-parameterisation of various components of the methodologies over the years. Nevertheless, these methods still have limitations and challenges associated with them. For instance, the EC method has a spatial scale limitation, energy balance closure issues and high costs to set up. Hence, this EC method is most suitable for ground-truthing of other methods. The P-M method, which has been improved significantly since the advent of remote sensing and advanced spatial science by coupling the method with remote sensing input data to produce products like e.g. MOD16 ET data (Mu et al., 2007), has been reported to perform poorly over certain environmental conditions and/or land covers (Hu et al., 2015a, Miralles et al., 2016, de Arruda Souza et al., 2018). Most of the poor performances recorded were despite the improvements made to algorithms like the MOD16 algorithm by Mu et al. (2011b), which included the re-parameterisation of several components of the method. These constant improvements are a necessity in the complex world of ET measurement and modelling. The EC system and MOD16 are arguably the most popular and widely accepted ground-truthing and global scale high resolution spatial ET product respectively. Regardless of the challenges and/or limitations of these methods, they have contributed immensely to the science of ET.

With the future of ET measurement clearly fused with remote sensing for regional scale estimations, there is the urgent need to develop, understand and improve the ET methods at optimal temporal and spatial resolutions. Scale issues have been identified as a challenge by studies using remote sensing data in ET models (Liu et al., 2016, Wang et al., 2016, Gaur et al., 2017). Notwithstanding the identified scale issues, there is paucity of research works that have evaluate the scale issue across remote sensing based ET models. Of the available studies that addressed the scale issues, Ruhoff et al. (2013) aggregated the high resolution MOD16 product to produce a better fit for the study area and Tang et al. (2015) observed better results from degrading the resolution of MOD16 product in validation exercises. Wang et al. (2016) used multi-scale remote sensing land cover images in modelling ET and observed an optimal image resolution for his datasets. While this study identifies the impact of the spatial component of remote sensing input data, analysis on spatio-temporal effects of scale is lacking in literature. With the increase in demand for higher resolution ET products, it is crucial to understand the spatio-temporal effects of scale using a multi-model approach. Improved understanding of optimal scales for ET estimation will significantly benefit the science of ET especially with regards to remote sensing data and catchment scale ET estimations.

ET is required for research, environmental, agricultural and other purposes, however the complexity of estimating ET significantly hinders these purposes. The development and free distribution of the MOD16 product, which has been extensively used in the last decade for comparison, validation and modelling hydrological systems, has significantly impacted the ET science positively. Evidently, the availability of such readily available, global ET data has aided researchers and other stakeholders requiring the use of ET data. The success of the MOD16 is premised on the availability, spatial resolution, coverage and relative accuracy. While a few other research efforts have created similar ET products such as the LSA-SAF MSG (Ghilain et al., 2011) over Europe and the AWRA-L (Viney et al., 2014) over Australia. While these ET products have contributed immensely to global ET studies. They all lump together the evaporation and transpiration components of ET together. For studies/purposes specific to only evaporation or transpiration, these products are unsuitable. Unfortunately, this is a significant challenge, which hinders several specific E and T studies and research efforts on specific vegetation type, lakes, rivers and open water research.

The Maximum Entropy Production (MEP) method is a relatively new approach to ET estimation developed by Wang and Bras (2011). The method can estimate E and T separately and is developed on the back of the information entropy principle (Shannon, 1948). The MEP method, which calculates the turbulent fluxes at the land surface as a function of temperature, specific humidity and available energy, is formulated on the principle

that the thermodynamic system at the land surface is constantly trying to achieve equilibrium through the maximisation of ET, subject to available energy at the land surface. The MEP method is a deviation from the conventional methods of ET estimation as it is the first ET estimation method which is primarily based on an information entropy model. The MEP's deviation from the norm with focus on driving the thermodynamic system towards equilibrium using ET allows focus on the thermodynamic state of the system rather than on the various physical processes involved in conventional ET methods which is expected to solve some physical based approach challenges to ET estimation. Some validation of the MEP model was conducted at the field scale (Wang et al., 2017, Hajji et al., 2018b) with excellent results but no rigorous spatio-temporal analysis has been conducted. An attempt was made to create a global scale MEP model by Huang et al. (2017). However, the resolution of 10,000 km^2 is too coarse for catchment or even regional scale use and it was not further developed into a product. The MEP model has the potential to be developed into a method that can be used at field, catchment and continental scales, which is a challenge of many of the more prominent methods. The MEP is not heavily reliant on temperature, which is another significant challenge of the other methods and costs much less to set up at the field scale. While the P-M method is widely accepted to be one of the most accurate methods of estimating ET, the difficulty of parameterising its components using several not readily available meteorological data(McMahon et al., 2013) has seen attempts at coupling the method with remote sensing for catchment to regional scale estimation achieve mixed results over different land covers and climate. The MEP has a significant advantage due to its requirement of few meteorological forcings to estimate ET hence is expected to perform differently by avoiding the complexity and biases introduced by uncertainties associated with individual meteorological forcings required by the PM method. This study intends to rigorously evaluate the MEP at various spatio-temporal resolutions and to effectively improve and/or propose areas of further development. The study will also develop a continental scale product over Australia at high resolution.

1.2 Research aims and PhD Contributions

This PhD aims to contribute to the science of ET, through the evaluation of the strengths and weaknesses of the MEP ET method, the use of a multi-model approach to qualitatively analyse the scale issues in ET and development of a continental scale E and T product using the MEP model. This thesis is structured into three sections;

1. The setup of an MEP field experiment in a mangrove forest with challenging environmental conditions different from previously evaluated sites and climatic conditions to evaluate the MEP and contribute to the challenges 1 and 2 stated in the introduction section above. This section evaluates the MEP at the hourly, daily, weekly and monthly temporal resolutions in an environment where temporal changes in flux is prevalent due to its proximity to the ocean. The overall performance was evaluated using a dedicated eddy covariance system setup beside the MEP station for the purpose. The limitations of the MEP were identified as well as its strengths.
2. The evaluation of four ET models on a catchment scale in a complex terrain. Scale challenges were evaluated and the drivers of different ET methods were analysed alongside possible challenges with the methods. Seasonal trends of the models were also analysed.
3. A high resolution continental scale E and T product was developed through re-parameterising of the MEP model components. The product was evaluated using several EC systems for accuracy on the daily time scales and was compared to existing products. The E, T and ET products contribution to the science of ET has been made publicly available for scientific and educational purposes similar to the popular and widely used MOD16 and LSA-SAF MSG products.

This PhD research work is a data intensive research where over 150 gigabyte (GB) of data was generated as part of the research output. A significant contribution of this research work is the creation of crucial continental wide datasets publicly available for research, environmental, agricultural, policy and climate studies. This research work will be the pedestal upon which other significant research works will build on. The produced datasets are freely available from the links below:

https://dap.tern.org.au/thredds/catalog/MEP/catalog.html

http://dx.doi.org/10.25901/5ce795d313db8

1 Evaluation of the MEP model for estimation of evapotranspiration over mangroves forest

Manuscript 1 to be submitted to Hydrology and Earth System Sciences (HESS)

Olanrewaju Abiodun[1], Okke Batelaan[1] Huade Guan[1], and Jingfeng Wang[2]

1. National Centre for Groundwater Research and Training, College of Science and Engineering, Flinders University, Australia
2. School of Civil and Environmental Engineering, Georgia Institute of Technology, Atlanta, USA

Corresponding author:

Lanre Abiodun, College of Science and Engineering, Flinders University, Bedford Park, Australia, lanre.abiodun@flinders.edu.au

Abstract

The goal of this study is to evaluate the maximum entropy production (MEP) model and test its performance in a hydrologically complex wetland environment using the eddy covariance (EC) method. We setup a turbulent flux measurement site with an EC system and other ancillary sensors required to parameterise the MEP model over a homogenous mangrove forest. A year's worth of data was collected from the MEP and EC systems and processed at an hourly temporal resolution.

The MEP model did not effectively capture latent heat flux at hourly temporal resolution when compared to the EC system. The MEP showed a correlation coefficient of 0.76, mean absolute error (MAE) of 0.08 mm/hr, percent bias of 1.8%, Nash Sutcliffe Efficiency (NSE) of -0.19 and root mean square error (RMSE) of 1.24 mm/hr for an average hourly ET from the EC method of 1.25 mm/hr. When the fluxes were aggregated to daily, 8-day and monthly values, the performance of the MEP improved progressively and at monthly aggregation, the correlation coefficient improved to 0.99. At the 8-day aggregation, correlation coefficient improved to 0.91, MAE of 3.04 mm/8-day, NSE of 0.76 and RMSE of 4.04 mm/8-day for an average ET of 21.5 mm/8-day. The diurnal influence of the horizontal advection and the systemic loss of the ground heat flux storage to tides are responsible for the reduced performances at the hourly temporal resolution.

2.1 Introduction

The science of evapotranspiration (ET) estimation has been considered a black art especially due to the complexity of parameterizing the turbulence at the atmospheric boundary layer (Jeffreys, 1918, Foken, 2006). Evapotranspiration estimation has however advanced significantly in the past decades, particularly since the derivation of the Monin-Obhukov Similarity Theory (MOST) (Monin and Obukhov, 1954). The MOST succeeded in parameterizing the turbulent fluxes of heat and momentum as functions of temperature and humidity, upon which most evapotranspiration methods have been developed (Brutsaert and Mawdsley, 1976, De Bruin, 1989, Suleiman and Crago, 2004, Koloskov et al., 2007, Savage, 2017). The performances of these methods have been observed in literature to vary depending on parameters (Amatya et al., 1995, Rana and Katerji, 2000) such as climate, vegetation cover and other biophysical parameters of the environment. Some of the most successful methods of turbulent flux quantification such as the Bowen-ratio method (Tanner, 1960) have benefitted from the MOST.

The Eddy Covariance (EC) method (Dyer and Hicks, 1970) has become the standard approach for validation of other emerging turbulent flux estimation methods (Cullen et al., 2017, Ruhoff et al., 2013). Although the EC method has been extensively tested, it has not been without challenges, with issues such as energy balance closure problems (Foken et al., 2006) and errors resulting from insensitivity of the EC system to high frequency turbulence (Loescher et al., 2006). While attempts have been made to address the challenges of the EC method over the years including several methods to solve the energy balance closure problem (Mauder et al., 2018), some concerns still remain (Widmoser and Wohlfahrt, 2018, Eshonkulov et al., 2019). Regardless of these challenges, the EC method has proven overwhelmingly popular due to the availability of equipment for measurement and the ease of calculation through proprietary processing software.

Since the turn of the millennium, remote sensing methods of ET estimation has evidently been the direction of the science due to the need of regional scale ET estimation for environmental planning, hydrological analysis, climate change modelling and other research needs. Many of the historically successful ET methods and emerging ones are coupled with remote sensing methods to produce the required evapotranspiration estimates. EC flux tower data is often used for ground-truthing the output of these remote sensing data driven models. FLUXNET, a network of continuous flux measurements from towers around the world at high temporal resolution has become the standard in ET flux validation (Running et al., 1999). Nevertheless, the high cost of setting up an EC system has impacted the growth of the network. The FLUXNET system has been successful in showing the need for

global flux measurement, hence more affordable methods of flux estimation without compromising the accuracy of the measured fluxes would be welcome. The maximum entropy production (MEP) model of surface heat fluxes (Sun et al. (2009) also benefits from the MOST for parameterizing thermal inertia of latent heat and sensible heat fluxes to use only three input variables (i.e. net radiation, surface temperature and surface specific humidity). The setup cost of the MEP estimation method is about 20% of the setup cost of the EC system. Although the MEP methodology is still considered an emerging technique, it has been very successful in macroscopic predictions of non-equilibrium systems (Dyke and Kleidon, 2010). The initial testings and validations of the MEP turbulent flux quantification method compared with measured data have been promising (Wang and Bras, 2011, Nearing et al., 2012, Huang et al., 2017, Wang et al., 2017, Hajji et al., 2018a, Xu et al., 2019, Yang et al., 2013). A recent review of evapotranspiration methodologies over the past 50 years (Liu et al., 2016) describes the MEP as an "alternative way to derive heat fluxes without getting into microscopic details of molecular conduction". The uniqueness of the MEP model method and the reported success in field tests warrant a rigorous review to determine if this is a viable ground-truthing method for evapotranspiration models. It must however be noted that the MEP model still requires comprehensive testing and validation across various environments to determine its strengths and weaknesses for further improvements. If the MEP is comprehensively tested and validated, it has the potential of complementing the EC method of flux validation in the future.

The objectives of this study are; (1) to evaluate the MEP method of flux quantification in a challenging hydrological environment (a mangrove forest with strong advection from the Gulf St. Vincent and high soil salinity), which has not been comprehensively assessed previously, i.e. determine the strengths and weaknesses of the MEP to estimate ET in a wetland environment and propose solutions where necessary; and (2) Evaluate the contributions of the sensible and latent heat fluxes to the energy balance as well as the evaporation and transpiration partitioning from the MEP model in the study area.

2.2 Model description

2.2.1 MEP model

The Maximum Entropy Model of turbulent flux estimation (hereafter referred to as MEP model) is developed on the back of the principle of Maximum entropy (MaxEnt) (Jaynes, 1957), which was advanced by Dewar (2003) and Dewar (2005) through the derivation of the Maximum Entropy Production theory as a subset of the MaxEnt. The MaxEnt is the maximization of the Shannon information entropy (Shannon, 1948) under a relevant constraint to develop a probability distribution from limited information. Dewar (2003) expatiated and expressed the link between the information entropy and thermodynamic entropy, where the Bayesian probabilities p_i for a certain variable x_i $(1 \leq i \leq n)$, are obtained through maximising the Shannon information entropy (S_I) under constraints.

$$S_I \equiv -\sum_{i=1}^{n} p_i \ln p_i , \tag{1}$$

Constrained by

$$\sum_{i=1}^{n} p_i \, f_k(x_i) = F_{k,}, \quad 1 \leq k \leq m \tag{2}$$

Where f_k are functions of x_i, F_k are the constraints parameterized from the available information on the variable x_i, m $(\ll n)$ is an integer, with the brackets denoting mathematical expectations. The MaxEnt probabilities distribution p_i can be derived from maximising Equation (1) under the constraint of Equation (2), yielding

$$p_i \propto \exp\left\{\sum_{k=1}^{m} \lambda_k \, f_k(x_i)\right\} \tag{3}$$

Where the $\lambda_k\ (1 \leq k \leq m)$ are the Lagrange Multiplier parameters, which are related with the constraint F_k (Dewar, 2005). The MEP theory is a direct offshoot of Equation (3) for the scenario of antisymmetric functions f_k. Based on the specific scenario of the anti-symmetric function where the MaxEnt distribution is driven by the exponential function in Equation (3), the MaxEnt is mathematically expressed as the entropy production function (Dewar, 2005)

$$D \equiv 2\sum_{k=1}^{m} \lambda_k F_{k,} \tag{4}$$

Sun et al. (2009) parameterized the entropy production function (also referred to as the dissipation function) in terms of sensible heat flux and ground heat flux with their respective thermal inertia and further developed the method in Wang and Bras (2011) through the addition of the latent heat flux term. The inclusion of the latent heat flux term and its thermal inertia in the MEP model dissipation function over land surfaces in Equation (5) is based on the theory that the macroscopic level turbulent thermodynamic system at the land surface is driven towards equilibrium stability by maximising evapotranspiration but constrained by available energy (Wang and Bras, 2011).

$$D(G,H,E) \equiv \frac{2G^2}{I_s} + \frac{2H^2}{I_a} + \frac{2E^2}{I_e} \tag{5}$$

where E, H and G are latent heat (W/m^2), sensible heat (W/m^2) and ground heat (W/m^2) fluxes, respectively. $I_e, I_a,$ and I_s are thermal inertia parameters relative to latent heat, sensible heat and ground heat fluxes respectively. The parameterization of the thermal inertia of the respective fluxes are discussed in detail in Sun et al. (2009).

The dissipation function derived in Equation (5) for the parameterisation of the land surface turbulent fluxes is constrained by the available energy on the land surface, given by the energy balance equation

$$R_n = E + H + G \tag{6}$$

By optimizing Equation (5) through the Lagrange Multiplier method and solving the resultant partial derivatives of E, H and G, we obtain the MEP evaporation equations over bare soil, Equation (7), which can be solved numerically. E and G in Equations (7) are direct results of solving the dissipation function in Equation (5) under the constraint of Equation (6). The formulation of Equation (7) and (8), which are MEP model parameters, are described in Wang and Bras (2011). For vegetated land surfaces, the dissipation function in Equation (5) is

optimized using the Lagrange Multiplier under the energy balance constraint in Equation (6) after eliminating the ground heat flux from both equations. The resultant Equation (9) is easily solved for H and E.

$$E_s = \beta(\sigma)H_s,\ G = \frac{\beta(\sigma)}{\sigma}\frac{I_s}{I_o}H_s|H_s|^{-\frac{1}{6}},\ R_{n,s} = E_s + H_s + G \tag{7}$$

$$\sigma = \frac{\lambda^2}{c_p R_v}\frac{q_s}{T_s^2}, \quad \beta(\sigma) = 6\left(\sqrt{1+\frac{11}{36}\sigma} - 1\right) \tag{8}$$

where σ is a dimensionless parameter characterizing the effect of surface thermal and moisture state on the energy budget (-), q_s the soil surface specific humidity (kg kg^{-1}), T_s the soil surface temperature, $\beta(\sigma)$ the inverse Bowen ratio (-), $R_{n,s}$ net radiation, I_s the thermal inertia of soil, I_0 the apparent thermal inertia of air parameterized using the Monin-Obukhov similarity equation of boundary layer turbulence (Wang and Bras, 2009), λ the latent heat of vaporization of liquid water (J kg^{-1}), c_p is the specific heat of dry air at constant pressure (J kg^{-1} K^{-1}), R_v is the gas constant of water vapor (J kg^{-1} K^{-1}). For vegetated surfaces Equation (7) becomes

$$E_v = \frac{R_{n\_v}}{1+\beta^{-1}(\sigma)},\ H_v = \frac{R_{n\_v}}{1+\beta(\sigma)} \tag{9}$$

where E_v, H_v are latent (transpiration) and sensible heat flux, respectively, $R_{n,v}$ net radiation over canopy surface. The other variables are defined as previously except that T_s, and q_s are canopy surface temperature and specific humidity, respectively. When calculating ET over canopy, where I_s is zero, G becomes zero, hence Equation (6) becomes $R_n = E + H$. Combining $R_n = E + H$ and $E = \beta(\sigma)H$, we obtain expressions for E and H in Equation (9) as a function of R_n and $\beta(\sigma)$. Note that E_v, H_v in Equation (9) satisfy the energy balance equation for canopy surface $E_v + H_v = R_{n,v}$ (Wang and Bras, 2011). Equation (7) is used to calculate evaporation while (9) is used to calculate transpiration. A summation of the evaporation and transpiration is the total ET for a given location.

The maximum entropy production (MEP) model of ET (Wang and Bras, 2011) was formulated based on the contemporary non-equilibrium thermodynamics, the Bayesian probability theory, information theory and the atmospheric boundary turbulence theory. The MEP theory has been applied to diverse fields of geosciences (Kleidon and Lorenz, 2005) including land surface hydrology (Kleidon and Schymanski, 2008), bio-ecological systems (Juretić and Županović, 2003, Kleidon and Fraedrich, 2004, Kleidon et al., 2010, Shipley, 2010) and surface heat fluxes at Earth-atmosphere interface (Wang and Bras, 2009, Wang and Bras, 2011, Wang et al.,

2014). The formulation of MEP ET model encompasses the dominant physical mechanisms underlying ET processes by including the four essential aspects of the evaporation physics (supply of energy, supply of water, evaporation potential and turbulent transport of water vapour). The MEP theory synthesizes the parameterizations of the physical processes and extracts the most relevant information about ET from fewer input variables than the traditional models. The unique features of the MEP ET model include the simultaneous solution of ET and other surface heat fluxes, closure of the surface energy budgets at all space and time scales, independence of temperature and humidity gradients, wind speed and surface roughness, covering the full range of soil moisture, and free of tuning empirical parameters.

The MEP model over water, snow and ice is different from the above described due to the energy budget calculations over water surfaces and the difference in thermal inertia of soil and water. Wang et al. (2014) optimized the dissipation function for the energy balance over water and derived unique equations below for the E, H and G over water, snow and ice; $R_n = \left[1 + \beta(\sigma) + \frac{\beta(\sigma)}{\sigma}\frac{I_{wsi}}{I_o}|H|^{-\frac{1}{6}}\right]H; E = \beta(\sigma)H; G = R_l^n - E - H;$

Where I_{wsi} is the thermal inertia of the media (water, snow or ice); R_l^n is the longwave radiated flux from the earth surface of medium water, snow or ice.

The above equations were evaluated for our mangrove site, however, the authors observed that the inundation on our site occurs intermittently for only a few hours on the days we carried out surveillance, with the soil surface exposed as a marsh for the greater part of the day. As the data obtained did not monitor the short periods of inundation, the equations for moist or wet land surfaces were used in this study, hence an open water evaporation analysis was not conducted.

2.2.2 Eddy covariance method

The EC method has been iteratively developed by several researchers globally over the past seven decades with the foundational theoretical basis of the method developed by Montgomery (1948), Obukhov (1951) and Swinbank (1951). The EC method has since gone through several improvements (Webb et al., 1980, Foken and Oncley, 1995, Lee, 1998) including instrumentation design (McBean, 1972, Ohtaki and Matsui, 1982). A comprehensive overview of the EC method is given by Aubinet et al. (2012).

2.3 Materials and methods

2.3.1 Study area and equipment

The study area is covered with dense mangrove forest in a coastal wetland of South Australia. The mangrove species is the *Avicennia marina* also known as grey mangrove. The grey mangrove grows along the South Australian coastline from Barker inlet in the south to the Tourville Bay in the north-west of South Australia. The site location is the St Kilda Mangrove trail close to the Barker inlet of South Australia. It is an area of homogenous dense grey mangrove extending 300 metres from the coastline at an elevation of 2 mAHD (metres Australian Height Datum). The equipment is located at latitude: 34°44'47.07744"S and longitude 138°32'15.90072"E on the St Kilda Mangrove Trail (Fig. 1) where the vegetation height is 4 m. The soil at the location is hypersaline with intermittent inundation dependent on tidal flows.

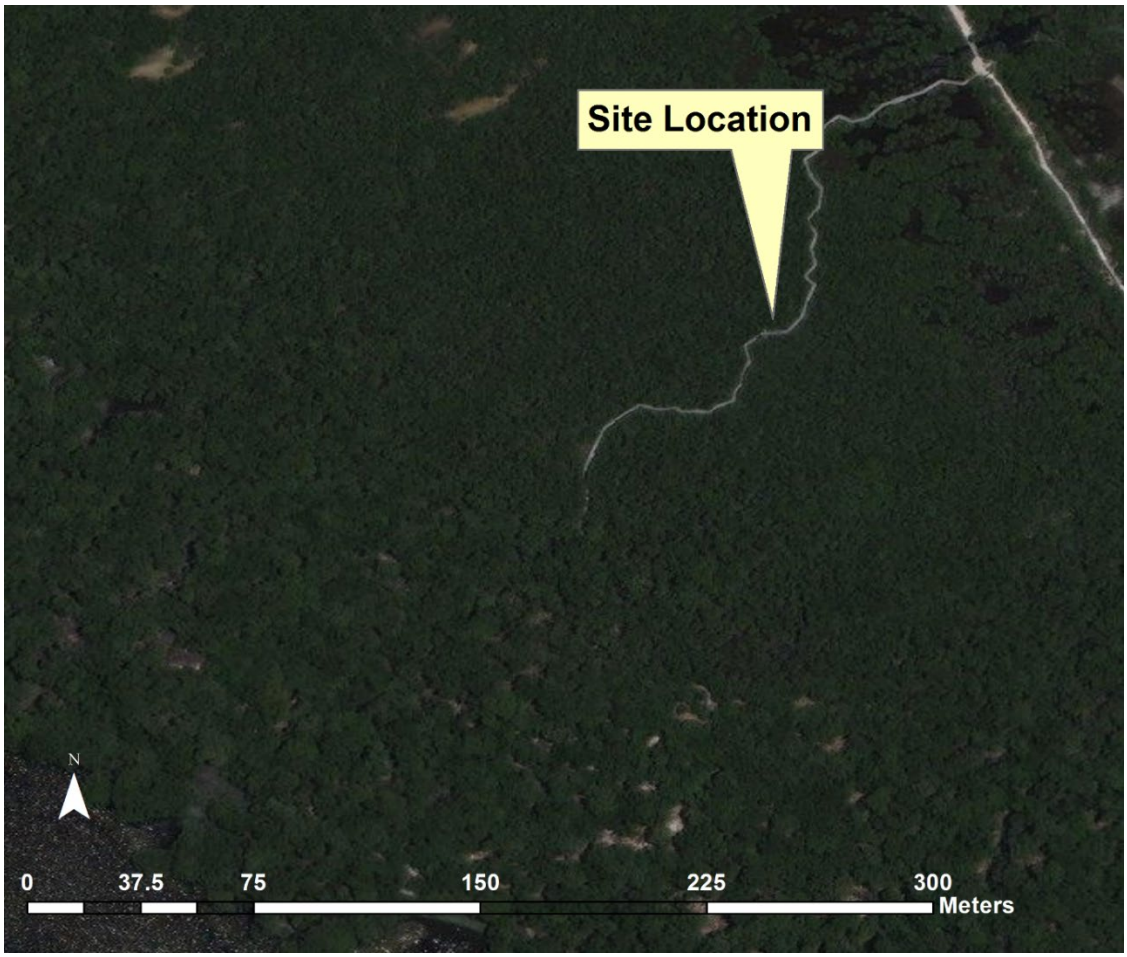

Figure 1: Equipment site location in mangrove forest

Two sets of equipment are installed at the site (Fig. 2); the EC system above the canopy to measure the turbulent fluxes and the "MEP station" which measures the meteorological variables required by the MEP method (net radiation, temperature and humidity at the canopy and soil surfaces). The EC system consists of the analyser interface unit, the gas analyser and the sonic anemometer installed at an elevation of 6.4 m above the soil surface, with the gas analyser set up at 15 degrees incline to align the air flow through it and the sonic anemometer. For the MEP station, infrared radiometer, net radiometer, relative humidity and air temperature sensors, are installed above the canopy, as well as just above the soil surface. Data from the MEP station sensors above the canopy are required for transpiration calculations while data from the sensors above the soil surface are required for evaporation calculations using the MEP model. The relative humidity, air temperature and infrared radiometer sensors above the canopy are installed at an elevation of 4.5 m above the soil surface while the net radiometer is installed at 5.5 m above the soil surface. The MEP station for measuring data above the soil surface is installed at 0.3 m. A logger box for the MEP is attached to the support structure for the equipment. While the MEP system only requires target surface temperature, we included both infrared thermometers and air temperature sensors at both the canopy and soil surface levels to evaluate the sensitivity of the MEP model to temperature.

The MEP model is very dependent on specific humidity data at the target surface hence the need to measure as close as possible to the target surface. However due to the intermittent inundation of the soil surface in the study location from tidal flows, sensors measuring near soil surface fluxes have been installed at the 0.3 m height.

The MEP and EC data are stored in the data logger and analyser interface unit respectively and sample at a frequency rate of 1 Hz.

Figure 2: MEP and EC equipment installed at St Kilda Mangrove Trail

Table 1: Installed instruments for MEP and EC

Instrument type (installation location)	**Observed component**
Infrared thermometer (canopy and soil surface) **Campbell Scientific SI-111** **Field of View: 22º half angle**	Target surface temperature
Net radiometer (above canopy and soil surface) **Kipp & Zonen NR-Lite2** **Field of View: 180º**	net radiation over target surface
Relative humidity and air temperature (soil surface) **Vaisala HMP 155**	Relative humidity and air temperature
Air temperature (canopy) **Environdata TA40**	Air temperature
Relative Humidity (canopy)	Relative humidity

Environdata RH40	
Logger Box **Campbell Scientific CR1000**	Data storage for all MEP data
Open path gas analyser (above canopy) **LiCOR Li-7500RS**	Latent heat flux and sensible heat flux
Anemometer (above canopy) **Gill instruments Windmaster pro 3-Axis Anemometer**	Wind speed and direction
Logger Box **LiCOR Li 7550 Analyzer interface**	Data storage for EC data

2.3.2 Data collection and processing

2.3.2.1 MEP model

The data collected from the MEP system were checked for quality but the net radiation data over the soil surface did not pass all quality checks. The net radiation over the canopy was preferred and a layer approach method described in Lhomme and Chehbouni (1999)was used in partitioning the net radiation between the canopy and soil surface. The Clausius-Clapeyron equation was used along with the relationship between relative humidity, vapour pressure and mixing ratio to obtain specific humidity over the target surfaces (Appendix A). Once the specific humidity is obtained, it is straight forward to compute the latent and sensible heat fluxes over the canopy using Eq. 9. The MEP model for evaporation over the soil surface was calculated using the "fsolve" function in Python programming language to solve the system of non-linear algebraic equation (7). The data stored in the MEP logger were averaged to 1-hourly interval for the flux computation.

2.3.2.2 EC method

The equipment was installed and ready for reliable data collection in January 2018. Data for this study were collected between 12 January 2018 and 5th of February 2019. Intermittent equipment faults occurred between April and September. The EC data were processed in the EddyPro 6.2.0 proprietary software from LiCOR for computing the turbulent fluxes from the EC system. Data quality control protocols were followed in the processing of the data such as rejection of hourly data with more than 3% of missing data. Data collected during periods of equipment malfunction were totally removed from the analysis. The data were averaged to 1-hour temporal resolution to align with collected data from the MEP system.

2.3.2.3 Flux footprint

The flux footprint can be a source of discrepancies in flux data analysis (Schmid, 2002, Göckede et al., 2004). The MEP and EC stations were installed as close as practicable to reduce the impact of flux footprint discrepancies. The study site has been carefully located in the centre of a homogenous grey mangrove forest (Fig. 2 and 3). Both the MEP and the EC equipment were installed at specific elevations to capture predominantly local flux footprints, with the grey mangrove forest stretching for several kilometres and a minimum radius of 200 m from the installed tower.

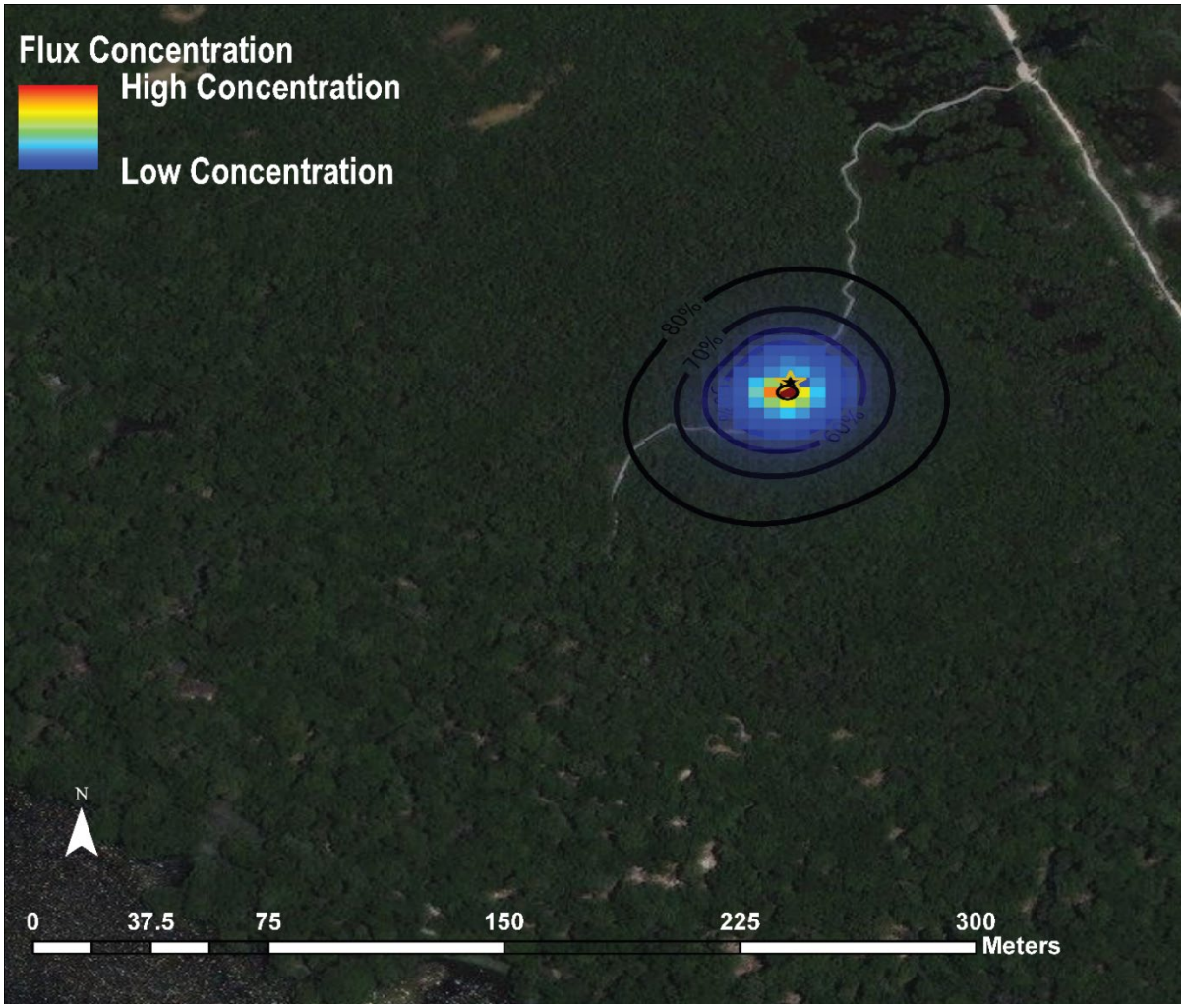

Figure 3: Average flux footprint for study period; Contour lines indicate radius of flux contributions to EC system

Relative humidity and air temperature sensors of the MEP station were installed at 0.5 m and 0.3 m above the canopy and soil surface, respectively. The net radiometer sensors are also close to the target surfaces at 1 m and 0.3 m above the canopy and soil surfaces respectively. From the EC flux footprint calculation, the Fig. 3 shows that 80% of the flux calculated by the EC system originates from a radius of about 100 m and the highest concentration of the measured fluxes occur within a 30 m radius. The flux footprints from the EC system were calculated using the methods by Hsieh et al. (2000), Kormann and Meixner (2001) and Kljun et al. (2004). The Kljun et al. (2004) method is the default method in the eddypro software but the method is subject to specific conditions, for instance, the friction velocity must be greater than 0.2 ms^{-1}. Where these conditions are not met the Kormann and Meixner (2001) methods is considered next. The mean cross wind integrated (CWI) footprint (Fig. 4) for our site for the 2018 period shows that the EC flux in our site is particularly localized with majority of the contributory flux to the footprint originating within 10 m of the flux tower.

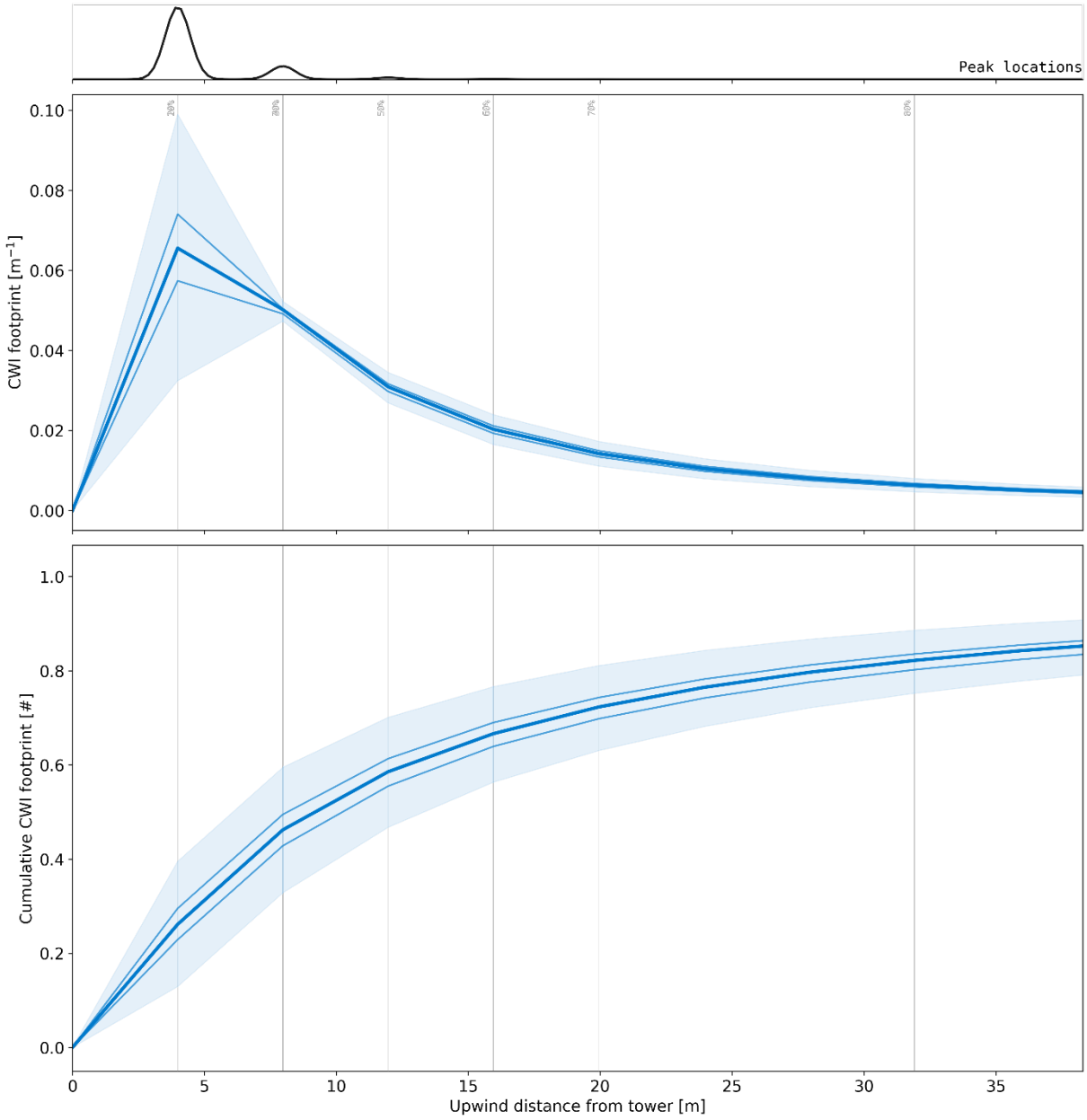

Figure 4: (a) Average crosswind integrated flux footprint vs distance from the EC tower over study period; (b) Cummulative flux footprint vs distance from EC tower. The thick blue line is the median, the upper and lower thin blue lines are the 75th and 25th quartile while the light blue spread is the range

2.4 Results and discussion

The ET results calculated by the MEP and EC systems were checked for outliers and improbable results. A total of over 6000 hourly data points across 280 days were used in the flux computation for each model. A comparison was carried out on the hourly timescale using the root mean square error (RMSE), mean absolute error (MAE), correlation coefficient (R), Nash Sutcliffe Efficiency (NSE) and PBIAS after replacing negative latent heat flux in the results which indicate condensation is zero, the energy balance closure improves significantly. The RMSE was 0.125 mm/hr; MAE of 0.08 mm/hr; correlation coefficient of 0.76 and a PBIAS of 1.8% (Table 2). The average hourly ET flux from the EC system was 0.124 mm/hr indicating a high RMSE. The percent bias of less than 2% flux volume between the two products over the study period of 280 days suggests good agreement in the ET estimates of both products. The results from both methods were also aggregated to the daily time step (Table 3), yielding RMSE of 1.19 mm/day, MAE of 0.9 mm/day, correlation coefficient of 0.65 and PBIAS of 1.8%. The RMSE improves significantly but the correlation coefficient degrades with the aggregation to daily timescale. The degradation of the correlation coefficient is attributed to the effect of the MEP latent heat data for night time which has poor statistics when compared to the EC (Table 2).

Table 2: Statistical comparison of EC vs MEP measurements for the duration of the study period

	Hourly (All)	**Hourly (Day)**	**Hourly (Night)**
Average MEP ET (mm/hr)	0.127	0.24	0.0002
Average EC ET (mm/hr)	0.125	0.19	0.05
RMSE (mm/hr)	0.125	0.16	0.07
R (mm/hr)	0.76	0.67	0.18
MAE (mm/hr)	0.08	0.12	-0.05
PBIAS (%)	1.8	22.7	99.6
NSE	-0.02	-0.57	-0.66

2.4.1 MEP ET vs EC ET at night time

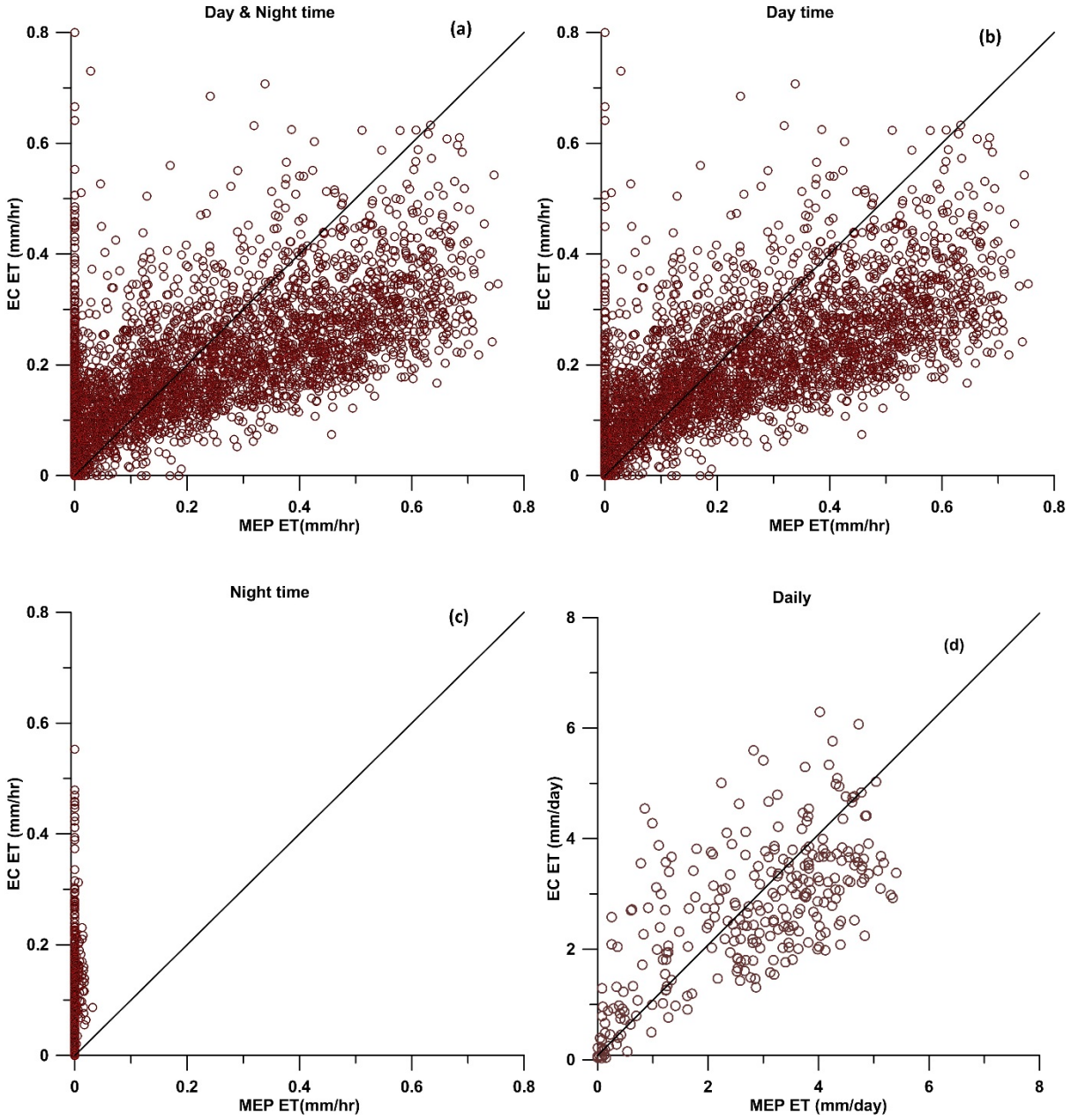

Figure 5: EC vs MEP ET; (a) All hourly data; (b) Day time; (c) Night time; (d) Daily

At night time when the net radiation is negative, the MEP turbulent fluxes are automatically negative which may lead to erroneous results (Fig. 5c) as shown by the poor agreement with EC latent heat flux when compared using RMSE, PBIAS, R and MAE statistical metrics (Table 2). The EC latent heat flux results show positive latent heat through most nights (Fig. 5c), thereby suggesting evapotranspiration occurs through the night time at our flux tower location. When net radiation is negative at night and positive latent heat is measured by the EC system, the result indicates that energy has been introduced into the thermodynamic system from non-solar radiation sources.

The MEP model formulation considers the net radiation as the only source of energy into the system and as such does not consider energy from other sources. At our flux tower location, horizontal advection is a significant source of energy input into the system with the interaction of land and sea breeze.

2.4.2 Sources of energy in the wetland environment

Horizontal advection is a significant source of energy in and out of the thermodynamic system at the site. The flux tower site is located 300 m from the gulf with sea breeze typically blowing north eastwardly towards the inland areas at day time especially in the summer months as seen in Fig. (6). The inland bound cool sea breeze travelling during the day time which accounts for 60% (Fig. 6a) of the air passing through the open-path gas analyser and anemometer impacts the turbulent fluxes by reducing the heat energy available at the land and canopy surfaces. During the summer nights, warm breeze from the inland and city locations flows towards the gulf (Fig. 6b), thus injecting heat energy into the system which drives evaporation over the wetland. This phenomenon leads to the EC system detecting positive latent heat even when the net radiation is negative. However, due to the parameterisation of the MEP model, this energy input is not captured in the thermodynamic system characterization. From Fig. (5a) it is evident that the MEP underestimates ET at lower flux thresholds and overestimates at higher flux thresholds.

Another possible explanation for the higher ET predicted by the MEP model during the daytime is the models high dependence on the accuracy of the humidity over the target surface. Typically, the specific humidity over the canopy surface usually represents the vapour sourced for transpiration but this is not the case for this location, due to the proximity to the sea where the humidity sensor may pick up water vapour over the canopy and from incoming wind from the sea.

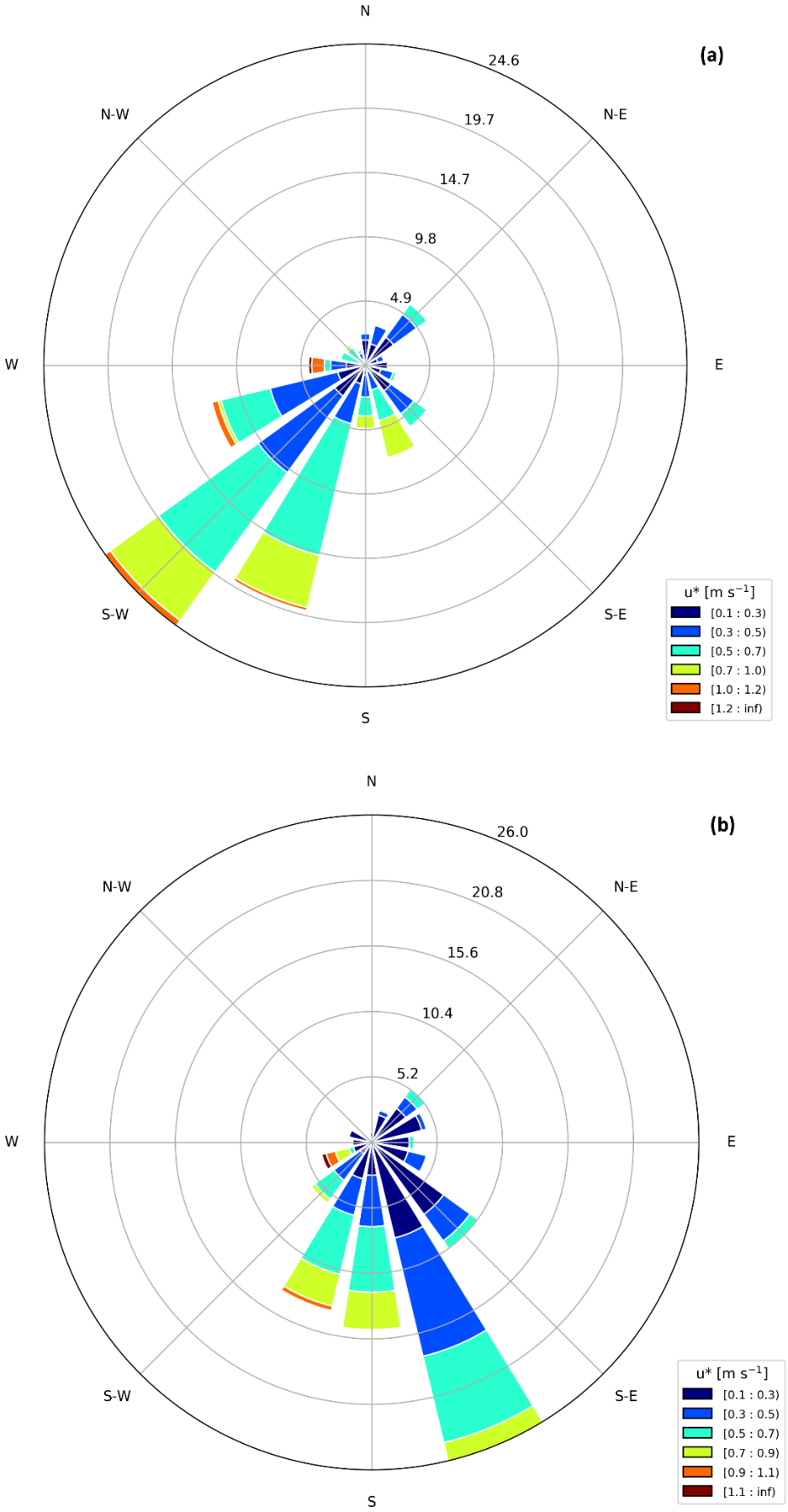

Figure 6: Summer wind rose driving horizontal advection; (a) Daytime; (b) Night time

Another source of energy inflow and outflow into the thermodynamic system at the site location is the flowing and ebbing tide. Due to the proximity of the site to the gulf, the site is intermittently flooded daily in cycles. This tide pattern influences the heat storage in the water and soil surface.

The effect of the horizontal advection as well as the tidal cycle effects leads to the MEP model overestimating and underestimating the latent heat at day and night times respectively (Fig. 5b and 5c). The horizontal advection is driven by the land and sea breeze, which is a function of atmospheric conditions over the land and sea surfaces which can last for days. Figure 5d shows the daily scatter plot of the MEP vs EC ET data. The net effect of the land and sea breeze with however balance out over the course of a few days, which may explain the better correlation with aggregation. The MEP aggregated 8-day and monthly flux data compared with the EC data shows remarkable agreement with significant improvement in the statistical analysis (Table 3). The cumulative 8-day and monthly analysis show that the MEP is able to predict the latent heat flux effectively when data is aggregated over time thereby suggesting that the net effect of the energy introduced and removed from the system by the horizontal advection and the tidal effects cancel out over several daily cycles. This suggests that to improve the ET estimation of the MEP method at high temporal resolution, the inclusion of a term to account for advection may be necessary. Nevertheless, at coarser temporal resolutions of 8-daily ET measurements, the MEP methods accuracy aligns significantly to the EC method affirming the validity of the MEP.

Table 3: ET aggregation statistical MEP ET table

	Daily (mm/ day)	**8-daily (mm/ 8-day)**	**Monthly (mm/ month)**
Average MEP ET	2.73	21.8	58.8
Average EC ET	2.68	21.5	57.8
RMSE	1.19	4.04	1.47
R	0.65	0.91	0.99
MAE	0.9	3.03	4.06
NSE	0.19	0.76	0.97

2.4.3 Sensible heat and latent heat contributions for daytime

One of the significant advantage of the MEP method over other ET methods is the ability to estimate the H and E over the canopy and soil separately. This allows for further analysis of the contribution of each surface to the overall evapotranspiration in the system. Due to the challenges and discrepancies between the EC and MEP at night time, the analysis of the contribution of the H and E have been considered only during the daytime.

In this environment, evaporation contributed 20% to the total evapotranspiration over the study period, with transpiration at 80% being the dominant contributor. This appears reasonable considering the dense vegetation cover at the site location.

During the daytime the energy balance between the EC and MEP is within 7% over the period of the study. The latent and sensible heat contributions of both methods is almost even at about 50% each of the total energy balance calculated by each method. This even contribution and the close energy balance give confidence regarding the MEP ET at lower temporal resolutions. However, the MEP predicts slightly higher sensible heat than latent heat over the canopy while the reverse is the case over the soil surface.

There is a percentage difference of 11% between the sensible heat from the MEP and EC with the MEP predicting higher sensible heat while also predicting higher latent heat by 3%. A possible explanation for this is the reduction of canopy surface energy by the incoming cool breeze from the sea during the daytime. The strength of the MEP is highlighted in this area by giving quantitative analysis on the latent and sensible heat fluxes at the canopy and soil surfaces separately.

2.5 Conclusion

The objectives of this study are to evaluate the performance of the MEP in a wetland environment adjacent to the gulf, compare the performance with the EC method and determine areas of improvement if any. Our study shows that the study environment is a complex thermodynamic system where diurnal horizontal advection and tides affect the fundamental characterization of the system. While the turbulent flux calculations from the MEP model on the hourly and daily timescales does not accurately characterize the thermodynamic system in the environment due to the effects of horizontal advection and tides, these influences are much less important over a few days of data aggregation. The results show the MEP can still be used in predicting fluxes over such environments but the

temporal resolution must be critically determined. Further studies are required on the performance of the MEP at higher temporal resolutions and in complex terrain regions.

The study shows that the MEP model is not as robust as the EC method in capturing the microscopic details, which impact the fluxes at high temporal resolution. However, the MEP model, which was introduced as a method requiring few input data (net radiation, temperature and specific humidity) to characterize the thermodynamic system based on the energy balance equation was able to achieve this at the expense of high temporal resolution output. Due to the flexibility of the MEP equation derived from the information entropy principle, it is entirely possible to parameterise further information such as the effect of horizontal advection into the MEP model. While this is beyond the scope of this study, this will most likely impact the simplicity of the MEP model of effectively characterising the thermodynamic system at the land surface with few easily accessible data.

The results of this study show the challenges of high temporal resolution ET modelling using the MEP model. Further study will seek to incorporate the parameterisation of the horizontal advection into the MEP model.

3 Comparison of MEP, AWRA-L, MODIS and SWAT Evapotranspiration over a Complex Terrain at Different Spatial Scales

Adapted and extended from the published article in Hydrology of Earth System Sciences

Abiodun, O.O., Guan, H., Post, V.E. and Batelaan, O., 2018. Comparison of MODIS and SWAT evapotranspiration over a complex terrain at different spatial scales. *Hydrology and Earth System Sciences*, *22*(5), pp.2775-2794.

Authors: Olanrewaju O Abiodun[1], Huade Guan[1], Vincent E.A. Post[1], Okke Batelaan[1]

[1]National Centre for Groundwater Research and Training, College of Science and Engineering, Flinders University, Australia

Correspondence to: Olanrewaju O. Abiodun (lanre.abiodun@flinders.edu.au)

Abstract

In most hydrological systems, evapotranspiration (ET) and precipitation are the largest components of the water balance, which are difficult to estimate, particularly over complex terrain. In complex terrain environments where ground based measurements are difficult, a multi-model approach to estimating ET can improve confidence on ET estimates In recent decades, the advent of remotely-sensed data based ET algorithms and distributed hydrological models has provided improved spatially-upscaled ET estimates. However, information on the performance of these methods at various spatial scales is limited. This study compares the ET from the MEP, AWRA-L, MOD16 and SWAT in a complex terrain. The finer spatial resolution MOD16 and SWAT ET were analysed on graduated spatial scales for the complex terrain of the Sixth Creek Catchment of the Western Mount Lofty Ranges, South Australia. The MEP model was able to estimate ET to with 20% of the SWAT, AWRA-L and MOD16. At the catchment scale, the MEP model accurately simulated the expected ET seasonal patterns but the SWAT and AWRA-L models predicted higher ET in the spring compared to summer, while the MOD16 predicted similar ET in spring and summer. At the sub-catchment scale, differences in ET estimation between the

SWAT and MOD16 methods of up to 31%, 19%, 15%, 11% and 9% were observed at respectively 1 km^2, 4 km^2, 9 km^2, 16 km^2 and 25 km^2 spatial resolutions. Based on the results of the study, a spatial scale of confidence of 4 km^2 for catchment scale evapotranspiration is suggested in complex terrain. Possible effects of drought on the specific humidity in the stomatal cavity as calculated in the MEP model, land cover differences, HRU parameterization in AWRA-L and catchment-scale averaging of input climate data in the SWAT semi-distributed model were identified as the principal sources of weaker correlations between the models.

Key words: Evapotranspiration, MEP, MOD16, SWAT, AWRA-L, complex terrain, spatial scale

3.1 Introduction

In most hydrological systems, evapotranspiration (ET) and precipitation are the largest components of the water balance (Nachabe et al., 2005) and yet the most difficult to estimate particularly over complex terrains (Wilson and Guan, 2004). In arid and semi-arid environments ET is a significant sink of groundwater with ET often exceeding precipitation (Domingo et al., 2001, Cooper et al., 2006, Scott et al., 2008, Raz-Yaseef et al., 2012). Reliable estimation of ET is integral to environmental sustainability, conservation, biodiversity and effective water resource management (Cooper et al., 2006, Boe and Terray, 2008, Zhang et al., 2008a, Tabari et al., 2013). Moreover, ET will be one of the most severely impacted hydrological components of the water cycle alongside precipitation and runoff as a consequence of global climate change (Abtew and Melesse, 2013).

Reliable, cheap and generally accessible methods of estimating ET are essential to understand its role in catchment processes. ET is principally measured and estimated using ground based measurement tools and/or through various modelling techniques often involving remote sensing (Drexler et al., 2004b, Tabari et al., 2013). Ground based measurement methods such as the Bowen Ratio Energy Balance (BREB), Eddy Covariance (EC), Large Aperture Scintillometers (LAS) and lysimeters have been regarded as the most accurate and reliable ET determination methods (Kim et al., 2012a, Rana and Katerji, 2000, Liu et al., 2013), but they are spatially and/or temporally limited (Wilson et al., 2001, Glenn et al., 2007). Despite the relative reliability of ground based measurement methods, there are inherent uncertainties associated with the different methods, which affect the accuracy of ET measurements (Baldocchi, 2003, Brotzge and Crawford, 2003, Drexler et al., 2004b, Zhang et al., 2008a). Ground based measurement methods are particularly prone to significant errors related to instrument installation (Allen et al., 2011). Mu et al. (2011a) observed that multiple EC towers on a site can have uncertainties

ranging between 10-30% and Liu et al. (2013) documented uncertainty ranges of over 27% between EC and LAS measurements over the same site on an annual scale. EC towers have also been observed to encounter energy balance closure challenges (Wilson et al., 2002), while other challenges of the EC method such as inaccuracies due to complex terrains have been documented by Feigenwinter et al. (2008). Furthermore, Kalma et al. (2008), conducted a review of 30 remote sensing ET modelling results relative to ground based measurements and contended that the ground based measurement methods were not incontrovertibly more reliable than the remote sensing ET modelling methods. Moreover, most of the ground based measurement methods are usually cost intensive thereby constraining measurements over large areas and thus making spatial extrapolation difficult (Moran and Jackson, 1991, Verstraeten et al., 2008, Melesse et al., 2009, Fernandes et al., 2012).

In more recent years, the spatial challenges associated with ET estimations are being eased by the increased availability of remotely-sensed data. The use of remotely-sensed input data in many surface energy balance algorithms and highly parameterized hydrological models have been extensively documented (Kalma et al., 2008, Hu et al., 2015a, Zhang et al., 2016). The advances in remote sensing have seen these methods become prominent in water resource assessment studies (Hong et al., 2009, Vinukollu et al., 2011, Anderson et al., 2011, Long et al., 2014, Zhang et al., 2016).

Several hydrological models and remotely-sensed based surface energy balance models are currently used in ET simulations globally (Zhao et al., 2013, Chen et al., 2014, Larsen et al., 2016, López López et al., 2016, Webster et al., 2017). However, the relative accuracy of these models relative to one another should be extensively explored to improve our understanding of the ET estimation from these algorithms.

Four ET models will be evaluated in this study; The Maximum Entropy Production model (MEP) (Wang and Bras, 2011), The Soil and Water Assessment Tool (SWAT) (Neitsch et al., 2011), the Australian Water Resource Assessment model (AWRA_L) (Viney et al., 2014) and the MOD16 (Mu et al., 2013) derived from remotely-sensed data from the Moderate Resolution Imaging Spectroradiometer (MODIS) instrument aboard the National Aeronautics and Space Administration (NASA) Aqua and Terra satellites. Of the four ET models (two hydrological and two energy balance based) to be evaluated in this study, one hydrological (SWAT) and one remote sensing based (MOD16) which are available in high spatial resolution (1 km^2) will be comprehensively evaluated at the catchment and sub-catchment scales. The sub-catchment scale analysis will include analysis at graduated spatial scales and the contributions of the temporal and spatial components to the variance. The sub-catchment scale analysis in this study was principally conducted between the SWAT and MOD16 due to the high

resolution of both products. The MEP and AWRA-L model analysis were conducted on catchment scale due to the coarser resolution of the products.

The MEP model which has been evaluated on the field scale at hourly, daily, 8-day and monthly temporal resolution in the previous chapter and will be evaluated on monthly temporal resolution at the catchment scale, i.e. 25 km^2 spatial resolution, using available remote sensing data. The evapotranspiration product from the Australian Water Resource Assessment model (AWRA_L) with the same spatial resolution with the MEP will also be evaluated temporally at the catchment scale.

While the MEP model is a relatively new algorithm derived from the information entropy principle (Shannon, 1948), the MODIS ET (MOD16) is based on the Penman-Monteith equation, the AWRA-L uses the Penman equation, while the SWAT ET algorithm also has the Penman-Monteith equation as one of the three user-selectable methods of estimating ET. In this study, the Penman-Monteith method in SWAT is used for a direct comparison with the MOD16 and the AWRA-L. However, to develop good confidence in ET estimations, especially in complex terrains where there are no ground-based measurements, a multi-model approach based on different parameterisation methodologies is required. The information entropy based MEP model uses an inference based methodology to estimate ET, the comparison of the results from the method with the three other methods with similar theoretical basis will significantly improve our confidence in the estimation. Although, the Penman-Monteith equation is regarded as one of the most reliable methods for ET estimation over various climates and regions (Allen et al., 2005, Allen et al., 2006), the MEP method has been shown to perform very well in various field tests (Wang and Bras, 2011, Hajji et al., 2018b). Moreover, although the performance of the MEP at the field scale in the previous chapter on a monthly timescale was excellent at the field spatial scale, it is imperative to evaluate the performance at the catchment scale with a greater complexity in ET estimation.

Notwithstanding, the similarities in the MOD16 and SWAT ET, which both use the Penman-Monteith equation, the methods for estimating the parameters of the equation are significantly different between them. For instance, the SWAT Penman-Monteith implementation requires wind speed data for the computation of the aerodynamic resistance, while the MOD16 Penman-Monteith variant does not require wind speed data but instead uses the Biome-BGC model (Thornton, 1998) to estimate the aerodynamic resistance. This study does not seek to evaluate the individual accuracy of any method, but rather to compare the ET results from the water balance-based hydrological models AWRA-L and SWAT and the energy balance-based models (MEP and MOD16) over a complex terrain catchment. Two different land cover products will also be used in the SWAT model in this study

(The Geoscience Australia and the MODIS land cover products). The rationale for this is to analyse the effect of land cover on the ET modelling in SWAT and also the use of the MODIS land cover allows for a direct comparison with the MOD16 which uses the same land cover product. The results will be compared temporally on catchment scale and spatio-temporally on sub-catchment scales to identify the effects of input data and other drivers of ET estimation in the MEP, MOD16, AWRA-L and SWAT ET algorithms.

While the MODIS evapotranspiration has been widely studied and compared to other methods, this is much less the case for SWAT ET, MEP and the AWRA-L. Moreover, a graduated spatial scale comparison of these evapotranspiration methods is yet to be documented over a complex terrain. The objectives of this study are therefore: (1) To compare four ET products (MEP, SWAT, MOD16 and AWRA-L) on catchment scale in a complex terrain catchment while also evaluating the two finer resolution products (SWAT and MOD16) on graduated spatial scale to evaluate their relative accuracy.; (2) To analyse and determine the spatial scale at which the graduated spatial scale models tend towards agreement to enhance the confidence in ET estimation in a complex terrain. A significant challenge of current ET estimation is the challenge of determination of a spatial scale where the results of each product tends towards agreement due to the availability of several products at various spatial scale. This study seeks to determine a spatial scale of agreement where the compared products tend towards agreement, this scale will be termed the "spatial scale of confidence".

Table 4: Literature studies of MODIS and SWAT evapotranspiration (see Table 5 for climate classification)

Study type	Reference	Method	Climate	Land Cover Cover	Spatial and temporal extents
MOD16 vs micrometeorological methods	Ruhoff et al. (2013)	EC validation at 2 sites	Cwa, Cfa	Savanna	3 km x 3 km area, 8 day
	Liu et al. (2013)	LAS validation at 3 sites	Dwa, Cwa	Orchards, Croplands	1 km x 1 km, annual
	Mu et al. (2011a)	EC validation at 46 site	Global	Global	Various
	Kim et al. (2012b)	EC validation at 17 sites	Af, Dfb, Dwa, Cfa, Bsk, Am, ET, Aw, Dwc, Dfc, Dfd	Forest, croplands, grassland	3 km x 3 km area, 8 day, 2000-2006
	Velpuri et al. (2013)	EC validation at 60 sites	Bsk, Cfa, Csa, Csb,	Cropland, Forest, Woody Savanna, Grassland,	Point scale at EC sites across the United States of America, monthly, 2001 - 2007

			Dfa, Dfb, Dfc	Shrubland, Urban	
MOD16 vs energy balance models	Jia et al. (2012)	MOD16 validation of ETWatch system	Dwa, Cwa	Farmland, Forest, Grassland,Shrub Forest, Beach land, Bare land, Urban, Paddy field	(1 km x 1 km grid over 318,000 km^2), annual , 2002-2009
	Velpuri et al. (2013)	MOD16 vs Gridded Fluxnet ET (GFET)	Bsk, Cfa, Csa, Csb, Dfa, Dfb, Dfc	Cropland, Forest, Woody Savanna, Grassland, Shrubland, Urban	50km, monthly, over the entire United States of America
MOD16 vs hydrological models	Ruhoff et al. (2013)	MOD16 vs MGB-IPH model	Cwa, Cfa	Forest, Shrubland, Savanna, Woody Savanna, Grassland, Cropland, Urban, Barren land	(1 km x 1 km grid over 145,000 km^2), 8 day, 2001
	Trambauer et al. (2014)	MOD16 vs GLEAM, ERAI, ERAL, PCR-GLOBWB, PCR-PM, PCR-TRMM, PCR-Irrig	Various	Various	$1km^2$, 0.25º, 0.5º, and ~0.7º resolutions over most of the African continent, daily and monthly, 2000 -2010
	Velpuri et al. (2013)	MOD16 vs Water Balance ET (WBET)	Bsk, Cfa, Csa, Csb, Dfa, Dfb, Dfc	Cropland, Forest, Woody Savanna, Grassland, Shrubland, Urban	(1 km x 1 km over the entire United States of America), Annual, 2002-2009,
SWAT vs energy balance models	Gao and Long (2008)	SWAT vs SEBS, SEBAL, P-TSEB, S-TSEB	Dwb	Woodland, Grassland, Cropland	1850 km^2 , 23 June 2005 and 25 July 2005 (2 days only)

Table 5: Köppen-Geiger Climate Classification system (Kottek et al., 2006)

Main climate	**Precipitation**	**Temperature**
A – equatorial	W – desert	h – hot arid
B – arid	S – steppe	k – cold arid
C – warm temperate	f – fully humid	a – hot summer
D – snow	s – summer dry	b – warm summer
E – polar	w – winter dry	c – cool summer
	m – monsoonal	d – extremely continental
		F – polar frost
		T – polar tundra

e.g Cwa – Warm temperate, winter dry, hot summer

3.2 Model Description

3.2.1 MEP Model

The MEP model predicts the turbulent heat fluxes (latent heat, sensible heat and ground heat) as a function of specific humidity (q_s), temperature (T_s) and net radiation (R_n). The model predicts the partitioning of the turbulent heat fluxes based on the available energy information and the thermal inertia driving the production of each of the turbulent fluxes. The MEP model theorises that the thermodynamic system at the land surface uses evapotranspiration as the principal source of driving the system to equilibrium based on the available energy. The MEP model which was derived by optimizing the dissipation function described in Wang and Bras (2011), operates as a two sources energy balance (TSEB) model by calculating the latent heat (evapotranspiration) over the canopy and soil surfaces separately. Unique equations for the evaporation over the soil surface and transpiration over the canopy are described in the Appendix A.

3.2.2 SWAT Model

The Soil and Water Assessment Tool (SWAT) is a physically based, semi-distributed hydrological model designed on the water balance concept. SWAT simulates catchment processes such as evapotranspiration, runoff, crop growth, nutrient and sediment transport on basis of meteorological, soil, land cover data and operational land management practices (Neitsch et al., 2011). The SWAT model has been used in hydrological modelling from sub-catchment scales of under 1 km^2 (Govender and Everson, 2005) to sub-continental scales (Schuol et al., 2008). The model discretises a catchment into sub-catchments and further into hydrological response units (HRU), which represent unique combinations of land cover, soil type and slope. The discretisation method employed by SWAT enables the model to simulate catchment processes in detail and to understand the response of unique HRU's on hydrological processes. Evapotranspiration is simulated at the HRU scale. A comprehensive outline of ET calculations in SWAT is included in Appendix B and Fig. (7) summarizes in a flowchart the SWAT ET algorithm. Where PET is the potential evapotranspiration, E_{can} is the evaporation from canopy surface, E_t is the transpiration, E_{soil} is the evaporation from the soil and Revap is the amount of water transferred from the underlying shallow aquifer to the unsaturated zone in response to water demand for evapotranspiration.

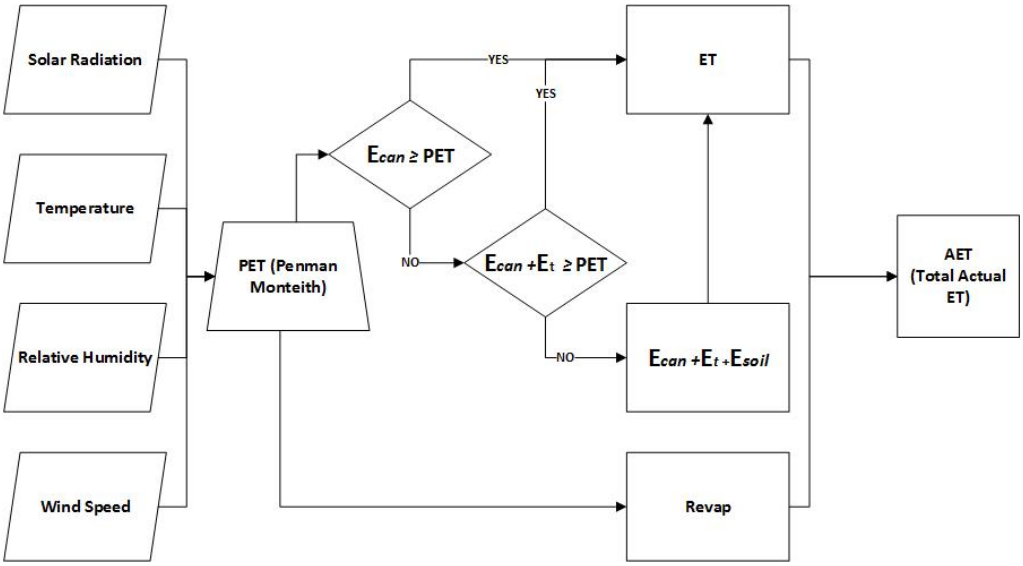

Figure 7: SWAT ET flowchart (Penman-Monteith method)

3.2.3 MOD16 Model

The MOD16 provides evapotranspiration estimates for 109.03×10^6 km^2 of global vegetated land area at 1 km^2 spatial resolution at 8 day, monthly and yearly temporal resolutions since the year 2000 (Mu et al., 2013). The initial version of the MOD16 algorithm used MODIS imagery as part of a Penman-Monteith method as described in Cleugh et al. (2007a). The MOD16 algorithm was significantly improved by the inclusion of a sub-algorithm for estimating soil evaporation as a component of total ET (Mu et al., 2007). Further improvements on the MOD16 algorithm such as the calculation and inclusion of night time evapotranspiration, partitioning of evaporation from moist and wet soils were incorporated in the newer version of the algorithm(Mu et al., 2013). In this study, the ET products from the newer version, are used. Details of ET calculations in MOD16 are included in Appendix C while Fig. (8) summarizes in a flowchart the MOD16 ET algorithm.

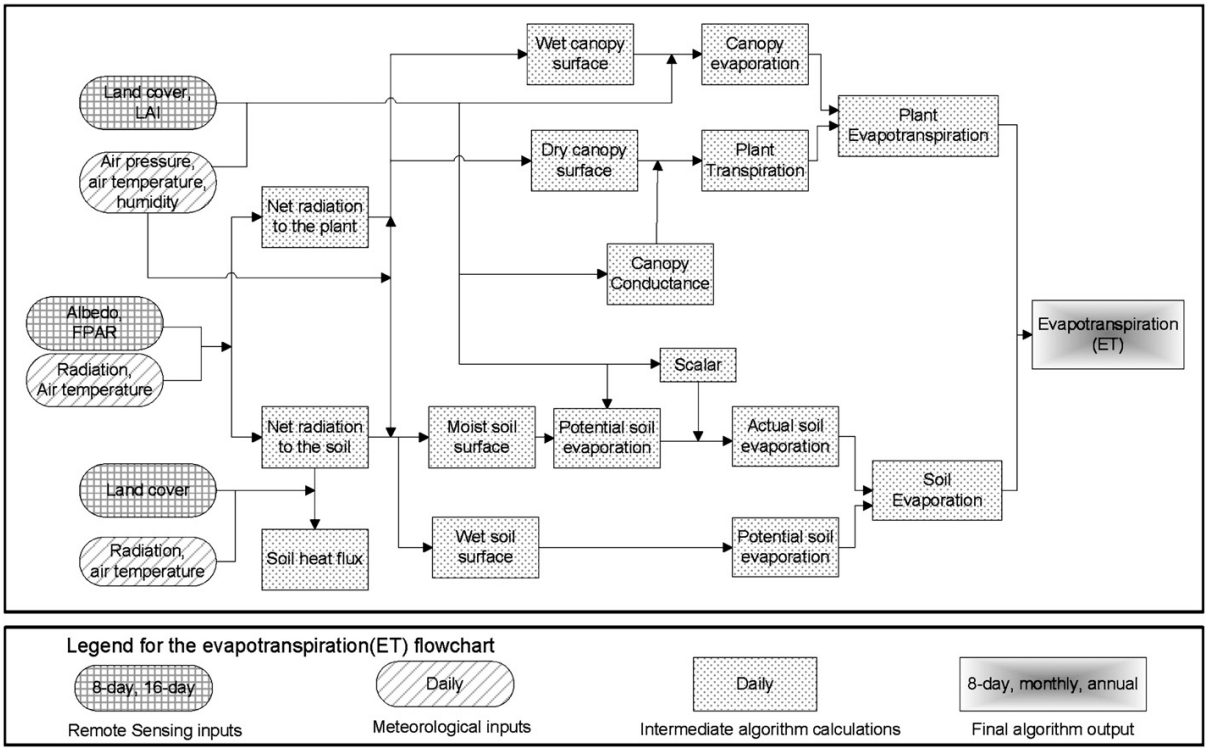

Figure 8: Flowchart of the MOD16 ET algorithm (Mu et al., 2011)

3.2.4 AWRA-L Model

The AWRA-L is a daily 25 km^2 grid based hydrological model designed on the water balance concept over Australia. The model conceptualises each grid as two distinct HRU's; shallow-rooted vegetation HRU and deep-rooted vegetation HRU. The shallow-rooted vegetation corresponds to grass while the deep-rooted vegetation corresponds to trees. The model conceptualises the soil into three layers with water storage capacity. The soil surface storage with a 0.1 m depth, the shallow storage from 0.1m to 1m and the deep storage from 1 m to 6 m. The principal difference between the two HRU's is that the shallow-rooted vegetation HRU can only access the first two soil storage layers while the deep-rooted vegetation HRU can access the 3 layers. The AWRA-L model simulates catchment hydrological processes such as evapotranspiration, infiltration, runoff, drainage, interflow, recharge and other catchment processes.

Evapotranspiration in the AWRA-L is a sum of six processes; canopy evaporation from intercepted precipitation, evaporation from soil surface, groundwater evaporation, shallow storage transpiration, deep storage transpiration and groundwater transpiration. The evaporation in the model is constrained by the Penman equation (Penman, 1948). For a detailed structure of the AWRA-L model, see Viney et al. (2014).

3.2.5 Penman-Monteith Algorithm Parameterization

The MOD16 and SWAT ET algorithm, which are both based on the Penman-Monteith equation but parameterized differently, suggests there will be similarities and differences in the results from both methods. Both algorithms are principally limited on temporal timescales by the available energy to convert liquid water to atmospheric water vapour. Their transpiration and soil evaporation algorithms are also very dependent on vegetation/biome type, VPD, and the soil moisture constraint parameterization (Fig. 9).

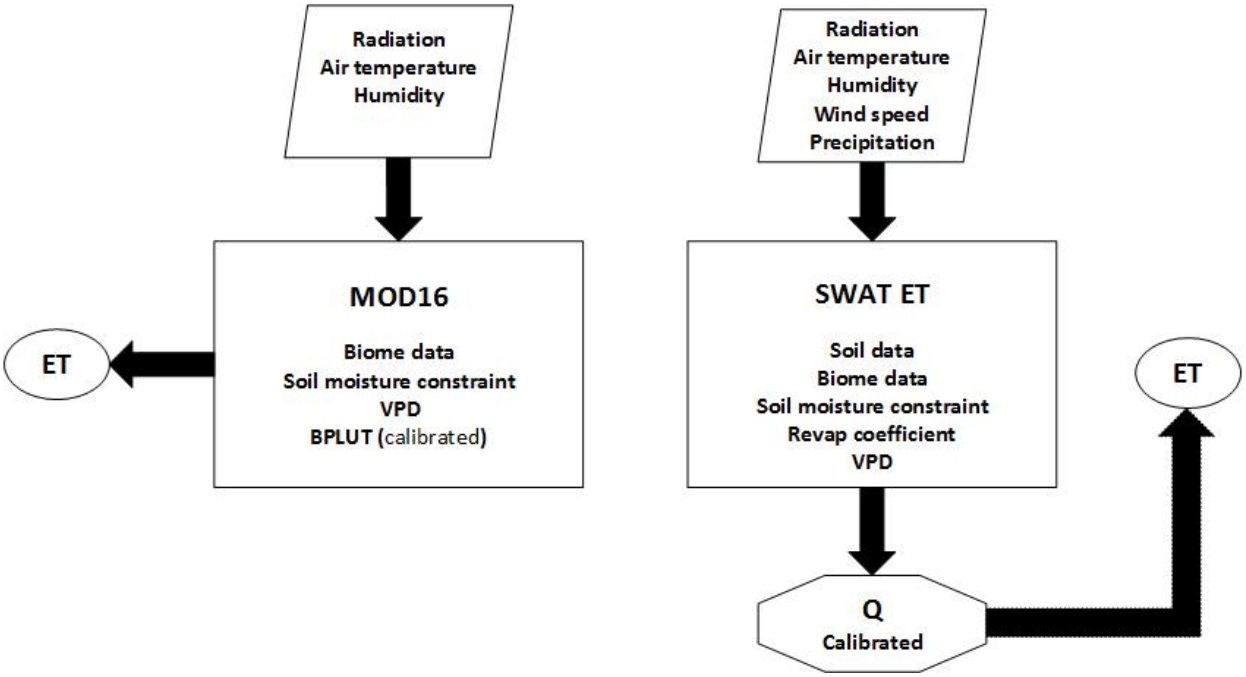

Figure 9: MOD16 and SWAT ET parameterization (Q: discharge, BPLUT: biome properties lookup table; VPD: vapour pressure deficit).

In the SWAT ET algorithm, the VPD significantly impacts the transpiration through the constraining of the stomatal conductance. Detailed soil data on HRU scale such as layer depth, number of layers, unsaturated hydraulic conductivity and water capacity are crucial for constraining the soil moisture content, which in turn regulates the percolation and recharge into the system. Similarly, the calculated MOD16 ET is significantly impacted by the biome properties lookup table (BPLUT) and the soil moisture constraint function. The BPLUT was calibrated using the response of biomes on flux tower sites globally. The BPLUT contains information on the stomatal response of each biome to temperature, VPD and biophysical parameters. The soil moisture constraint function is applied in the estimation of the soil evaporation and is an important parameter in regions where the saturated zone is close to the ground surface such as our study area.

3.3 Data and Methods

3.3.1 Study Area

The study area is the Sixth Creek Catchment of South Australia, located in the western part of the Mount Lofty Ranges, which is a range of highlands separating the Adelaide Plains in the west from the Murray-Darling basin in the east. The western part of the Mount Lofty Ranges runs 90 km north to south, its summit is at 680 mAHD (metres Australian Height Datum) (Sinclair, 1980). It extends from the southernmost part at McLaren Vale on the Fleurieu Peninsula to Freeling in the north over an area of 2189 km^2. The Sixth Creek Catchment is a complex area, with acute elevation changes over few hundred metres (Fig. 10). The catchment is located close to the summit of the Western Mount Lofty Ranges.

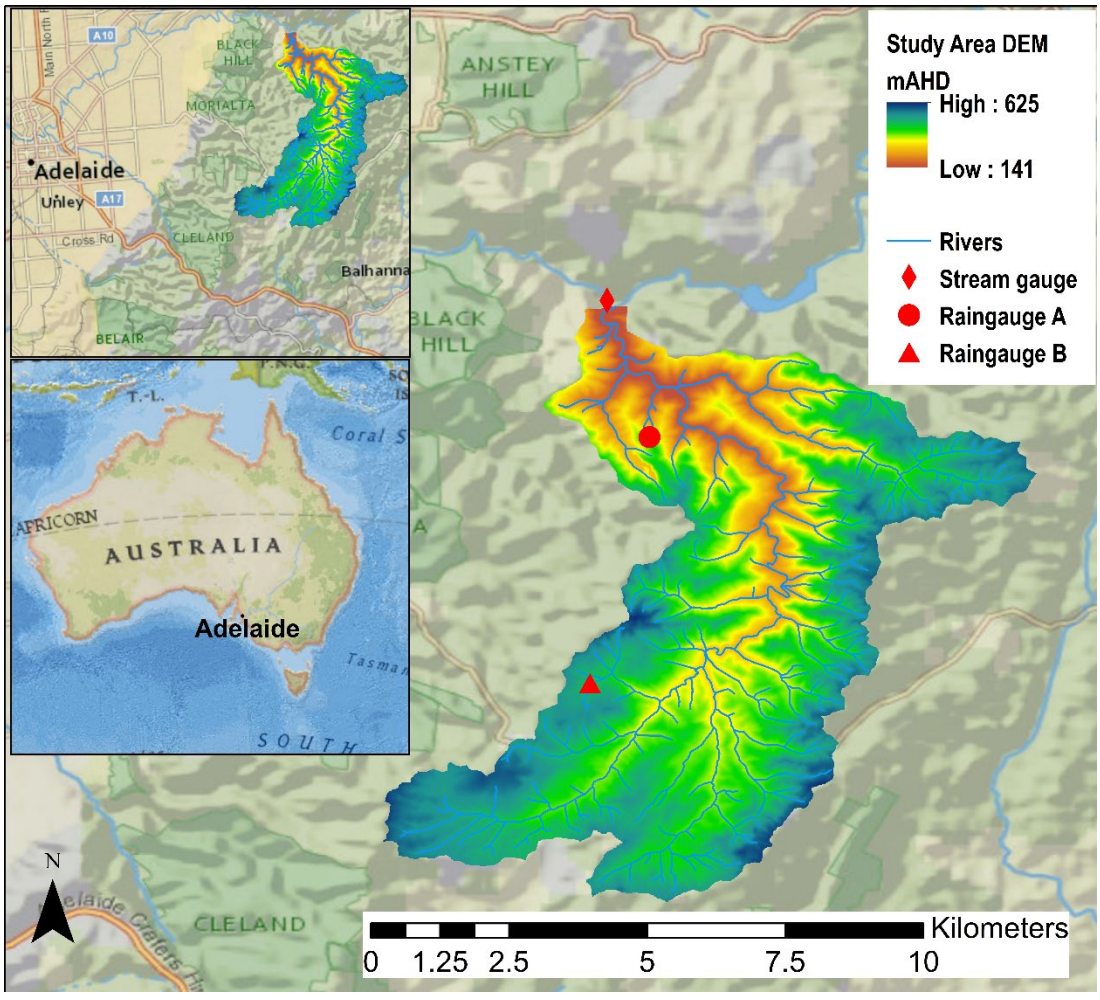

Figure 10: Digital elevation model of the Sixth Creek Catchment study area (Gallant et al., 2011)

It covers an area of 44 km^2 between 34°52′6.098″ to 34°57′54.541″S and 138°42′55.855″ to 138°49′27.174″E and has an elevation range of 140 - 625 mAHD (Fig. 10). The land cover consists of 95% forestland with significant deep-rooted Eucalyptus plantation and 5% pasture, shrubs and grasslands (Fig. 11b). Most of the native vegetation is under conservation. The climate is Mediterranean, with warm dry summers and cool wet winters, and is of the type "Csb" according to the Köppen-Geiger classification. The Sixth Creek is a perennial stream with mean annual discharge of 0.25m^3/s which accounts for 20 – 25 % of the mean annual rainfall in the catchment. The Sixth Creek did however experience a total of 35 days of no flow in the 13-year period of this study, which encompasses the "millennium drought years" (2000 – 2009) in Australia. The Sixth Creek is a gaining stream with groundwater discharging into the stream and sustaining it especially during the dry summer months. The depth to groundwater varies greatly across the complex terrain catchment, from less than 1 m to over 20 m across the seasons.

The Sixth Creek Catchment's complex terrain plays a significant role in its hydrology, with highly localised precipitation events recorded from the two weather stations in the catchment within the study period. The weather stations are located 4.5 km apart with elevation difference of over 200 metres (Fig. 10). Differences in annual rainfall of over 400 mm have been recorded between the two weather stations.

The annual precipitation for the period 2002 till 2016 for Station A ranges between 500 – 900 mm and 750-1500 mm for Station B, while the temperature ranges between 10.5 °C and 22.2 °C in the summer months and 3.4 °C and 10 °C in the winter months.

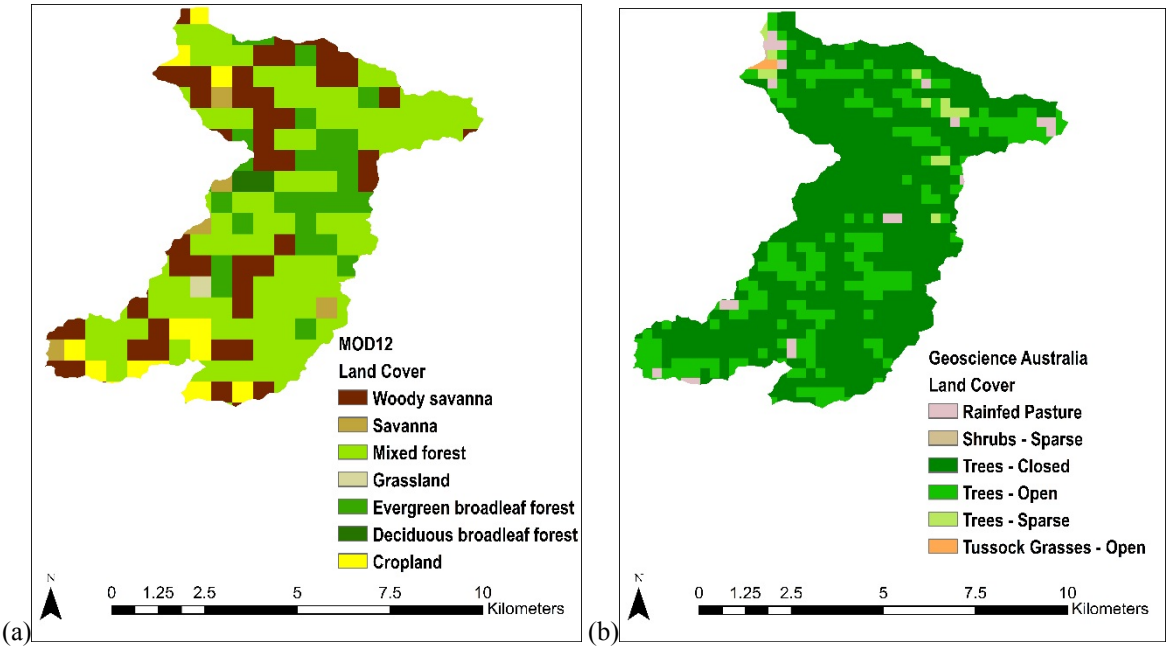

Figure 11: (a) MOD12 land cover used in MOD16 (Friedl et al., 2010); (b) Land Cover (Lymburner et al., 2010)

3.3.2 Input datasets

3.3.2.1 MEP

The MEP ET over the Sixth Creek Catchment was calculated at the 25 km^2 resolution using (temperature, relative humidity and solar radiation) climate data from the Scientific Information for Land Owners (SILO) repository of Australian weather data. The relative humidity data was used in obtaining specific humidity, solar radiation data was used in calculating net radiation using the method described in Allen et al. (1994) and the temperature data from SILO was also used in calculating the evapotranspiration. The algorithms for producing the SILO climate data over Australia are discussed in Jeffrey et al. (2001).

3.3.2.2 SWAT

The GIS interfaced version of SWAT (ArcSWAT) was used in the hydrological modelling. A 30 m Digital Elevation Model (DEM) (Dowling et al., 2011) of the Sixth Creek Catchment was used to extract the stream network and the catchment area. A detailed soil properties database for the catchment was created from the soil data obtained from the Australian Soil Resource Information System (Johnston et al., 2003a). The 250 m land cover map of Australia from Geoscience Australia's Dynamic Land Cover database (Fig. 11b) is typically preferred to be used in the SWAT model ahead of the 500 m MOD12 land cover map (Fig. 11a) due to its finer spatial resolution and better biome match with local field knowledge but for direct comparison with MOD16 which uses the MOD12 land cover, both maps are used to run separate SWAT models. In this study, the 1 km^2 wind speed data (McVicar et al., 2008), and the 25 km^2 relative humidity, temperature, rainfall, solar radiation (Jeffrey et al., 2001) from SILO, were preferred to weather station data. Four 25 km^2 gridded data cells fall within the boundaries of the catchment and are therefore comparable to the climate components of the two weather stations in the catchment while also maintaining uniformity of input data with the MEP model. Moreover, the gridded data used in this study are calibrated using the weather stations across Australia including the two weather stations in the Sixth Creek Catchment, thus maintaining excellent correlation when compared to the weather stations' measured data. Details of the gridded data methodology and algorithm used in this study can be found in Jeffrey et al. (2001) and McVicar et al. (2008). The daily gridded climate datasets were simply averaged over the Sixth Creek Catchment, to obtain values used in this study.

The monthly MOD16 datasets for the years 2000 to 2013, at 1 km^2 spatial resolution were used in this study(Mu et al., 2013). Catchment averages were calculated by simple averaging of all the 1 km^2 cells that fall within the catchment area. AWRA-L ET data at the 25 km^2 were also used in catchment scale comparison. A percentage area weighted average of the cells overlapping in the catchment was calculated and used in the analysis.

3.3.3 SWAT Model Setup and Calibration

The soil, land cover and DEM derived slope data were classified into classes and used to create 124 and 119 unique HRU's for the Geoscience Australia and MOD12 land covers respectively, ranging from 0.001 km to 6 km in area. While each unique HRU has specific set of properties several small areas with the same land cover, slope and soil type make up the total area of a single HRU. The properties of each unique HRU determine how it responds to precipitation, and how different hydrological processes such as streamflow, runoff, lateral flow and evapotranspiration are modelled in the catchment. The runoff from each HRU is accumulated and routed through the river network to the outlet of the catchment. Driven by the meteorological input, the model simulates catchment hydrological processes with a daily time step for the period 2000 to 2013.

The SWAT model is calibrated by fitting simulated streamflow to observed streamflow with the SUFI-2 algorithm. This semi-automatic Latin hypercube sampling algorithm optimizes SWAT model parameters while attempting to fit the simulated data as close as possible to the observed data using the user preferred objective function from those detailed below as measurement of simulation accuracy (Abbaspour, 2007). Although a single user objective function is used in the calibration and validation, the results of the other objective functions are also recorded for the optimal model run.

Nash Sutcliffe Efficiency (N_{SE}) (Nash and Sutcliffe, 1970),

$$N_{SE} = 1 - \frac{\sum_{n=1}^{N}(Q_n - \widehat{Q_n})^2}{\sum_{n=1}^{N}(Q_n - \overline{Q})^2} \quad (10)$$

where Q_n (m^{3}s^{-1}) is the measured discharge at time n, $\widehat{Q_n}$ (m^{3}s^{-1}) is the simulated discharge at time n, $\overline{Q}$ (m^{3}s^{-1}) is the mean measured discharge and N is the number of time steps.

Ratio of root mean squared error to the standard deviation of measured data (R_{SR}) (Moriasi et al., 2007),

$$R_{SR} = \frac{\sqrt{\sum_{n=1}^{N}(Q_n - \widehat{Q_n})^2}}{\sqrt{\sum_{n=1}^{N}(Q_n - \overline{Q})^2}} \quad (11)$$

Percent bias (P_{BIAS}),

$$P_{BIAS} = 100 \ \frac{\sum_{n=1}^{N}(Q_n - \widetilde{Q_n})}{\sum_{n=1}^{N} Q_n} \tag{12}$$

Coefficient of determination (R^2),

$$R^2 = \left(\frac{(\sum_{n=1}^{N}(Q_n - \overline{Q})(\widetilde{Q_n} - \widetilde{Q_n}))}{\sqrt{\sum_{n=1}^{N}(Q_n - \overline{Q})^2}\sqrt{\sum_{n=1}^{N}(\widetilde{Q_n} - \widetilde{Q_n})^2}} \right)^2 \tag{13}$$

where $\widetilde{Q_n}$ (m^3s^{-1}) is the mean simulated discharge.

Kling-Gupta Efficiency (K_{GE}) (Gupta et al., 2009),

$$K_{GE} = 1 - \sqrt{(r-1)^2 + (\alpha - 1)^2 + (\omega - 1)^2} \tag{14}$$

where r is the linearcorrelation coefficient between the simulated and measured variable, $\omega = \frac{\widetilde{Q_n}}{\overline{Q}}$, $\alpha = \frac{\sigma_s}{\sigma_m}$, σ_s and σ_m are the standard deviation of simulated and measured data.

After obtaining a satisfactory fit between the simulated and observed streamflow data during calibration, the model is validated by running the model for a different time period using the same parameters from the calibration period. SUFI-2 further incorporates the unitless P and R-factor metric, which gives an indication of the confidence in the calibration exercise. The P-factor which is also referred to as the 95 Percent Prediction Uncertainty (95PPU), is the percentage fraction of observed data captured which falls between the 2.5 and 97.5 percentiles, while the R-factor is the width of the 95PPU. The P and R-factors are iteratively determined using Latin Hypercube Sampling. For streamflow calibration and validation to be considered reliable, combined satisfactory values should be obtained of P-factor (> 0.7), R-factor (< 1) (Abbaspour, 2007) and of one of the objective functions, N_{SE} (> 0.5), R_{SR} (≤ 0.7) and P_{BIAS} (±25%) (Moriasi et al., 2007). In this study, the NSE objective function combined with the P and R factors are used. The result of the other objective functions at the optimal NSE are also recorded. For a comprehensive explanation of the SUFI-2 algorithm, see Abbaspour (2007).

The calibration process was conducted on daily timescales for the years 2000 to 2005 while the validation was conducted for the years 2007 to 2013. A warm up period of 5 years between 1995 and 1999 was used in the SWAT model to equilibrate the model mass budget and internal reservoirs. The relatively long periods of streamflow calibration and validation on daily timescales were specifically used to address the potential problem of equifinality of parameters to be optimized. The principle of equifinality has been known to affect semi-distributed

models such as SWAT (Qiao et al., 2013). Nevertheless, the use of many observation points has been observed to effectively constrain it (Tobin and Bennett, 2017). In this study, 21 sensitive SWAT model parameters (Table 6) are optimized with SUFI-2 to fit simulated streamflow to the observed streamflow data. In the SUFI-2 algorithm preparation for calibration, an "r_" and a "v_" prefix before a SWAT model parameter (Table 6) are indicative of a relative change (a percentage increase or decrease in the SWAT modelled value) and replacement change of the original SWAT modelled values respectively. The relative change is often used to fine tune parameters that have been modelled within the acceptable range while the replacement change is used when modelled parameter values are at odds with local field knowledge or established values.

The resultant SWAT simulated ET was compared with the MOD16 ET using the root mean square error (R_{MSE}), mean difference (M_D), Pearson's correlation coefficient (R) and coefficient of determination (R^2) metrics.

$$R_{MSE} = \sqrt{\frac{\sum_{n=1}^{N}(x_{1,n}-y_{1,n})^2}{N}} \quad (15)$$

Where x_1 and y_1 are SWAT and MOD16 monthly ET values respectively.

$$M_D = \left(\frac{x_1+x_2\ldots x_N}{N}\right) - \left(\frac{y_1+y_2\ldots y_N}{N}\right) \quad (16)$$

$$R = \frac{(\sum_{n=1}^{N}(Q_n-\overline{Q})(\widehat{Q_n}-\widetilde{Q_n})}{\sqrt{\sum_{n=1}^{N}(Q_n-\overline{Q})^2}\sqrt{\sum_{n=1}^{N}(\widehat{Q_n}-\widetilde{Q_n})^2}} \quad (17)$$

Table 6: Optimized SWAT parameters and their final range

Parameter Name	Parameter Description	Final Parameter Range
r_CN2.mgt	SCS Runoff Curve Number for moisture condition II	$[1 + (-0.048 - 0.122)] \times Actual\ value$
v_ALPHA_BF.gw	Baseflow recession constant	$0.58 - 0.93$
v_GW_DELAY.gw	Groundwater delay time	$1.89 - 3.70$
v_GW_REVAP.gw	Groundwater "Revap"	$0.12 - 0.2$
v_ESCO.hru	Soil evaporation	$0.2 - 0.5$
v_CH_N2.rte	Manning's "n" value for the main channel	$0.05 - 0.15$
r_SURLAG.bsn	Surface runoff lag	$[1 + (0.22 - 1.2)] \times Actual\ Value$
v_ALPHA_BNK.rte	Baseflow alpha factor for bank storage (days)	$0.5 - 1$

v_SOL_AWC(..sol	Available water capacity of the soil layer (mm/mm)	$0.24 - 0.71$
r_SOL_K(..).sol	Saturated hydraulic conductivity (mm/hr)	$[1 + (-0.99 - -0.39)] \times Actual\ Value$
r_SOL_BD(..).sol	Moist bulk density (g/cm^3)	$[1 + (-0.37 - -0.04)] \times Actual\ Value$
r_SOL_Z(..).sol	Depth from soil surface to bottom of layer (mm)	$[1 + (-0.25 - -0.04)] \times Actual\ Value$
v_EPCO.bsn	Plant uptake compensation	$0.77 - 1$
v_GWQMN.gw	Threshold depth of water in the shallow aquifer required for return flow to occur	$0 - 500$
v_DEEPST.gw	Initial depth of water in the shallow aquifer (mm)	$20000 - 30000$
v_SHALLST.gw	Initial depth of water in the deep aquifer (mm)	$10000 - 20000$
r_HRU_SLP.hru	Average slope steepness	$[1 + (-0.24 - 0.15)] \times Actual\ Value$
r_OV_N.hru	Manning's "n" value for	$[1 + (-0.84 - -0.05)] \times Actual\ Value$
r_SLSUBBSN.hru	Average slope length (m)	$[1 + (-0.9 - -0.24)] \times Actual\ Value$
v_REVAPMN.gw	Threshold depth of water in the shallow aquifer required for Revap to occur (mm)	$0 - 100$
v_CH_K2.rte	Effective hydraulic conductivity in main channel alluvium (mm/hr)	$^{6} - 30$

3.3 Results and Discussion

3.4.1 Streamflow

The streamflow was calibrated and validated on daily timescales according to the guidelines set out in Moriasi et al. (2007) and Abbaspour (2007) (Table 7, Fig. 12). The result indicates an observed data bracketing of between 87% and 89% for both calibration and validation with R-factors under 1.

Table 7: Streamflow calibration and validation results

Model		P-factor	R-factor	N_{SE}	R^2	K_{GE}	R_{SR}	P_{BIAS}
SWAT with Geoscience Land Cover	Calibration	0.89	0.66	0.61	0.62	0.71	0.62	-11.1
	Validation	0.87	0.91	0.78	0.78	0.88	0.47	-0.1
SWAT with MOD12 Land Cover	Calibration	0.88	0.69	0.62	0.64	0.74	0.61	-13.5
	Validation	0.87	0.98	0.79	0.80	0.87	0.46	-6.5

Table (7) shows better results for the validation than calibration for the N_{SE}, R^2, K_{GE} and R_{SR} metrics, however slightly lower for the P-factors. The results of the calibration and validation exercise on daily timescales show that the model effectively represents the high and low flow periods (Fig. 12).

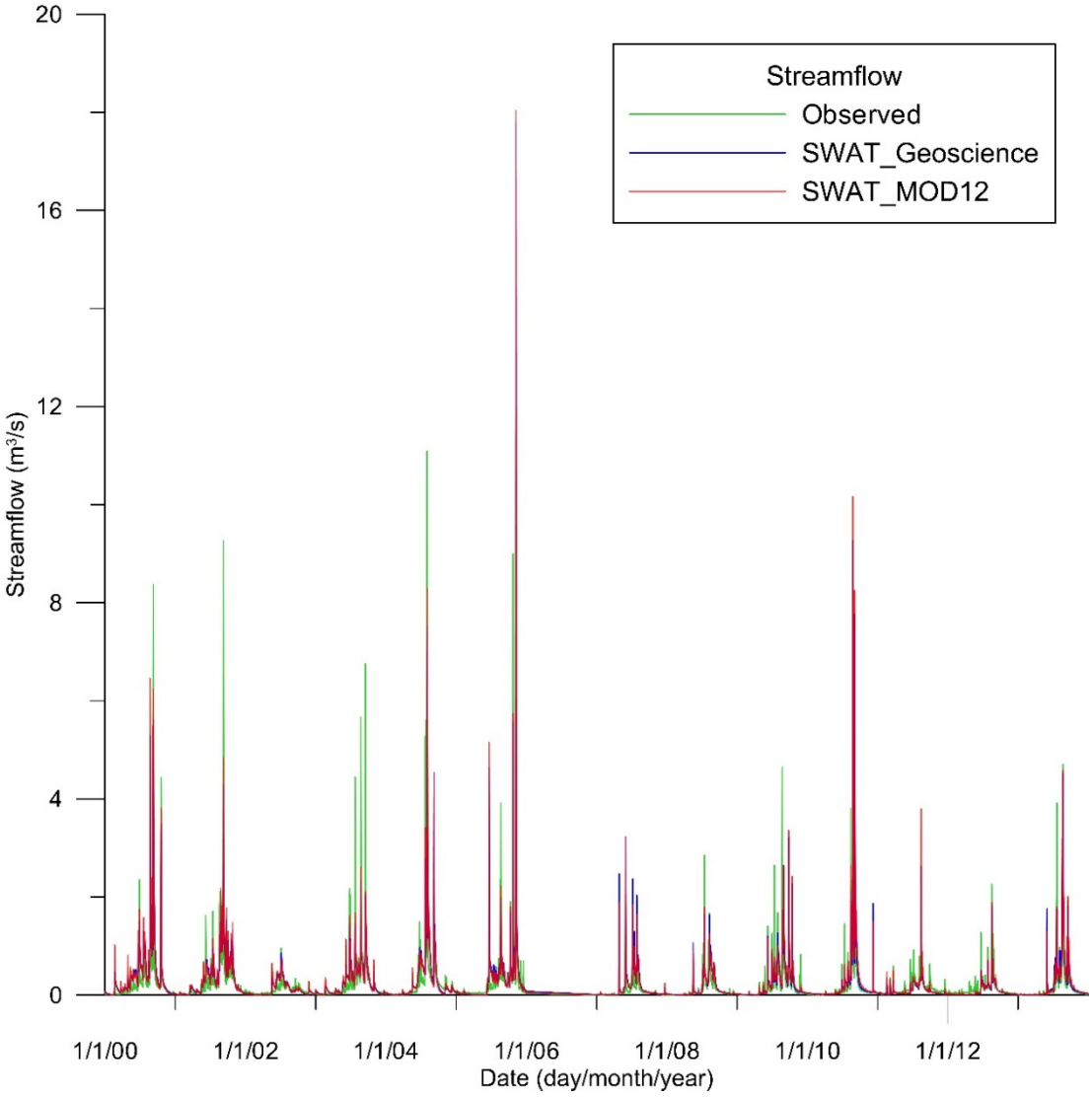

Figure 12: Streamflow calibration (2000-2005) and validation (2007-2013)

3.4.2 Sub-catchment scale evapotranspiration

The SWAT ET model is calculated at the HRU scale (Fig. 13a and 13b), however for direct comparison with the MOD16 ET (Fig. 13c), the HRU ET results were reprocessed into 1 km^2 cells using simple averaging. For cells on the boundary, which do not aggregate up to the 1 km^2 resolution, a percentage weighting based on the area covered is applied. Figure (13d) shows the mean annual difference between both SWAT models (the SWAT model with Geoscience land cover as SWATGEO and the SWAT model with MOD12 land cover as SWATMOD12) over the validation period at the 1 km^2 spatial resolution. The SWATMOD12 and the MOD16 maps (Fig. 13b and 13c) can be seen to show some spatial resemblance in the north, south, east and west corners of the catchment principally due to the use of the MOD12 map in both models. Generally, a trend of higher ET in the north-east and central part of the catchment is seen while lower ET is observed in the south-western parts of the catchment. The spatially distributed mean annual ET difference of the SWAT models compared to the MOD16 show about 40% of the catchment with a difference of ±100 mm/year at the 1 km^2 spatial scale. Clear spatial difference between the SWAT models are seen at the HRU scale but at the 1 km^2 resolution, the maximum mean annual difference between the SWAT models is 12%.

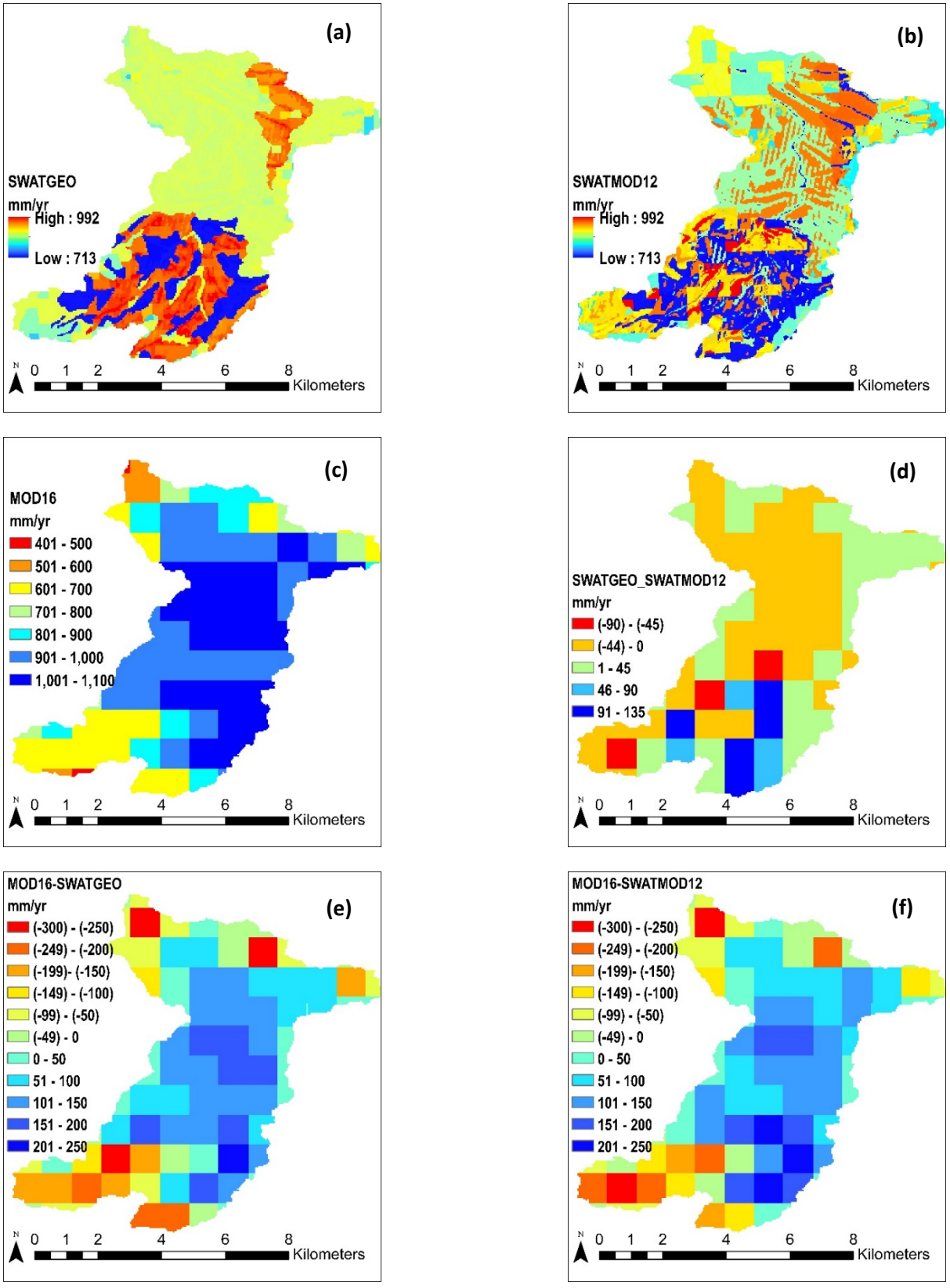

Figure 13: (a) HRU scale SWATGEO mean ET (2007-2013); (b) HRU scale SWATMOD12 mean ET (2007-2013; (c) 1 km² grid MOD16 mean ET (2007-2013); (d) Mean difference between SWATGEO and SWATMOD12 for corresponding 1 km² grid cells (2007-2013); (e) Mean difference between MOD16 and SWATGEO for corresponding 1 km² grid cells (2007-2013); (f) Mean difference between MOD16 and SWATMOD12 for corresponding 1 km² grid cells (2007-2013)

Further analyses were carried out to determine the effect of spatial aggregation on the correspondence between the ET methods. For the spatial aggregation analysis, the SWATGEO model was used due to its improved land cover accuracy based on field knowledge. The box and whisker plot in Fig. (14) shows the spread of the difference between the SWAT ET and the MOD16, with the bottom, middle and top of the box indicating the 25th, 50th and 75th quartiles of the distribution. The lowest and highest bars in the plot indicate the minimum and maximum differences between the ET products at the different spatial scales. Figure 14 shows that with increasing cell aggregation the difference in the ET between SWAT and MOD16 decreases. At 1 km^2, 4 km^2, 9 km^2, 16 km^2 and 25 km^2 the maximum cell difference between the SWAT and MOD16 ET are 31%, 19%, 15%, 11% and 9% respectively.

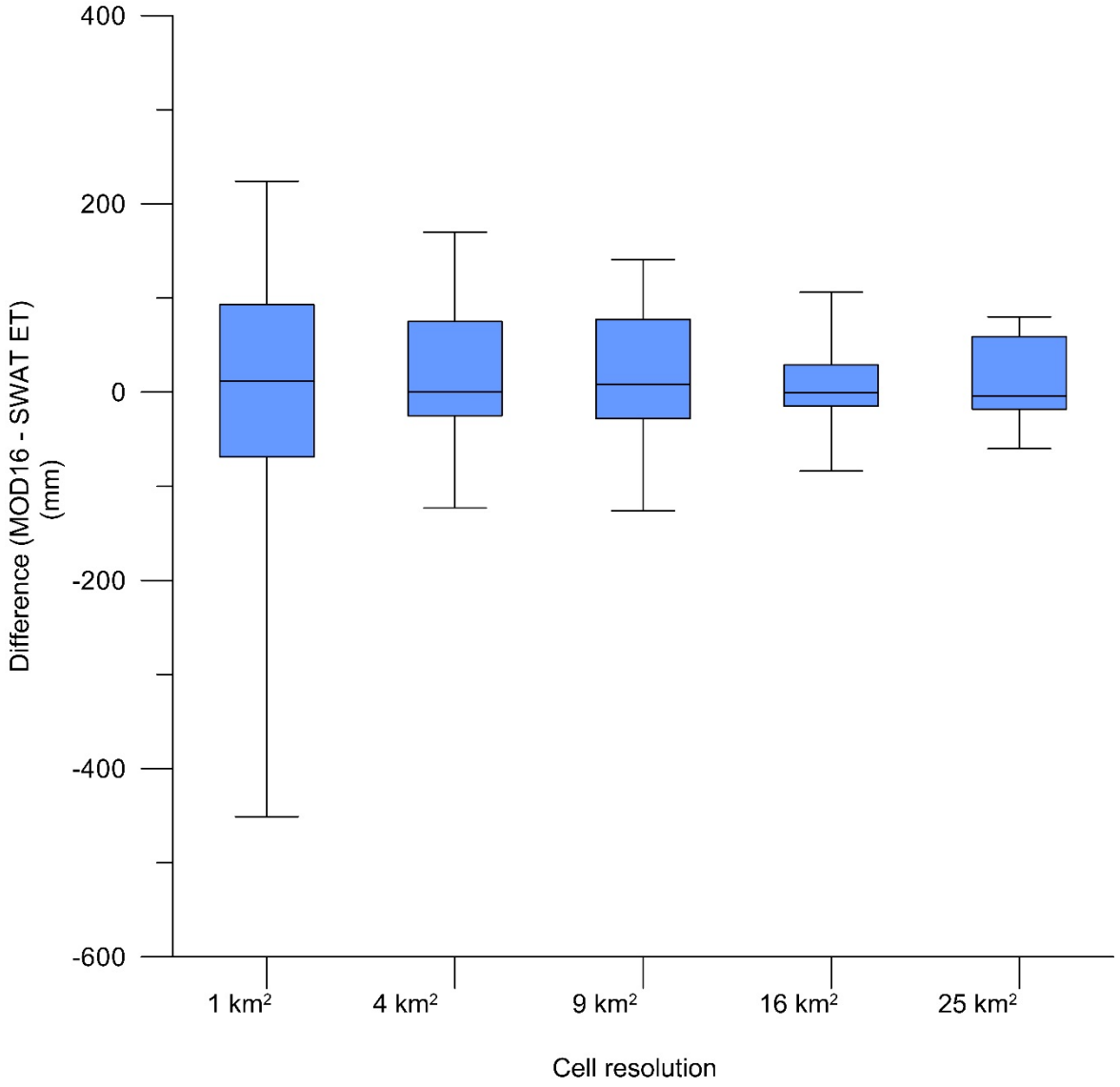

Figure 14: Differences between SWATGEO ET and MOD16 for spatial aggregations between 1 and 25 km². The bottom, middle and top of the whisker indicate the 25th, 50th and 75th quartiles of the distribution, the lowest and highest bars indicate the minimum and maximum differences.

The grand variances for the monthly data of the three models were calculated and partitioned into the spatial and temporal components at the 1 km^2, 4 km^2, 9 km^2, 16 km^2 and 25 km^2 resolutions (Table 8) using the Time-First formulation described in Sun et al. (2010). The partitioning presents the average of the temporal variances for each of the regions in the catchment as the temporal component and the spatial variance of the evapotranspiration as the spatial component. The result shows the spatial component consistently higher across the three models. The partitioning shows that at the finer resolution the variance in the evapotranspiration in the models are principally associated with the spatial component but the temporal component of the variance increases with spatial aggregation.

Table 8: Variance partitioning into space and time components at various spatial resolutions

Spatial Resolution	**Model**	**Spatial Component in mm^2 (%)**	**Temporal Component in mm^2 (%)**
1 km^2	SWATMOD12	74.4 (80.9)	17.6 (19.1)
	SWATGEO	75.5 (80.6)	18.2 (19.4)
	MOD16	82.5 (84.9)	14.7 (15.1)
4 km^2	SWATMOD12	239.9 (79.8)	60.6 (20.2)
	SWATGEO	241.1 (79.4)	62.72 (20.6)
	MOD16	265.0 (84.04)	50.34 (16.0)
9 km^2	SWATMOD12	434.4 (77.7)	124.9 (22.3)
	SWATGEO	434.8 (77.2)	128.4 (22.8)
	MOD16	479.2 (82.0)	105.1 (18.0)
16 km^2	SWATMOD12	586.2 (74.8)	198.0 (25.2)
	SWATGEO	590.7 (74.3)	204.8 (25.7)
	MOD16	637.3 (80)	159.4 (20)
25 km^2	SWATMOD12	665.9 (68.3)	308.7 (31.7)
	SWATGEO	669.9 (67.6)	320.6 (32.4)
	MOD16	738.8 (73.5)	266.4 (26.5)

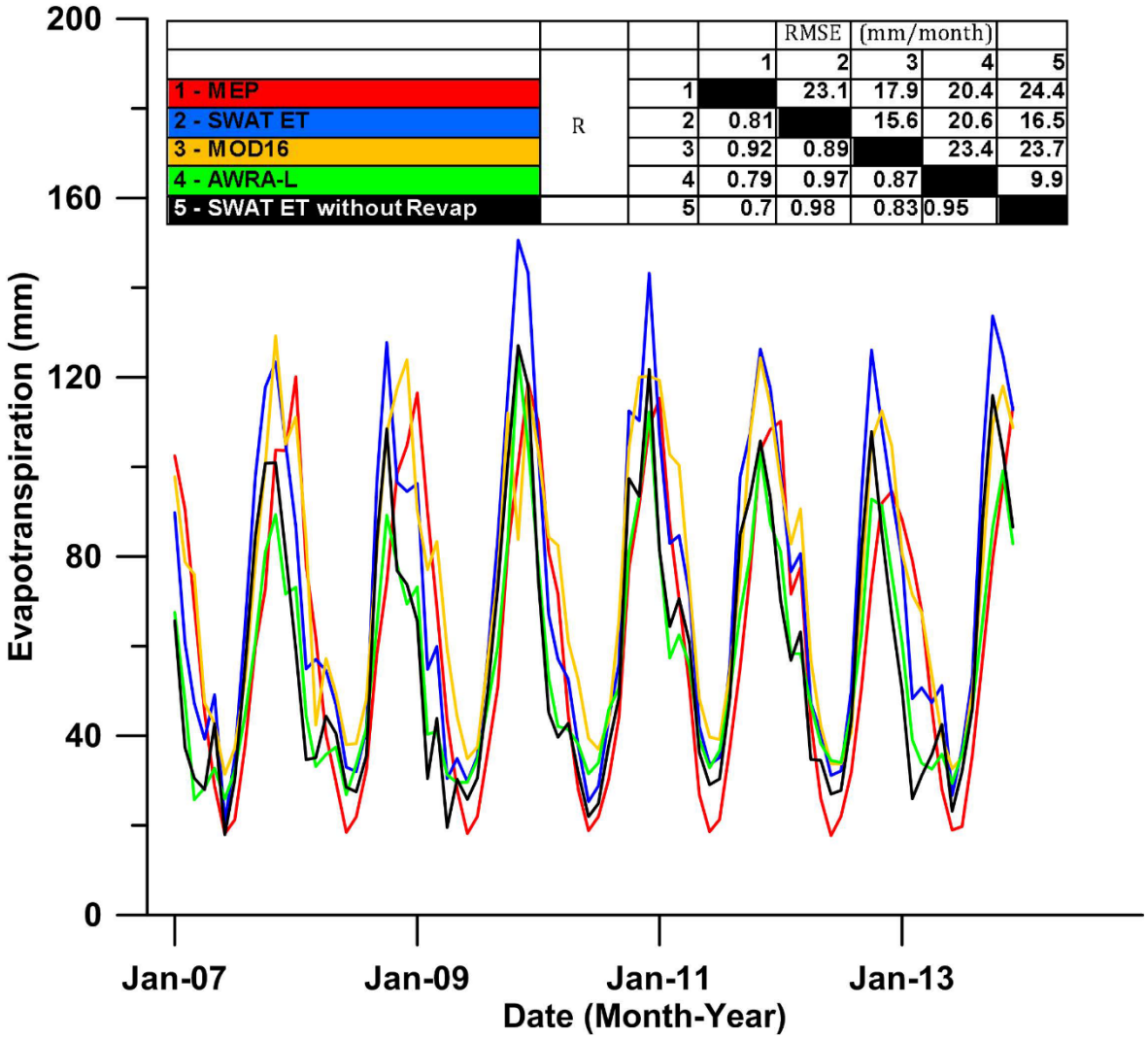

Figure 15: Monthly Comparison of MEP, SWAT, AWRA-L and MOD16 at Catchment scale

3.4.3 Spatial Aggregation

The mean annual graduated spatial scale analysis across the SWAT models and the MOD16 for 2007-2013 exhibits a wide spread at the 1 km^2 spatial resolution with a maximum cell difference of 31%. When the data was aggregated to 4 km^2 using the simple averaging method, the maximum difference reduced to an acceptable 19%. Further aggregation to 9 km^2 reduced the maximum difference by a further 4% but also sees a significant degradation in the resolution of the evapotranspiration data. Table (8) also shows the impact of the spatial aggregation on the variance of the monthly ET data across the SWAT and MOD16 models. It is observed that the

aggregation from 1 km^2 to 4 km^2 altered the percentage variance between the spatial and temporal by about 1% across the three models but beyond the 4 km^2 resolution the spatial component of the variance which accounts for the larger portion of the variance begins to degrade further. Hence our finest resolution spatial scale of confidence for catchment scale ET analysis is the 4 km^2 resolution based on the comparison of the SWAT and MOD16 ET over a complex terrain. This result is supported by the findings of Tang et al. (2015) which found that MOD16 performed better at coarser resolutions. The differences between regions in the catchment are more significant at finer spatial resolutions due to the diverse input data and their associated errors, these impacts become less significant as the outputs are up-scaled (Fig. 14). This trend was also observed by Hong et al. (2009). The simple averaging method was preferred in this study over the bilinear, cubic and other methods as the simple averaging method has been observed to be the best in flux aggregation after a study of various methods (Ershadi et al., 2013).

3.4.4 Catchment Scale Evapotranspiration

At catchment scale, the mean annual ET from the MEP, SWAT, AWRA-L and MOD16 models for the period of 2007 – 2013 are 744, 873, 680 and 897 mm respectively. The highest correlations occur between the hydrological models and the energy balance based models (Fig 15). This may be related to the use of precipitation data and net radiation data as major constraints in hydrological and energy balance models respectively. The use of the same land cover product in the MOD16 and SWAT models are thought to contribute to good agreement.

To compare the temporal dynamics of the MEP, MOD16, SWAT ET and the AWRA-L ET, the data were aggregated to catchment scale. As both SWAT models tend towards unity at the catchment scale with less than 1% difference in their annual mean ET, only the SWATGEO model is evaluated at catchment scale as the more accurate model to keep with the philosophy of the study.

Monthly MOD16 ET, MEP and AWRA-L ET values were averaged to catchment scale values using the spatial analyst tools in ArcGIS, while ET values from the validated SWAT model on catchment spatial extent and daily timescales were aggregated to monthly timescales. Using the R_{MSE} and R metrics the analysis shows a good correspondence between all the models (Fig. 15). The mean ET from the MEP model is within 20% of the other three models while all models are within a 25% range. The agreement in the ET results from the four models gives some confidence regarding the estimation in the complex terrain catchment, considering the error range observed in some ground-based measurements approach 30% (Liu et al., 2013).

3.4.4.1 Seasonal Trends

Table 9: Seasonal ET trend across the models

	MOD16 (mm)	AWRA (mm)	MEP ET (mm)	SWAT ET (mm)
Summer	296	209	299	274
Autumn	182	117	142	155
Winter	122	110	74	114
Spring	297	243	220	330

The four methods perform differently seasonally with the MOD16 having the highest mean ET estimate in the summer months while the MEP predicts the lowest ET in the winter months (Fig. 15). Although the MEP predicts the lowest ET in the winter months, its correlation with the three models is high with a minimum of 0.91 across the models when statistically analysed. The seasonal trend of the MEP also appears the most realistic with highest ET recorded in the summer, followed by the spring growing season, then the autumn when leaves fall and lastly the winter season (Table 9). The MOD16 calculates similar ET across the summer and spring seasons, with lower ET in the autumn and winter. The SWAT and AWRA-L water balance driven models estimate highest ET in the spring season followed by the summer season. This seems less plausible as the study area is classified as an evergreen broadleaved forested catchment with shallow groundwater suggesting that availability of moisture thus making solar radiation a principal driver of ET. The solar radiation in the summer months is usually significantly higher than other seasons making the MEP seasonal trend more agreeable.

3.4.5 Sources of differences across the four models

The possible principal sources of differences between the four ET methods are associated with specific humidity in the MEP, land cover, the Revap component in SWAT and the HRU parameterization in the AWRA-L; they are discussed in the following sections.

3.4.5.1 Specific humidity in the MEP

The MEP model is very dependent on the accuracy of the specific humidity data to effectively determine transpiration over the canopy. The specific humidity over the leaf surface is not always equal to the that in the stomatal cavity (Wang and Bras, 2011). A model parameter η_s is proposed to constrain the specific humidity depending on the environment (see Appendix A). The parameter η_s represents the opening and closing of the

stomatal cavity where complete closure is equivalent to 0 and totally opened cavity corresponds to 1. As the sixth creek catchment study area is underlain by a shallow aquifer, η_s is assumed to be equal to 1. Nevertheless, the study period encompasses the "millennium drought period", which may have some effect on the complete openness of the stomatal cavity even in the evergreen broadleaved forest. The analysis of the effect of drought on the degree of openness of the stomatal cavity for this specific catchment is however beyond the scope of this study.

3.4.5.2 Land Cover

The land cover is an important parameter in the MOD16 and SWAT ET algorithms as it determines the values allocated to biophysical properties such as leaf conductance and boundary layer resistance, which significantly impact ET calculations. The impact of the land cover on the SWAT models is evident from the spatially divergent high-resolution SWAT models (Fig. 13a and b), at the HRU scale, though the streamflow calibration and validation parameters and results were similar. With the spatial aggregation of the SWAT models to 1 km^2 resolution, the obvious spatial differences at the HRU scale reduces significantly and begins to disappear beyond the 1 km^2 resolution. Differences in the land cover in the SWAT models were responsible for the difference spatial distribution of the ET across the catchment between the models. The effect of the land cover on the MOD16 was not evaluated, however, the SWATMOD12 model with the same land cover expectedly showed better agreement when compared with the MOD16 with mean for the period of 2007-2013 within 1 mm at the catchment scale. The Geoscience Land cover map has 95% percent forests, while the MOD12 has a classification of 67% forests and 24% woody savanna, with most of the region misclassified as woody savanna having some similar properties of the forests. At catchment scale, the data averaging contributes to the convergence of the MOD16 and SWAT ET results albeit with closer agreement between the MOD16 and SWATMOD12, which share land cover.

3.4.5.3 Revap

The Revap component of the AET in SWAT is mostly significant in forested catchments with deep rooted trees that can access the saturated zone and as such are governed by land use parameters (Neitsch et al., 2011). However, the relative accuracy of the Revap component of the ET on HRU scales has been questioned (Liu et al., 2015) due to the linear relationship between the Revap coefficient and potential evapotranspiration in SWAT (see Eqn. B23). The Revap component in this study appears consistent with the studies by Benyon et al. (2006) in south-eastern

Australia with similar climatic condition as the Sixth Creek Catchment. Benyon et al. (2006) observed that under the combined conditions of highly permeable soils, available groundwater resources of low salinity (<2000 mg/L), a high transmissivity aquifer and groundwater of depths up to 6 m, annual groundwater ET contribution to total ET ranged from 13 – 72% for sampled Eucalyptus tree species. The Sixth Creek Catchment is principally underlain by the highly transmissive and permeable Aldgate Sandstone aquifer, with salinity levels well below 2000 mg/L (Gerges, 1999). Monitoring bores in the Sixth Creek Catchment have recorded standing water levels of less than 1.5 metres at the end of the rainy winter months in parts of the catchment. The Sixth Creek Catchment has been identified as one of the principal recharge zones in the Western Mount Lofty Ranges based on the catchment geology and hydrochemical analysis (Green and Zulfic, 2008). A significant portion of the 95% forested part of the Sixth Creek Catchment is a mosaic of various Eucalyptus tree species, thereby corroborating the results of Benyon et al. (2006). However, the seasonal partitioning of the Revap component is questionable. The AWRA-L ET model does not appear to include a separate groundwater ET model in its algorithm such as is found in the SWAT model (B23-26), hence the correlation and strong agreement between the AWRA-L models when the Revap is unaccounted for in the SWAT ET. The results suggest the Revap is a significant contributor to ET in the Sixth Creek Catchment (Fig. 16) with mean annual contribution of 20% for the years 2007 – 2013, while monthly contributions ranged from 15 – 52 % over the same period. The possibility exists that the linear relationship with PET employed in its calculation on HRU scale may be contributory to the higher range of ET fluctuation seen in the SWAT model on the 1 km^2 scale when compared to the MOD16, however, that is beyond the scope of this study.

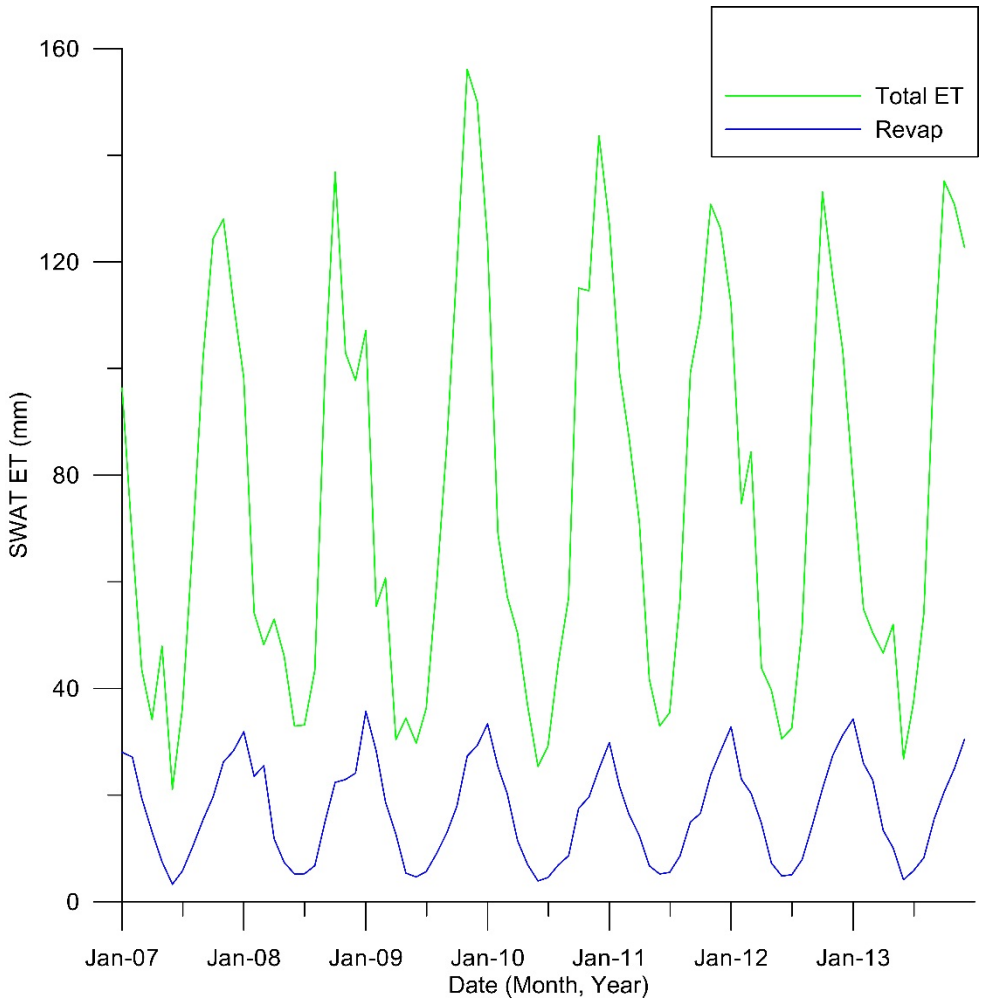

Figure 16: Monthly comparison of Revap component of the ET and total ET in SWAT.

On catchment scale, the results show that MOD16 simulates higher ET in the winter periods while SWAT simulates higher ET during the summer periods (Fig. 15). Generally, the agreement between the products is more consistent during the winter seasons when ET is lower. The lesser correlation during higher ET seasons may be related to the linearly determined Revap component of the ET, which is a more dominant process in the summer months when the demand for soil evaporation, plant transpiration and groundwater ET is significantly higher.

3.4.5.4 HRU parameterization in AWRA-L

The HRU parameterization method in AWRA-L significantly impacts the evapotranspiration modelling process. While the AWRA-L does not use a robust land cover product that distinguishes between vegetation including trees, it uses a fraction of tree cover product to parameterise the HRU. AWRA-L discretises each 25 km^2 grid cell into two HRU's; the shallow-rooted HRU and the deep-rooted HRU. The determination of the area of the grid

apportioned as deep-rooted and shallow rooted HRU are solely based on the satellite derived product of the persistent and recurrent photosynthetically active absorbed radiation (fPAR) from the Advanced Very High Resolution Radiometer (AVHRR) (Donohue et al., 2008). The fraction of the persistent fPAR is regarded as the fraction of tree cover, hence it is used as the fraction of the deep-rooted HRU in each grid cell. The Sixth Creek Catchment has an average of under 60% persistent fPAR according to the AVHRR fPAR product. The discretisation of the AWRA-L HRU in the Sixth Creek catchment which suggests only about 60% tree cover in the Sixth Creek Catchment severely limits the access of the model to groundwater ET computation in the catchment, hence the close correlation and agreement of the AWRA-L model with the SWAT model when the Revap (groundwater ET) is unaccounted for is reasonable.

3.4.5.5 Input data Challenges

The four methods have challenges associated with input data, which are subsequently propagated through the algorithms. The remote sensing based MOD16 have cloud cover challenges affecting input parameters. The MEP, SWAT and AWRA-L models use interpolated spatial data, which includes rainfall data specific to the SWAT and AWRA-L. These datasets have inherent uncertainties associated with them. For instance in semi-arid environments such as the Sixth Creek Catchment, high intensity rainfall events are common occurrences, which impacts hydrologic processes such as infiltration and evapotranspiration differently from if the precipitation were evenly distributed through the day (Syed et al., 2003). Yang et al. (2016) observed that the use of hourly rainfall in SWAT significantly improved the modelling of streamflow and hydrological processes. In this study, due to the unavailability of hourly precipitation data, daily precipitation data were used thus neglecting the impact of high intensity precipitation events in the catchment.

Another challenge encountered with the SWAT model is associated with the semi-distributed model methodology. The use of a single value for wind speed, relative humidity and solar radiation for a sub-catchment with spatial scale, which could be in the order of tens of square kilometres, affects the accuracy of hydrological processes at the HRU scale. The “elevation band” method of temperature and precipitation distribution with respect to elevation changes across a catchment was introduced into the SWAT algorithm to attenuate orographic effects in complex terrain catchments (Neitsch et al., 2011). The elevation band algorithm in SWAT has performed well in predominantly snowy, complex terrain catchments, which are significantly larger than the Sixth Creek Catchment with elevation changes in the order of kilometres (Abbaspour et al., 2007, Zhang et al., 2008b, Pradhanang et al.,

2011). However, the application of the elevation band algorithm in the non-snowy Odiel River basin (Spain) with Mediterranean climate similar to the Sixth Creek Catchment yielded less than satisfactory results (Galván et al., 2014). In the non-snowy Sixth Creek Catchment, the orographic effects are a dominant atmospheric process when winds are moving from the lower elevations in the north of the catchment to the higher elevations in the South particularly during the winter months. The orographic lift leads to significantly higher precipitation in the south-westerly direction in the Sixth Creek Catchment, which the elevation band algorithm in SWAT does not represent accurately in non-snowy catchments.

The various meteorological and remote sensing input data used in the processing of the MOD16 all have their inherent uncertainties, with cloud cover challenges and coarse resolution resampling (Mu et al., 2011a), while errors have been associated with the land cover product used (Ruhoff et al., 2013). The land cover map (MOD12) used in MOD16 (Fig. 11a), in conjunction with the calibrated biome properties lookup table (BPLUT) significantly influences the ET output from the various land covers under different climatic conditions. A more detailed map and local knowledge of the Sixth Creek Catchment indicates that the MOD12 land cover spatially mismatches some biomes (Fig. 11a and b). Besides the obvious land cover mismatches that were observed between the input data of the two models, the variety of accepted national, regional and global land cover classification system contributes to the challenges of hydrological modelling. In this MOD12, the “mixed forest” category covered over 50% of the catchment while the category does not exist in the local field map land cover classification. The global standardization and harmonization of land cover maps and biome classification at high resolution may improve model performance.

3.5 Conclusion

The main objectives of this paper are to compare the four ET products (MEP, SWAT, MOD16 and AWRA-L) on catchment scale to evaluate their relatively accuracy particularly the performance of the newer MEP against conventional methods, while also evaluating the two finer resolution products (SWAT and MOD16) on graduated spatial scale. We also attempted to determine the spatial scale at which the models tend towards agreement. While also seeking to understand the sources of disagreements between the models.

The four models could simulate ET to within a 25% difference range. The mean annual ET agreement across the models produced using different algorithms suggests that all four models have the capacity to estimate ET in the

complex terrain catchment. Although the terrain of the catchment is complex, the MEP, which does not parameterise the slope of the study area, was able to effectively model the catchment ET. Nevertheless, the models exhibited seasonal differences with the MEP model predicting plausible seasonal trends in the catchment, while the SWAT and AWRA-L appeared to underestimate in the summer and/or overestimate in the spring season.

The calibrated SWAT model using the SUFI-2 algorithm and various objective functions could simulate ET to within 6% of the MOD16 on catchment scale, annually. The P and R factors metrics were observed to be very reliable indicators of a good calibration exercise. Abbaspour (2007) proposed P and R factor minimum benchmarks of >0.7 and <1 respectively for streamflow calibration, in this study the P and R factors >0.8 and <1 were found to produce reliable ET estimates on catchment scales. We observed that at a spatial scale of 4 km^2 we obtained cell differences of under 20% annually which gave confidence to our study in the complex terrain that the 4 km^2 spatial resolution is our "spatial scale of confidence". The result of the spatial resolution analysis corroborates the view that prevailing ET algorithms and measurement methods will have certain degree of variability due to the complexity of ET estimation and various drivers of the contributory processes. The study shows that correlation at catchment scale does not necessarily translate to correlation at finer spatial scales. However, our study shows that as ET is aggregated to a spatial scale of 4km^2 and beyond, the results converge.

At the catchment scale, the MEP and MOD16 energy balance models had very good agreement as well as the SWAT and the AWRA-L models. These agreements could be attributed to the solar radiation and precipitation as dominant drivers of the energy balance and water balance models respectively. Biome differences and input spatial scale contribute to poor agreement at finer spatial scales. The challenge of the lack of a globally accepted and harmonised land cover classification system at high resolution was encountered in the study, with two products derived from the MODIS satellite data classifying land cover differently and thus impacting the results from the SWAT models. The use of different land covers with different classification systems and parameters are observed to have limited impact on evapotranspiration modelling at coarse spatial resolutions due to spatial averaging. Nevertheless, the tree cover fraction used in place of a land cover product in the AWRA-L is also observed to impact the ET modelling, particularly in a groundwater dependent catchment like our study area. The inherent differences and uncertainties associated with these land cover products will continue to be propagated through the models, thereby promoting divergence in the drive towards more accurate and finer resolution evapotranspiration data products. While many concerted research efforts have been made in the past (Latham, 2009, Friedl et al., 2010), a globally accepted harmonised world land cover database at high resolution can significantly improve correlation and confidence in high resolution ET products. It is however refreshing that the MEP model can predict

ET at the catchment scale effectively and does not suffer from the land cover challenges which plagues the SWAT and MOD16.

4 A Maximum Entropy Production Evaporation - Transpiration Product for Australia

Manuscript 3 in review for Earth System Sciences Data

Olanrewaju Abiodun[1], Okke Batelaan[1] Huade Guan[1], and Jingfeng Wang[2]

1 National Centre for Groundwater Research and Training, College of Science and Engineering, Flinders University, Australia

2 School of Civil and Environmental Engineering, Georgia Institute of Technology, Atlanta, USA

Corresponding author:

Olanrewaju Abiodun, College of Science and Engineering, Flinders University, Bedford Park, Australia, lanre.abiodun@flinders.edu.au

Abstract

The aim of this research is to develop evaporation and transpiration products for Australia based on the maximum entropy production model (MEP). We introduce a method into the MEP algorithm of estimating the required model parameters over the entire Australia through the use of pedotransfer function, soil properties and remotely sensed soil moisture data. Our algorithm calculates the evaporation and transpiration over Australia on daily timescales at the 5 km^2 resolution for 2003 – 2013.

The MEP evapotranspiration (ET) estimates are validated using observed ET data from 20 Eddy Covariance (EC) flux towers across 8 land cover types in Australia. We also compare the MEP ET at the EC flux towers with two other ET products over Australia; MOD16 and AWRA-L products. The MEP model outperforms the MOD16 and AWRA-L across the 20 EC flux sites, with average root mean square errors (RMSE), 8.21, 9.87 and 9.22 mm/8 days respectively. The average mean absolute error (MAE) for the MEP, MOD16 and AWRA-L are 6.21, 7.29 and 6.52 mm/8 days, the average correlations are 0.64, 0.57 and 0.61, respectively. The percentage Bias of the MEP ET was within 20% of the observed ET at 12 of the 20 EC flux sites while the MOD16 and AWRA-L ET were within 20% of the observed ET at 4 and 10 sites respectively. Our analysis shows that evaporation and transpiration contribute 38% and 62%, respectively, to the total ET across the study period which includes a significant part of the "millennium drought" period (2003 – 2010) in Australia.

Keywords: Evaporation; transpiration; Maximum Entropy Production; remote sensing

4.1 Introduction

The use of remote sensing data in existing and new methods for evapotranspiration (ET) estimation is incontrovertibly the current and future trend of ET flux quantification on catchment, regional and continental scales (Bhattarai et al., 2016, Zhang et al., 2016, Najmaddin et al., 2017). The use of remote sensing observations is an unprecedented advancement in regional scale ET estimation due to its spatiotemporal flexibility and/or economic viability (Chirouze et al., 2014, Long et al., 2014, Xiong et al., 2014, Yang et al., 2015, Bhattarai et al., 2016). Various methods have been developed for improving ET estimates (Allen et al., 2007, Cleugh et al., 2007b, Mu et al., 2011b, Xiong et al., 2014, Tang et al., 2009). However, the relative accuracy of these methods differ across different climates, vegetation and soil types (Jia et al., 2012, Kim et al., 2012b, Velpuri et al., 2013, Bhattarai et al., 2016). The performance of the ET models depends on the parameterization of physical processes underlying ET (Liaqat and Choi, 2017). A major challenge is to produce accurate ET estimates of various spatial and temporal resolutions (Senay et al., 2013, Wang et al., 2016, Gaur et al., 2017) when using remote sensing data (Kalma et al. (2008).

A remote sensing based ET model is empirical or physically-based (Xiong et al., 2014). In the past two decades, several physically based ET models have been developed including the single source energy balance (SSEB) (Bastiaanssen et al., 1998b, Roerink et al., 2000, Allen et al., 2007) and two-source surface energy balance (TSEB) (Kustas and Norman, 1999, Norman et al., 2003, Sun et al., 2009) models using remote sensing input data. The SSEB models provide total ET without partitioning it into soil evaporation (E) and transpiration (T), while the TSEB models do the partition. The TSEB models have been shown to be more accurate over partially vegetated surfaces (Timmermans et al., 2007, Gao and Long, 2008, Choi et al., 2009). A fundamental challenge of TSEB models is their reliance on land surface temperature (LST) and the partitioning methodology of the LST into soil and canopy temperature components for modelling (Colaizzi et al., 2012, Yang et al., 2018). Different techniques have been applied to partition the canopy and soil temperatures from the LST in the TSEB models (Norman et al., 2000, Zhang et al., 2005), with varying degree of success over different vegetation types (Chavez et al., 2009, Song et al., 2016, Diarra et al., 2017). The more pertinent challenge of the TSEB models becomes apparent when creating high resolution regional to continental scale ET, which requires accurate LST data as the principal input.

Frequent clouds plague remotely sensed LST products such as the widely accepted Moderate Resolution Imaging Spectroradiometer land surface temperature product (MODIS LST) (Wan et al., 2002).

The limitations of the LST dependence of the traditional TSEB models was further highlighted by Mu et al. (2007) who found that the use of the 8-day composite of all cloud free data in the MODIS LST suite did not produce accurate estimates of global scale evapotranspiration. The MODIS LST yielded erroneous results of partitioned soil and canopy temperatures across various biomes, hence the development of a new algorithm is needed for estimating soil and canopy temperatures for improving the MODIS ET product (MOD16), which is widely accepted for comparison and validation purposes on catchment to continental scales. There are, however, unresolved issues of accuracy (Tang et al., 2015, de Arruda Souza et al., 2018, Khan et al., 2018). With the challenge surrounding the LST partitioning in TSEB models and the MOD16 challenges, a different perspective to the TSEB modelling on regional scale is required.

The Maximum Entropy Production (MEP) model of ET (Wang and Bras, 2011) is a new approach to modelling ET. The MEP model was formulated as a unique TSEB model for soil and vegetated surface where ET and the other surface heat fluxes result from the partition of net radiation. The MEP model requires three main inputs: surface temperature, specific humidity and net radiation. A major departure of the MEP model from the traditional TSEB models is that the MEP model is less sensitive to temperature and more sensitive to the moisture content of immediately above the target surface and the available energy.

Case studies have shown that the MEP ET for small catchments outperformed several other models (Nearing et al., 2012, Yang and Wang, 2014, Shanafield et al., 2015). However, the MEP ET model is yet to be comprehensively tested over various vegetation covers. A global product of the MEP ET at a 100 km^2 spatial resolution has been produced (Huang et al., 2017). However, at this scale, individual vegetation cover type validation and analysis is problematic. The ET data over the diverse Australian landscape at catchment to continental scale has been produced by Guerschman et al. (2009) using MODIS surface reflectance data; by Mu et al. (2011b) using MODIS remote sensing data (MOD16); and the Australian Water Resource Assessment Landscape (AWRA-L) model by Viney et al. (2014). To the best knowledge of the authors, there is no dedicated evaporation (E) and/or transpiration (T) product over Australia available in the public domain at moderate to high spatial and temporal resolution.

The goal of this paper is to develop a daily MEP E & T product for Australia on a 0.05° spatial resolution. We have generated the data for 2003 – 2013 for demonstration and testing of result. The skill of the MEP ET model will be evaluated using eddy covariance tower data across various vegetation covers and compared with the results of the MOD16 and the AWRA-L products. The evaluation period covers the climatological highly variable "millennium drought" period (2003-2010).

4.2 Method and data

The energy balance equation over the land surface is expressed as,

$$E + H + G = R_n \tag{18}$$

where E, H, G and R_n are evapotranspiration (W/m^2), sensible heat (W/m^2), ground heat (W/m^2) and net radiation (W/m^2), respectively. The MEP ET model provides a solution of $Es, Hs,$ and G over non-vegetated land surface satisfying the energy balance equation Eq. (18) (Wang and Bras, 2011) for a given net radiation Rn, surface temperature T, and surface specific humidity q,

$$\sigma_S = \frac{\lambda^2}{c_p R_v}\frac{q_s}{T_s^2} \ , \ \beta(\sigma_s) = 6\left(\sqrt{1+\frac{11}{36}\sigma_s} - 1\right) \tag{19}$$

$$G = \frac{\beta(\sigma_S)}{\sigma_S}\frac{I_s}{I_o} H_s|H_s|^{-\frac{1}{6}} \tag{20}$$

$$E_s = \beta(\sigma_s)H_s \tag{21}$$

where σ_s (Sigma) is a dimensionless parameter characterizing the effect of (soil or canopy) surface thermal and moisture state on the phase change of liquid water (-); λ is the latent heat of vaporization of liquid water (J kg^{-1}); c_p is the specific heat of dry air at constant pressure (J kg^{-1} K^{-1}); R_v is the gas constant of water vapor (J kg^{-1} K^{-1}); q_s the specific humidity at the soil or vegetation surface (kg kg^{-1}); T_s is the soil or canopy surface temperatures (K); $\beta(\sigma_s)$ is the inverse Bowen ratio (-); I_s is the thermal inertia of soil (J m^{-2} K^{-1} s$^{-1/2}$); I_o is the thermal inertia of turbulent air (J m^{-2} K^{-1} s$^{-1/2}$). For vegetated land surface where G is neglected, equations (19) – (21) become;

$$E_v = \frac{R_{n\_v}}{1+\sigma_s{}^{-1}} \ , H_v = \frac{R_{n\_v}}{1+\sigma_s} \tag{22}$$

where E_v is the canopy transpiration and H_v sensible heat flux over canopy surface satisfying energy balance equation $R_n = E_v + H_v$.

The MEP ET algorithm calculates soil evaporation and canopy transpiration separately. Total evapotranspiration is the sum of the two fluxes weighted by the fractional coverage of soil and canopy (Fig. 17). In this paper, we apply temporally varying vegetation fraction cover in the algorithm to partition the radiation energy for soil and canopy.

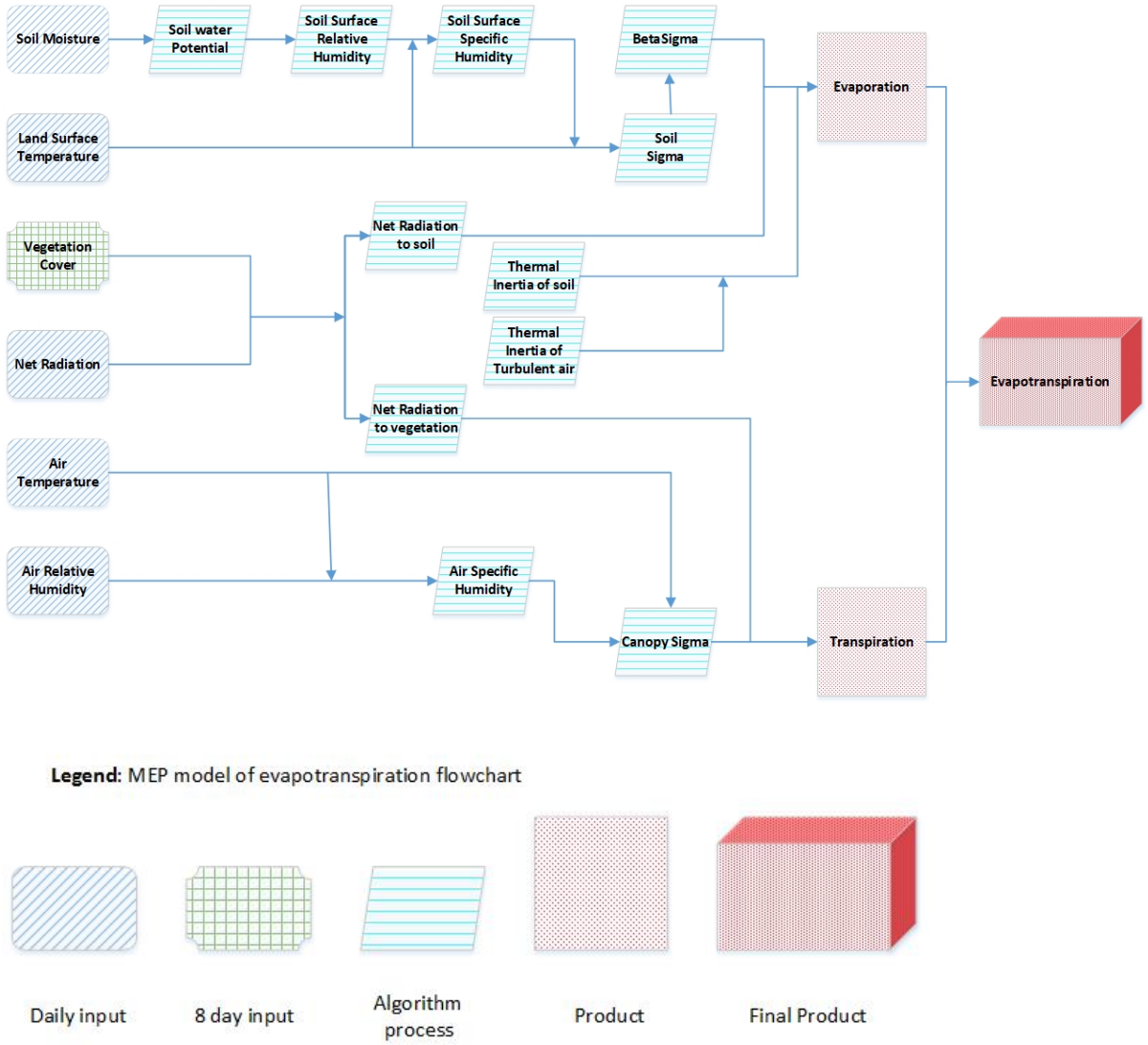

Figure 17: Flowchart of MEP ET algorithm; BetaSigma is the inverse Bowen ratio

4.2.1 Net radiation (R_n)

Daily net radiation at 0.05° spatial resolution over Australia is partitioned between soil and canopy within a grid cell according to vegetation fraction cover. Photosynthetically active radiation (FPAR) product MOD15A2H (Myneni et al., 2015) is used in this study. While the MEP model is very sensitive to net radiation as a model input with pronounced diurnal cycle, 8-day vegetation cover data were used as vegetation cover changes at seasonal time scale. Net radiation over canopy and soil surface within a grid cell is expressed as,

$$R_{n\_v} = F_c\, R_n \;\; , \;\; R_{n\_s} = (1 - F_c)\, R_n \tag{23}$$

where, R_{n_v} is the net radiation over vegetation (W/m^2), R_{n_s} is the net radiation over soil (W/m^2), and F_c is the vegetation fraction (-).

4.2.2 Evaporation

The MEP model as in Eqs. 18, 20 and 21 provides a unique solution of E, G and H for given surface temperature (T_s), soil/canopy surface specific humidity (q_s), and R_{n_s}. The land surface temperature (T_s) is provided by the MOD11C1 product (Wan, 2014) derived from the MODIS observations. The daily data for Australia from 2003 to 2013 was extracted from the global dataset. Missing T_s data, due to cloud cover, were filled using the lowest value within a month for each grid cell. The rationale is that cloud cover reduces the amount of solar radiation reaching the land surface, hence the lowest observed T_s value within a month is used.

Due to the difficulty of obtaining q_s over the entire Australia, an empirical equation is used to calculate q_s as a function of soil surface relative humidity and land surface temperature. The soil surface relative humidity is calculated from the soil surface water potential. The Hutson and Cass function (Hutson and Cass, 1987) is used for estimating soil surface water potential. The Hutson and Cass function requires two empirical coefficients calibrated for each grid cell using two methods: the empirical equation derived in Williams et al. (1992), and the pedotransfer functions to estimate the soil water content at wilting point (-1.5MPa) and at field capacity (-10kPa). The water content at the wilting point and field capacity for each 0.05° grid cell, estimated from the pedotransfer

functions, are subsequently used to determine the coefficients, by applying the two-point method (Cresswell and Paydar, 1996) (see Section 4.2.2.1). Several pedotransfer functions for determining the wilting point and field capacity (Minasny et al., 1999, Minasny and Mcbratney, 2002, Rab et al., 2011) were considered. Eq. 12 and 13 in Rab et al. (2011) were selected due to their minimal data requirement and relative accuracy. The pedotransfer function combined with the two point method was preferred to the empirical equations described in Williams et al. (1992) as they yielded significantly better estimates of ET after validation with flux tower data. Soil properties as the inputs of the pedotransfer functions and empirical equations are obtained from the Australian Soil Resource Information System (ASRIS) (Johnston et al., 2003b).

An important parameter of the MEP model is the distance above target surface for which the Monin-Obukhov similarity theory is valid (z) in the formula of the thermal inertia of turbulent air above soil surface. Huang et al. (2017) suggested that the distance above target (z) vary with the land cover types as shown in the look-up table (Table 10) used in this study. z for each land cover is specified for each 0.05^{o} grid cell using the MODIS land cover product (MOD12C1) (Mark and Damien, 2015) of the same resolution.

Table 10: Distance above target surface (z) in (m) for Australian Land cover

Land Cover	Distance above target (z) in (m)
Evergreen Needleleaf Forests (ENF)	10
Evergreen Broadleaf Forests (EBF)	10
Deciduous Needleleaf Forests (DNF)	10
Deciduous Broadleaf Forests (DBF)	10
Mixed Forests (MF)	10
Closed Shrublands (CSH)	5
Open Shrublands (OSH)	4
Woody Savannas (WSA)	8
Savannas (SAV)	7
Grasslands (GRA)	5
Croplands (CRP)	5
Urban and Built up (URB)	3
Cropland/Natural Vegetation Mosaics (CRV)	5

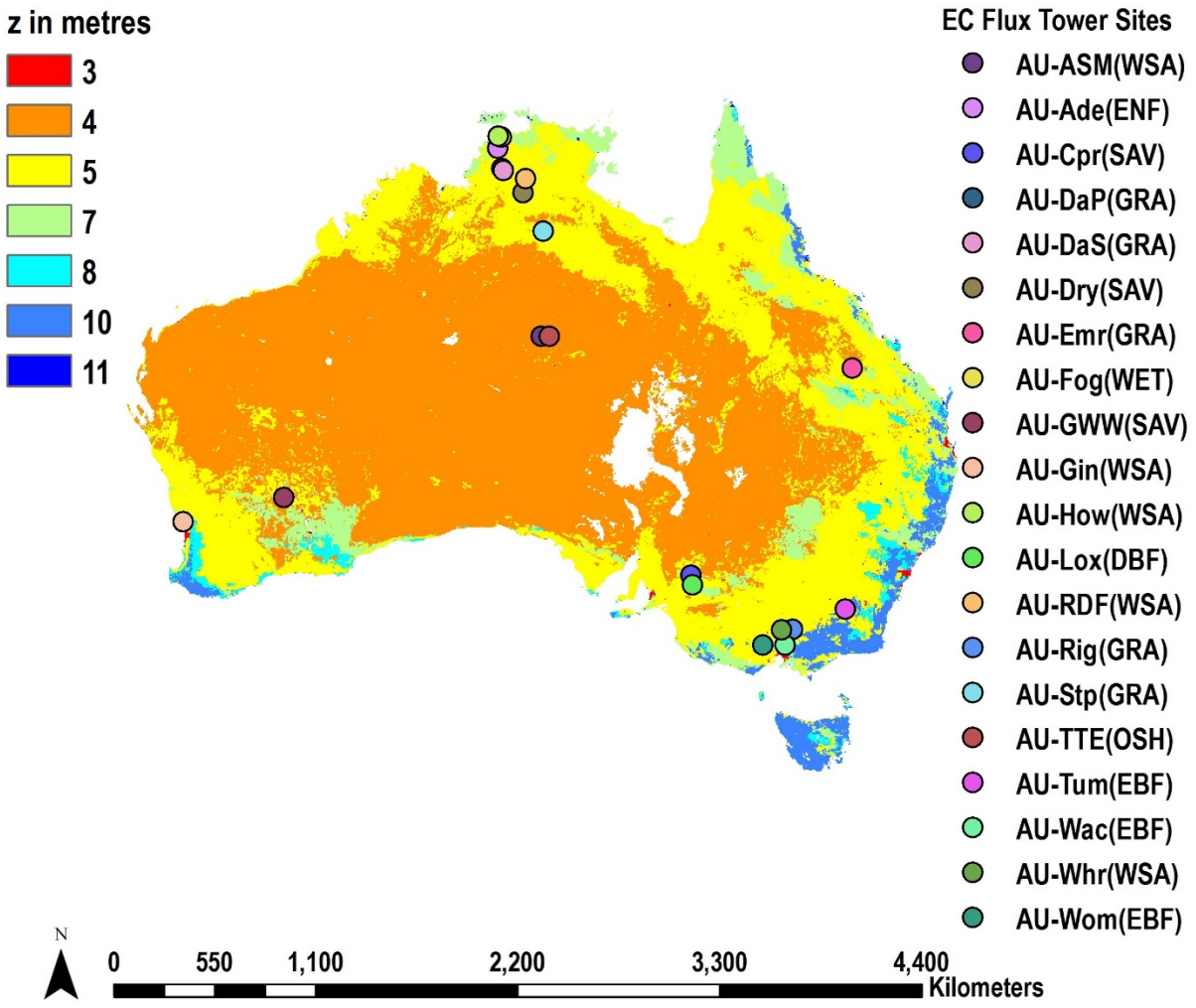

Figure 18: Target height (z) in (m) above vegetation with location of Eddy Covariance flux towers and the land cover types.

4.2.2.1 Hutson and Cass function with the two-point method

To determine the Hutson and Cass coefficients "a" and "b" (Eq. 24) for each 0.05° grid cell across Australia, we solve the pedotransfer with the two-point method. The two values used are the volumetric soil moisture (θ1 and θ2) at the field capacity and the wilting point soil water potentials (Ψ1 and Ψ2) of -10 kPa and 1500 kPa respectively. Combining both equations, we obtain the model parameters "a" and "b" for each 0.05° grid cell.

$$\Psi = a\left(\frac{\theta}{\theta_p}\right)^{-b} \quad (24)$$

$$\theta_p = 1 - (\rho / \rho_s) \quad (25)$$

where Ψ is the soil water potential (kPa); a (kPa) and b (-) are curve-fitting parameters; θ_p (-) is the porosity; ρ (kg/dm^3) is the bulk density of soil; and ρ_s =2.65 (kg/dm^3) is the mineral density.

4.2.2.2 Soil moisture

The soil moisture data used in this study are obtained from the European Space Agency's Climate Change Initiative Soil Moisture Project (ESA CCI SM) at 0.25^{o} and daily resolution available from 1978 to 2018 (Dorigo et al., 2017), hereafter referred to as the ESA CCI SM. The ESA CCI SM consists of three products; Active, Passive and Combined (Liu et al., 2012, Gruber et al., 2017). The ESA CCI SM is preferred in this study as it offers the most suitable spatio-temporal resolution compared to other available soil moisture products. The ESA CCI SM was validated using ground-based soil moisture measurements (Dorigo et al., 2015), while the underlying methodology has been extensively evaluated by Gruber et al. (2019). The combined product is selected in this study as the validation exercise by Dorigo et al. (2015) suggests the combined product outperforms both the active and passive products and also because its algorithm unifies the Active and Passive products to have better spatial coverage than either the Passive or Active products with more stringent quality control. While the combined product has good spatial-temporal resolution for remote sensing applications, missing data are filled through an average of the day before and after. Multiple-days data gaps are filled using multiple-days average. The ESA CCI SM is also resampled at 0.05^{o} resolution to be consistent with the spatial resolutions of the other input data.

4.2.3 Transpiration

The MEP method requires specific humidity and temperature very close to the target surface nevertheless Wang and Bras (2011) experimented with temperature profiles above and below the target surface and determined the use of air temperature as surrogates of leaf surface temperature had negligible effect on the ET measurements. By the MEP method. Hence, due to the difficulty of obtaining leaf surface temperature and specific humidity at regional scales, air temperature and air specific humidity are used as surrogates. Air temperature and relative humidity data above canopy are obtained from the interpolated field observations over Australia (Jeffrey et al., 2001). The Clausius-Clapeyron equation is used in obtaining the specific humidity from air temperature and relative humidity.

4.2.4 Model Evaluation

For the evaluation of the MEP model results over Australia, data from 20 eddy covariance (EC) flux towers across different land covers are used. The model performance is evaluated using six statistical metrics: the root mean square error ($RMSE$), mean difference (MD), mean absolute error (MAE), Pearson's correlation coefficient (R), Nash-Sutcliffe Efficiency (NSE) and Percent Bias ($PBIAS$).

The MEP ET product at 25 km^2 resolution is validated across the 20 EC tower flux data with footprints ranging from 100 m^2 up to about 2 km^2 depending on the measuring height of the EC system and vegetation height. The effects of the differences in footprints of the EC towers and the data to be validated are not considered in this study.

A three-product comparison (MEP, AWRA-L and MOD16) with the field data from the 20 EC flux towers across Australia was conducted as part of this study. While the MEP and the AWRA-L models are produced on daily timescales, the MOD16's highest temporary resolution is an 8-day product. For a direct comparison, MEP and AWRA-L are aggregated to 8-day resolution. Since the MOD16 dataset has missing data points due to cloud cover or sensor failures, the days with missing data are removed across all models and the EC tower data before comparison. While the MEP model could be run with the field data at the EC sites, for a fair comparison of the three products, the Australia wide product for all three products were used in the comparisons.

Mean annual maps are produced for the three products between 2003 and 2013 with the MOD16 resampled to the 25 km^2 resolution to match that of the MEP and AWRA-L data for direct comparison for 280,000 pixels covering the entire Australian using the R, RMSE, MAE and NSE statistical metrics.

4.3 Results and discussion

4.3.1 Mean spatial-temporal MEP ET Analysis

The daily MEP evaporation and transpiration over Australia for 2003 – 2013 are relatively high in the northern vegetated parts of Australia (Fig. 19a and 19b) and around the eastern coastline (Fig. 19b). Evaporation and

transpiration account for 38% and 62% of total ET, respectively, over Australia. ET is highest in the high rainfall shrub-lands and forested regions in the northern Australia as well as around the coastline (Fig. 19c). The west central parts of Australia have the lowest ET with mean annual ET 440 mm for Australia for 2003-2013, while the mean ET along the coastline exceeds 1000 mm for the same period.

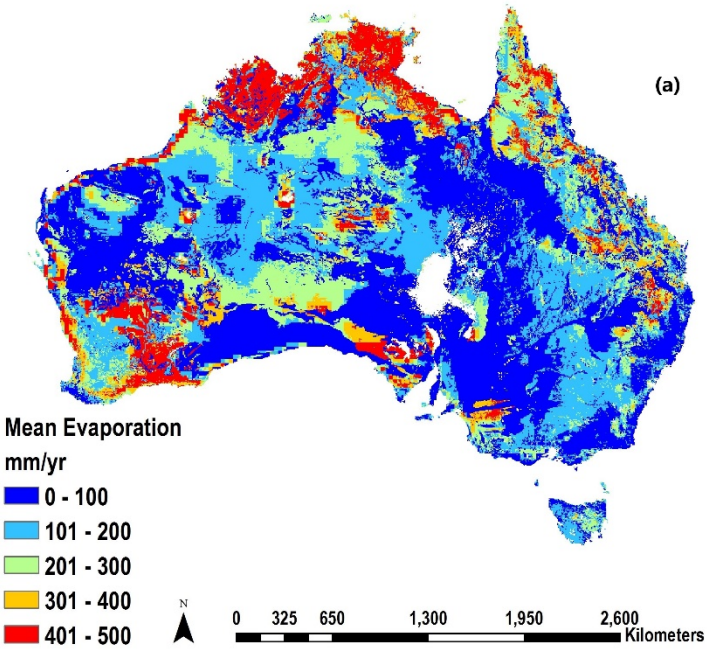

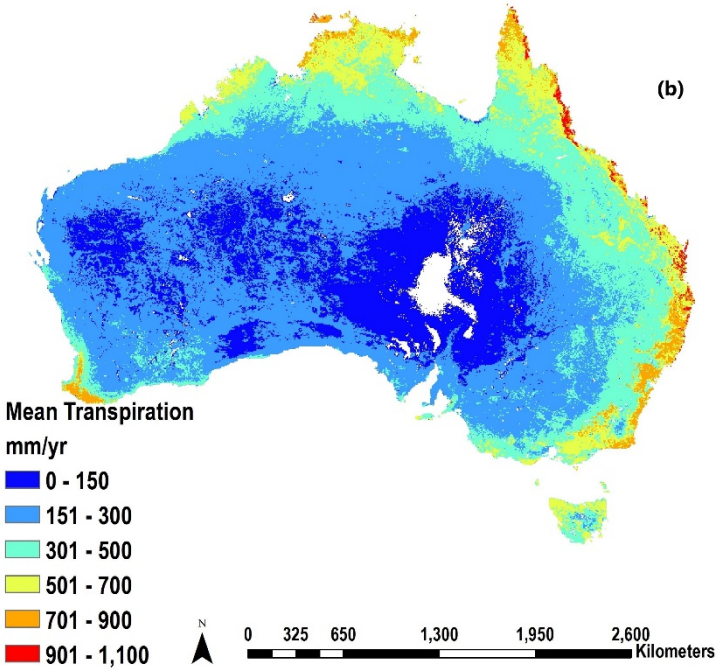

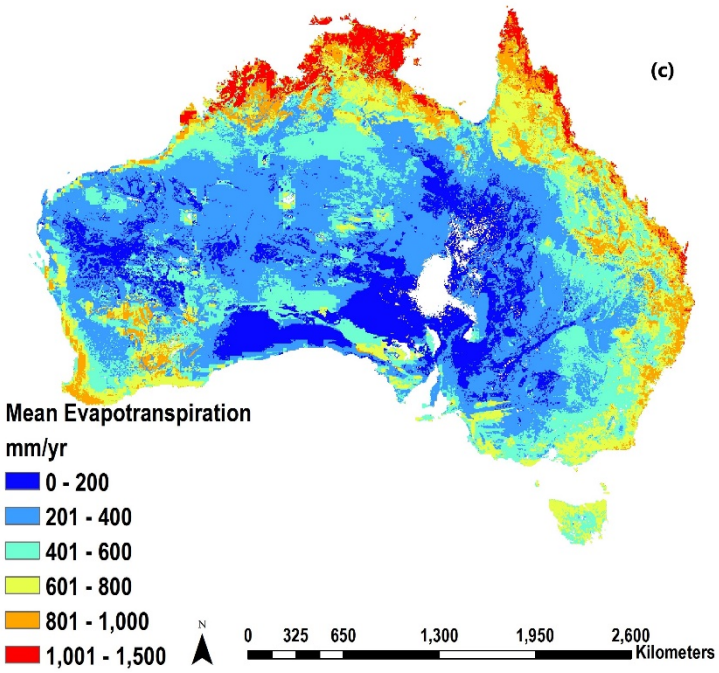

Figure 19: (a) Mean evaporation; (b) Mean transpiration; and (c) Mean evapotranspiration in mm/yr for 2003-2013

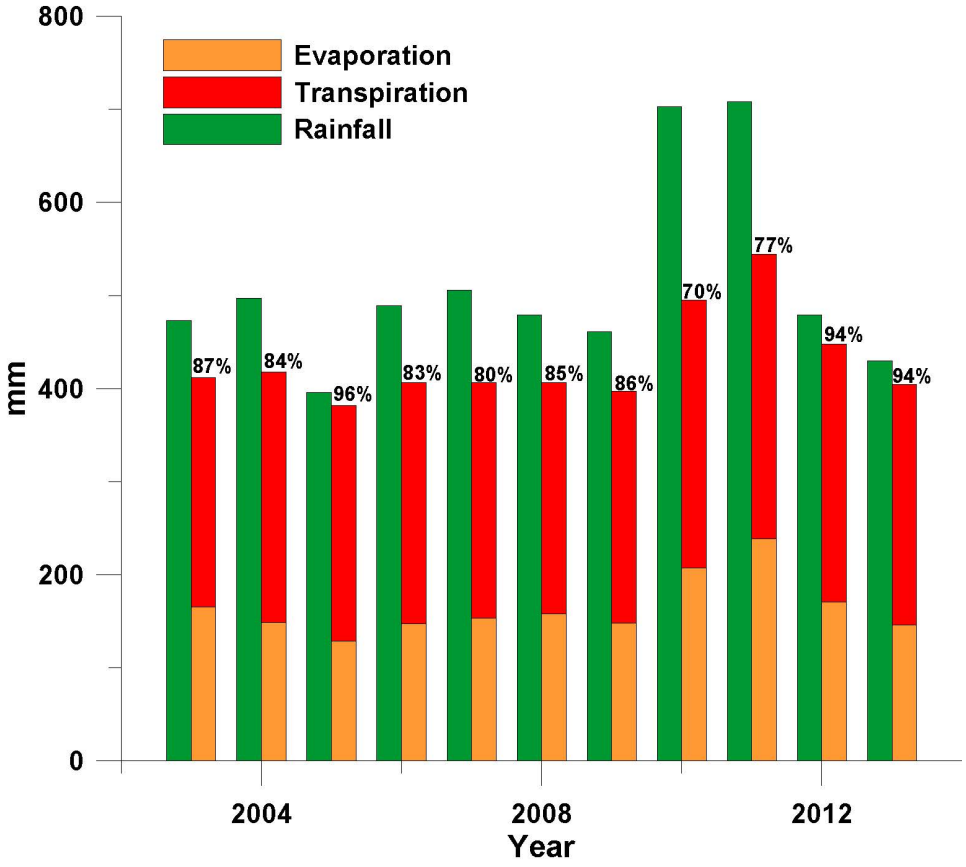

Figure 20: MEP E and T vs rainfall

Annual ET fluctuates during the study period (Fig. 20) with the correlations for annual evaporation and transpiration relative to annual rainfall calculated to be 0.94 and 0.84, respectively. Although the MEP model does not use rainfall as an input, the strong correlation between rainfall and ET, the largest components of the hydrologic system in Australia, suggests the MEP model captures the Australian hydrological system effectively. These results are consistent with the findings of Jung et al. (2010) who observed a drop in the global evapotranspiration due to reduced ET over Australia between 1998 and 2008. The reduction in ET over Australia can be seen through the "millennium drought" years with the immediate increase in ET observed in 2010 at the end of the prolonged drought.

Table 11: EC validation of the MEP, MOD16 and AWRA-L products. Eddy Covariance Tower Site name (Site Name); Fluxnet site ID and IGBP land cover type (Site ID); Average observed ET at flux tower (OBS_ET); Root Mean Square Error (RMSE); Mean Absolute Error (MAE); Correlation Coefficient (R); Percent Bias (PBIAS); EC sites citations

Site Name	**Site ID**	**Obs_ET (mm/ 8 days)**	**RMSE (mm/ 8 days)**			**MAE (mm/ 8 days)**			**R**			**PBIAS (%)**			**Citations**
			MEP	MOD16	AWRA-L	MEP	MOD16	AWRA-L	MEP	MOD16	AWRA-L	MEP	MOD16	AWRA-L	
Adelaide River	AU-Ade (WSA)	15.34	**9.06**	11.09	9.65	7.04	9.22	**5.73**	0.64	0.57	**0.71**	26.18	-34.38	**22.26**	(Beringer, 2014a)
Alice Springs	AU-ASM (ENF)	8.45	**6.12**	8.82	7.13	**4.80**	6.05	6.03	**0.74**	0.69	0.63	**-6.78**	-62.1	-23.9	(Derek and James, 2014a)
Calperum	AU-Cpr (SAV)	8.39	**3.38**	4.69	3.55	**1.01**	2.79	1.27	0.62	0.33	**0.72**	**-12.04**	-33.25	-15.15	(Koerber, 2014)
Daly River Cleared	AU-DaS (GRA)	18.6	**4.62**	9.74	6.05	**3.63**	8.21	4.43	**0.88**	0.74	0.78	-12.23	-38.6	**0.21**	(Beringer, 2014b)
Daly River Savanna	AU-DaP (GRA)	12.24	10.43	10.75	**9.78**	8.64	6.93	**6.89**	0.63	0.74	**0.77**	17.32	**13.86**	41.49	(Beringer, 2014c)
Dry River	AU-Dry (SAV)	19.55	**9.95**	13.63	12.58	**4.7**	8.14	5.02	**0.62**	0.43	0.58	**-24.2**	-41.77	-25.8	(Beringer, 2014c)
Emerald	AU-Emr (GRA)	11.56	**5.69**	5.96	9.91	**4.22**	4.35	7.32	0.47	**0.48**	0.43	**-10.92**	-14.38	21.25	(Schroder, 2014)
Fogg Dam	AU-Fog (WET)	35.35	**15.45**	22.53	18.9	**13.97**	20.72	16.33	0.26	0.6	**0.61**	**-35.71**	-58.4	-42.79	(Beringer, 2013a)
Gingin	AU-Gin (WSA)	15.47	6.27	7.21	**5.49**	5.20	6.09	**4.1**	0.39	0.37	**0.51**	**-3.0**	-36.49	-17.02	(Silberstein, 2015)
Great Western Woodlands,	AU-GWW (SAV)	7.65	**2.78**	5.15	3.47	**2.04**	3.9	2.62	**0.63**	0.08	0.37	11.08	-47.45	**-11.06**	(Craig, 2014)
Howard Springs	AU-How (WSA)	24.96	**7.13**	9.92	7.96	**5.53**	8.13	6.18	0.67	0.79	0.79	**-3.2**	-30.0	-9.87	(Beringer, 2014d)
Loxton	AU-Lox (DBF)	27.3	27.31	**27.09**	32.63	17.78	**17.51**	22.8	**0.51**	0.37	-0.12	-63.48	**-60.0**	-82.7	(Ewenz, 2008)
Red Dirt Melon Farm	AU-RDF (WSA)	14.66	**9.56**	11.36	12.17	**8.25**	8.65	8.88	**0.66**	0.55	0.58	**3.45**	-25.39	12.53	(Beringer, 2013b)
Riggs Creek	AU-Rig (GRA)	13.22	5.72	9.07	**4.53**	4.67	4.23	**3.28**	0.71	0.70	**0.83**	-14.96	-22.21	**11.62**	(Beringer, 2014e)
Sturt Plains	AU-Stp (GRA)	10.24	**7.95**	8.20	8.5	6.17	5.64	**4.79**	0.73	**0.79**	0.78	25.77	-40.4	**17.9**	(Beringer, 2013c)
Ti Tree East	AU-TTE (OSH)	2.81	4.45	**4.32**	6.99	3.69	**2.63**	4.95	**0.43**	0.08	0.20	96.17	**-42.34**	146.08	(Derek and James, 2014b)
Tumbarumba	AU-Tum (EBF)	20.86	6.72	6.54	**5.97**	4.75	4.98	**4.31**	0.83	0.86	0.86	-13.82	14.07	**-6.57**	(Woodgate, 2014)
Wallaby Creek	AU-Wac (EBF)	15.35	6.76	11.13	**5.76**	5.82	9.31	**4.84**	**0.85**	0.77	0.78	34.67	57.75	**25.57**	(Beringer, 2014f)
Whroo	AU-Whr (WSA)	13.73	6.51	**5.08**	5.86	5.09	**4.10**	4.52	0.54	**0.59**	0.46	**-2.54**	-23.07	-10.8	(Beringer, 2014g)
Wombat	AU-Wom (EBF)	23.28	8.24	**5.13**	7.45	7.11	**4.16**	6.02	**0.89**	0.88	0.81	-30.12	**-0.29**	-21.24	(Beringer, 2014h)

4.3.2 MEP, MOD16 and AWRA-L performances at the Eddy Covariance flux sites

The 20 eddy covariance flux tower sites used for the validation of the MEP, MOD16 and AWRA-L products include 8 land cover types according to the International Geosphere-Biosphere Programme (IGBP), i.e. 4-Evergreen Broadleaved Forest (EBF), 4-Woodland Savanna (WSA),4-Savanna (SAV), 1-Wetland (WET), 4-Grassland (GRA), 1-Evergreen Needle Forest (ENF), 1-Deciduous Broadleaved Forest (DBF), and 1-Open Shrubland (OSH). The MEP model outperforms the MOD16 at 15, 13, 14 and 16 sites measured by the RMSE, MAE, R and PBIAS metrics respectively. The MEP also performed better than the AWRA-L at 13, 11, 11 and 12 sites measured by the RMSE, MAE, R and PBIAS metrics, respectively. The MEP model also outperforms the MOD16 and AWRA-L measured by the average RMSE, MAE and R across the 20 EC flux sites. The average RMSE across the 20 EC flux sites for the MEP, MOD16 and AWRA-L are respectively 8.21, 9.87 and 9.22. The average MAE are respectively 6.21, 7.29 and 6.52 for the MEP, MOD16 and AWRA-L. The average correlations are 0.64, 0.57 and 0.61 for the MEP, MOD16 and AWRA-L, respectively. The MEP PBIAS was within 20% of the observed flux at 12 sites while the MOD16 and AWRA-L were within 20% of the observed flux at 4 and 10 sites, respectively.

Some consistency is seen across the models at many sites, with the three models seeming to perform best for the evergreen broadleaved forests with correlations ranging from 0.77 to 0.89 at the three sites. Similar correlation consistency of the models is obtained across the five grassland sites. Generally, the MOD16 underestimated ET significantly at most sites with 12 sites over 30%. Consistent underestimation is also observed across the Fogg Dam wetland site with the three models underestimating ET by 35% or higher. The MEP ET exhibited the lowest correlation at the Fogg Dam site. The Fogg Dam is a seasonally flooded wetland where water evaporation is a principal component of ET. However, due to the coarse resolution of the soil moisture data, the MEP model may not effectively capture the local evaporation, while scale mismatch may also contribute to the weaker performance of the MEP. Less accurate ET estimates were also observed at the Loxton site by the three models with underestimation at least 60%. The flux data at the Loxton site appear unrealistic presumably caused by sensor failures suggested by 1800 mm ET while only 500 mm rainfall is recorded at the site, unfortunately due to the closure of the site it was difficult investigating further.

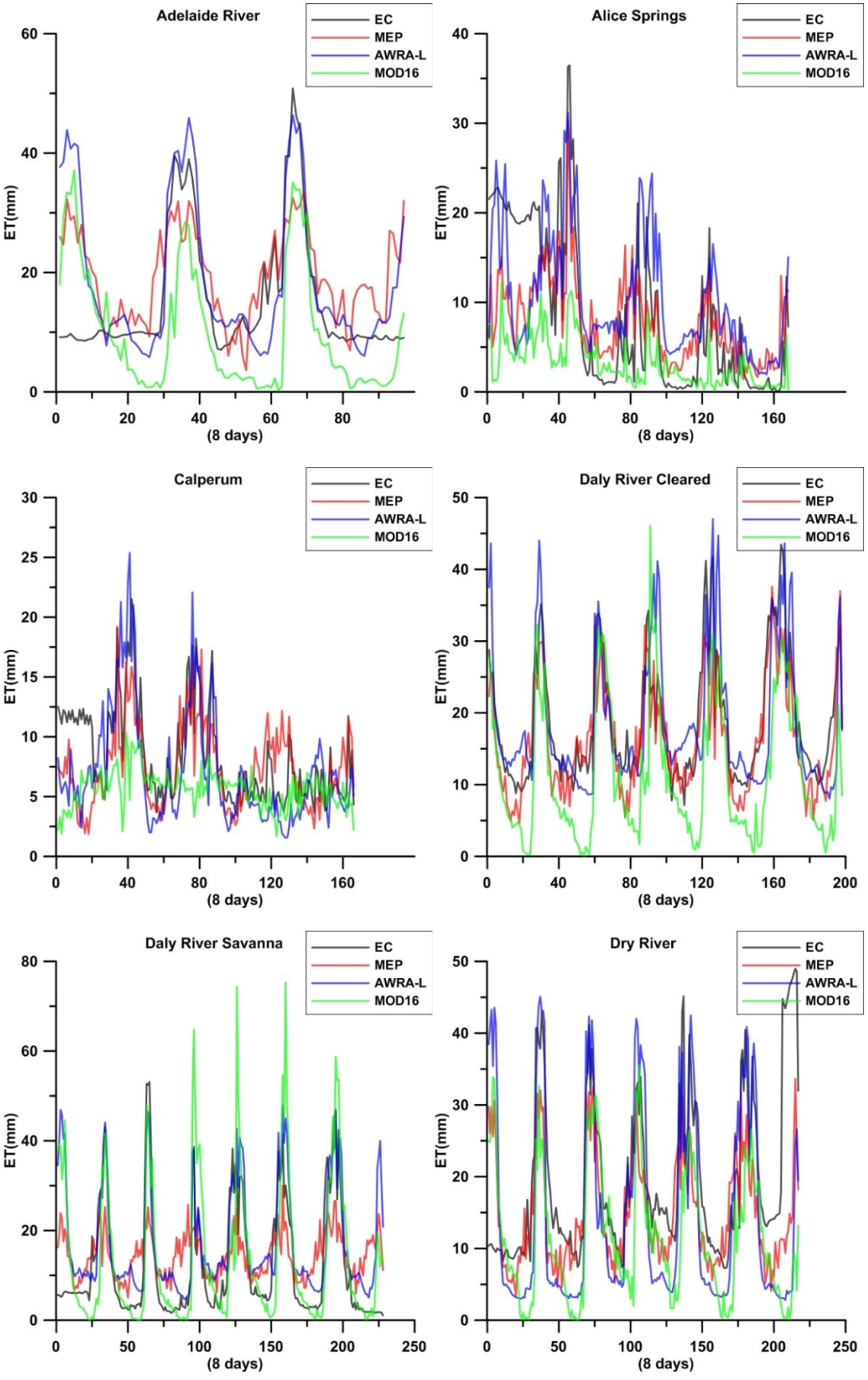
Adelaide River
EC
MEP
AWRA-L
MOD16
ET(mm)
(8 days)
Alice Springs
Calperum
Daly River Cleared
Daly River Savanna
Dry River

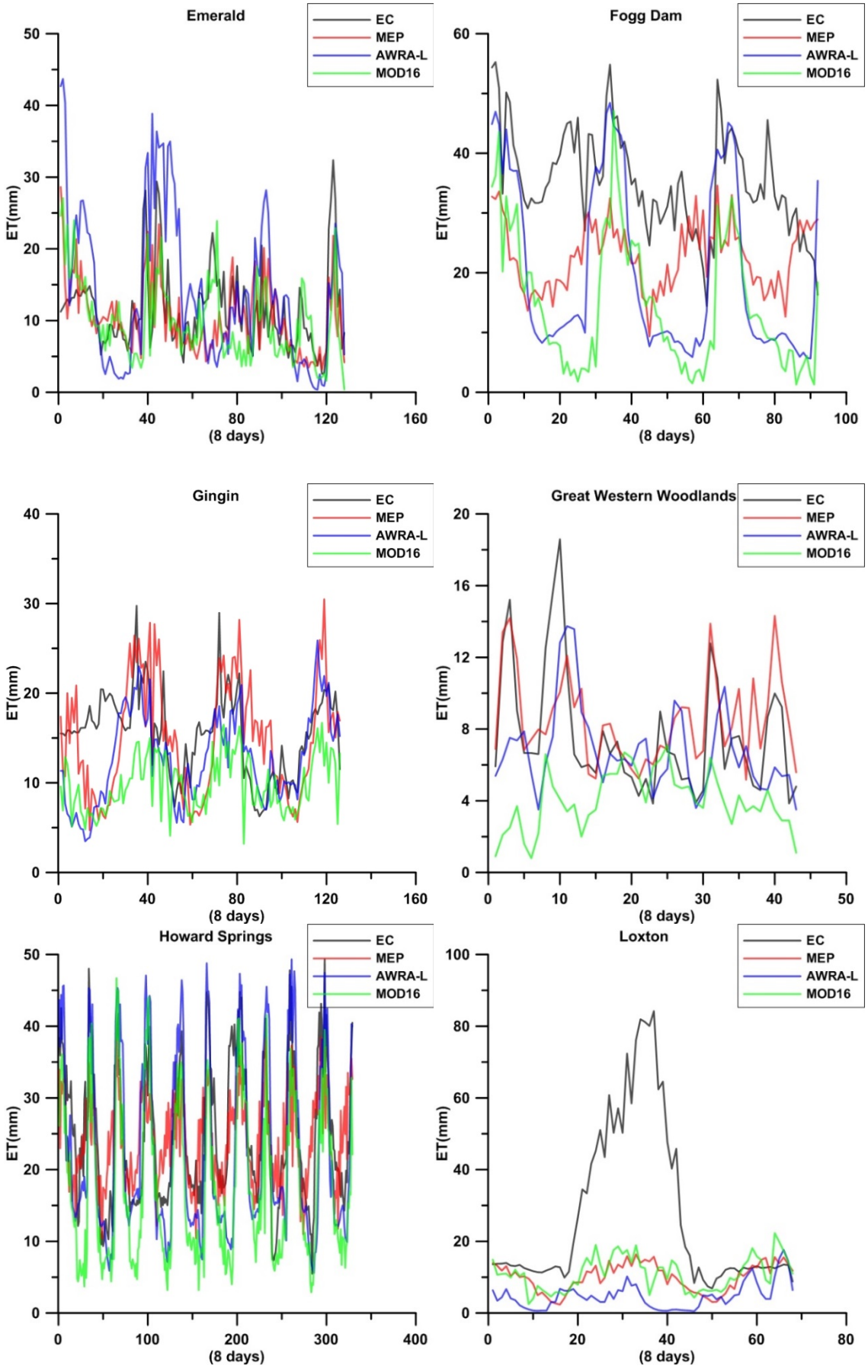
Emerald
EC
MEP
AWRA-L
MOD16
ET(mm)
(8 days)
Fogg Dam
Gingin
Great Western Woodlands
Howard Springs
Loxton

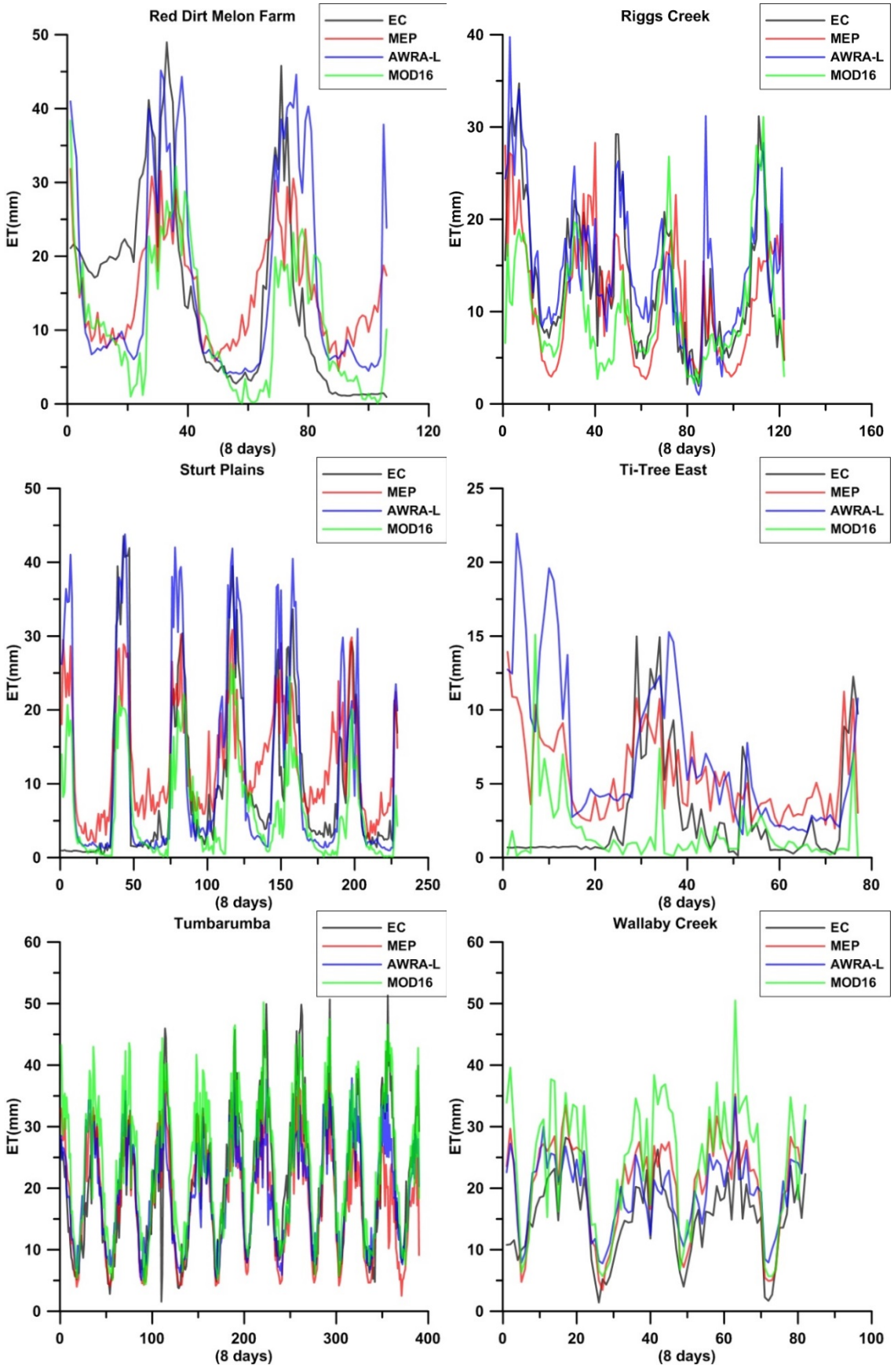
Red Dirt Melon Farm
EC
MEP
AWRA-L
MOD16
ET(mm)
(8 days)
Riggs Creek
Sturt Plains
Ti-Tree East
Tumbarumba
Wallaby Creek

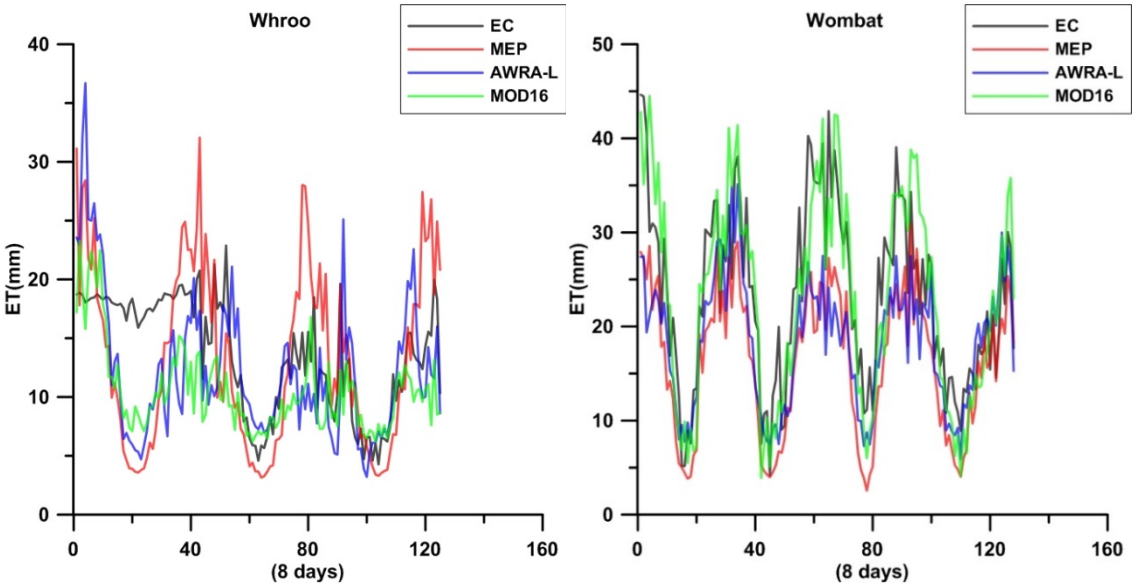

Figure 21: Continuous plot of the MEP, EC, AWRA-L and MOD16 ET

Figure (21) shows that the MEP model reasonably captures the temporal trends of ET relative to the EC flux at most sites. The MEP model appears to underestimate ET in the winter months and overestimate ET in the summer months at the Whroo site. A possible reason for this trend in the MEP model is the wrong classification of the vegetation at the Whroo site. The Whroo site, a box woodland revegetation from the gold mining era currently covered with pasture and eucalyptus species vegetation, is incorrectly classified by the IGBP as an evergreen broadleaved forest. The FPAR product used in partitioning net radiation between soil and canopy show large inter-annual variation, leading to seasonal under- or overestimation of ET.

The MOD16 performs the best at forested sites showing consistent temporal patterns relative to the EC observations. The calibrated AWRA-L model also effectively replicates the temporal trends across most sites and outperforms the MOD16 at most sites.

The accuracy of the modelled ET is strongly affected by the estimated soil water potential using the pedotransfer function. The difference in the footprints of the flux towers may also contribute to the underestimation of ET particularly at flux tower sites with mixed vegetation.

4.3.3 Comparison of the MEP, MOD16 and AWRA-L at Continental scale

A continental scale comparison of the MEP, MOD16 and AWRA_L ET products was carried out after calculating a mean annual ET over the study period from each product over the entire Australia. All 260,000 pixels of 5 km resolution across the three models are used in the analysis. Annual mean ET over Australia from the MEP, MOD16 and AWRA_L products over the 11-year study period were calculated as 440, 262 and 428 mm, respectively. All the corresponding cells were also used to calculate the correlation R, RMSE, NSE and MAE (Table 12). The spatial agreements across the products was evident with all three products showing higher ET around the coastline and lower ET in inland Australia. The NSE between the MEP and AWRA-L shows a better agreement than between the MEP and MOD16 products, which have a negative NSE. The MAE and RMSE were also significantly lower between the MEP and AWRA-L. The total ET from the MEP and AWRA-L appears more reasonable relative to the annual rainfall over Australia (Fig. 20). The annual MEP ET as a percentage of rainfall (Fig. 20) is consistent with other studies that about 90% of annual rainfall in Australia is returned to the atmosphere through ET (Chiew et al., 2002, Prosser, 2011). Moreover, significant underestimation of ET by the MOD16 model was observed across the flux tower sites.

Spatial analysis of the three products were also carried out using the percentage difference for MEP vs MOD16, MEP vs AWRA-L and AWRA-L vs MOD16 (Fig. 22). MEP ET was significantly higher than MOD16 ET for large swaths of inland Australia while MOD16 was higher around the coastlines, particularly the eastern coastlines and Tasmania. The underestimation of the MOD16 ET at the EC flux tower sites (section 4.3.2) shows that MOD16 underestimated ET at 17 of the 20 flux sites and by more than 30% in 12 of the sites) is confirmed as shown in Fig. 22(a) and (c). The MOD16 performed better at the evergreen broadleaved forest tower sites close to the coastline where it has better agreement with the MEP. However due to mixed performance of the MEP and MOD16 model at the flux towers around the south-eastern coastline, it is difficult to draw a definite conclusion on which model performs better. The percentage difference between the MEP and AWRA-L model has a narrower range over large areas of Australia with both models within 50% for Australia. There are two large areas in the south-central to Western Australia where the AWRA-L model significantly underestimates ET. The AWRA-L ET is in the range of 1 – 10 mm/yr over large portion of Western Australia with numerous pixels having mean ET less than 1 mm/yr between 2003 and 2013, which may be due to water balance errors in the AWRA-L algorithm. The historic average precipitation in the partially vegetated region is in the range 200-500 mm/yr and it appears implausible for ET to be less than 10 mm/yr. The large swath is also conspicuous in the AWRA-L and MOD16

percentage difference map (Fig. 22c). The MOD16 model also produces higher ET than the MEP and AWRA-L specifically in regions classified as evergreen broadleaved forests along the coastlines. The overestimation of MOD16 at evergreen broadleaved forests has been documented in literature (Ruhoff et al., 2013, Hu et al., 2015b).

Table 12: The correlation coefficient (R), Root Mean Square Error (RMSE), Nash-Sutcliffe Efficiency (NSE) and Mean Absolute Error (MAE) for comparison of the MEP, MOD16 and AWRA_L products over the entire Australia

RMSE (mm/yr)					MAE (mm/yr)				
R		MEP	MOD16	AWRA-L	NSE		MEP	MOD16	AWRA-L
	MEP		242	162		MEP		203	126
	MOD16	0.75		205		MOD16	-0.05		187
	AWRA-L	0.77	0.86			AWRA-L	0.51	0.25	

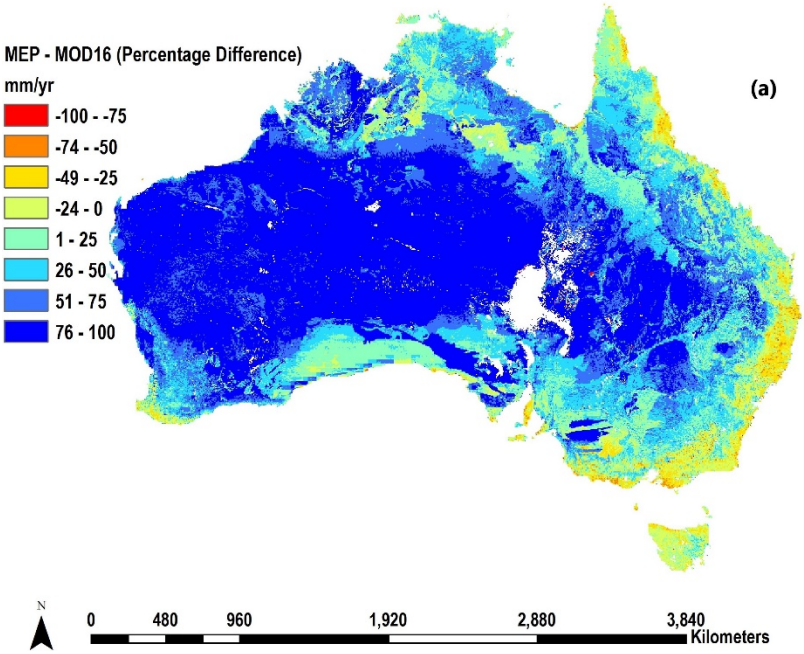

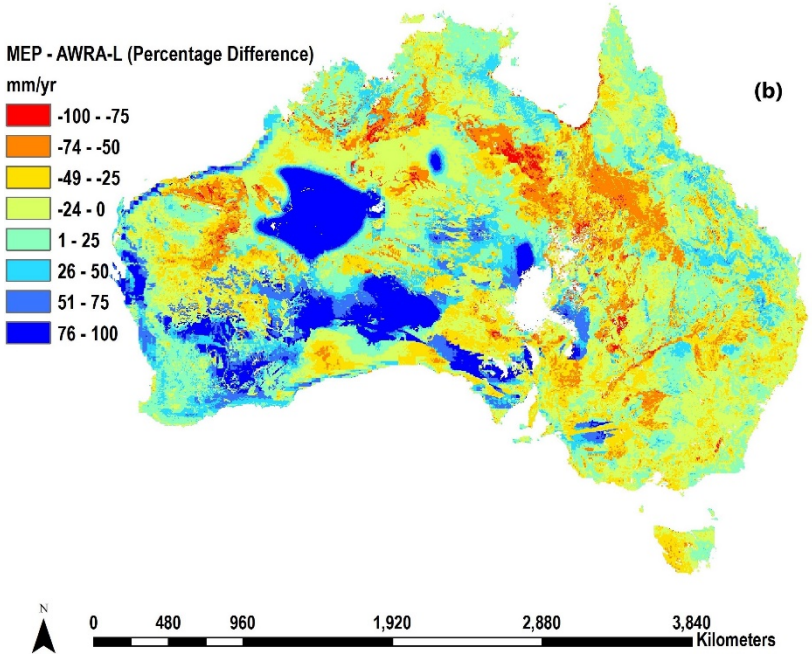

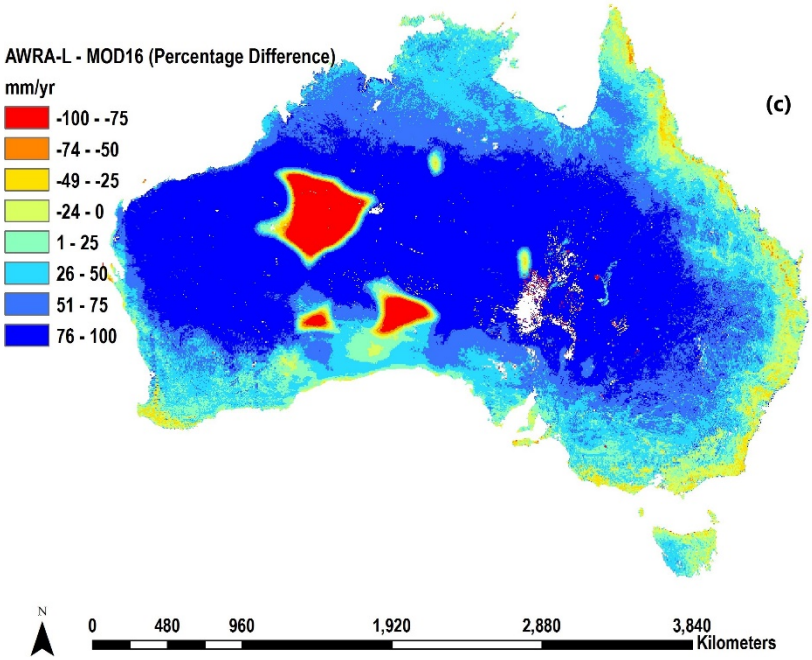

Figure 22: Mean annual percentage difference between (a) MEP – MOD16; (b) MEP-AWRA-L; (c) AWRA-L- MOD16

4.3.4 Possible challenges with the MEP model

The MEP model appears lacking spatial continuity, probably due to the use of pedotransfer functions to determine the wilting point and field capacity, since surface specific humidity is a crucial input of the MEP model. Hence, further improvement to the MEP model may be achieved by improving the parameterization of the pedotransfer functions for each soil type. Another challenge is the spatial resolution of soil moisture data for the regions where soil moisture is spatially more variable. The low correlation of the MEP model in the Fogg Dam wetlands may be related to high spatial variability of the soil moisture with intermittent flooding occurring at the site.

4.4 Conclusion

We have implemented the MEP model for estimating ET on a continental scale using readily available remote sensing datasets to produce daily evaporation and transpiration at 5 km^2 resolution dataset over the entire Australia.

The MEP modelled ET was validated at 20 EC flux tower sites and compared to the MOD16 and AWRA-L model ET. The MEP model outperforms both models at most EC flux sites with the AWRA-L model performing the next best. The MEP ET has the best average RMSE, MAE, R and PBIAS across all 20 EC flux sites. The MEP annual mean ET over Australia corroborates previous studies on the ET trend over Australia indicated by close correlation between MEP ET and rainfall during and after the "millennium drought" period.

The MEP model is the simplest of the three models in terms of model formula and input data. This study shows that the MEP model as a two-source surface energy balance model effectively estimates ET on regional scales using fewer input data to produce evaporation and transpiration separately.

The MEP method has the potential to be further improved for modelling ET. Further study will seek to improve the resolution of the MEP ET product while focusing on the development of a daily global MEP product.

4.5 Acknowledgement

We would like to acknowledge the invaluable advice of Dr John Hutson on soil hydrology during the preparation of this manuscript.

This work used eddy covariance data acquired and shared by the FLUXNET community, including these networks: OzFlux-TERN. The ERA-Interim reanalysis data are provided by ECMWF and processed by LSCE. The FLUXNET eddy covariance data processing and harmonization was carried out by the European Fluxes Database Cluster, AmeriFlux Management Project, and Fluxdata project of FLUXNET, with the support of CDIAC and ICOS Ecosystem Thematic Center, and the OzFlux, ChinaFlux and AsiaFlux offices.

5 Conclusions, data availability and future work

5.1 Conclusions

The specific findings of the three principal studies are condensed below:

1. The MEP model at field scale in the mangrove forest was able to predict the ET with good accuracy on the 8 day cycle when compared to the EC ET results. The results show that the MEP model only captures energy input through net radiation into the system. Other sources of energy are neglected. Horizontal advection from and to the sea, which is not captured in the MEP model is principally responsible for the weaker correlation of the MEP and the EC system at hourly resolution. In areas with strong advection, the advection cycle may impact the ET estimation negatively at high temporal resolutions. With aggregation of the data from hourly to 8 days, the MEP model results improved consistently until the effect of the advection was balanced out on the temporal scale. The MEP was determined to performefficiently at the 8-daily timescale

2. In a homogenous Eucalyptus dominated catchment, with acute elevation changes and highly variable rainfall, mean annual ET from the MEP was within 20% of the SWAT, MOD16 and AWRA-L models. Such a mutli-model approach is a way to gain confidence in ET measurements in challenging environments due to terrain. Seasonal variations differed between the four models with the MEP appearing to simulate the seasonal ET accurately. The spatio-temporal analysis on a graduated spatial scale show that the variance in the ET was dominated by the spatial component and with aggregation, the spatial component of the variance reduces. A spatial scale of confidence of 4 km^2 was proposed for catchment to regional scale ET modelling based on the graduated spatial scale analysis of SWAT and MOD16.

3. The MEP ET was developed into a continental scale product over Australia at the 0.05^o resolution on daily timescales. The results of the E and T show that evaporation contributed 38% and 62% respectively to the ET for the period of 2003-2013. The MEP ET results were validated at 20 EC flux sites and simultaneously compared to the MOD16 and AWRA-L ET products. The MEP outperformed both models in the majority of the 20 flux sites as measured by four statistical metrics. The analysis of the MEP model and the findings at the field, catchment and continental scales will contribute to the knowledge base regarding the MEP model

method. The E, T and ET products will open up new frontiers of research and understanding of the contributions, behaviour and trends of the E and T component in different environments and land covers with the newly available data.

5.2 MEP ET Product Data availability

The MEP ET over Australia is the only known independently available E and T products over the entire Australia to the author. The initial dataset produced as part of this PhD research is on daily timescale covering the period of 2003 – 2013. The product required significant programming in the Python language which was principally used in creating the product. Some processing was also completed using the ArcGIS suite. The product was created in the GeoTIFF raster format for easy import into GIS software for viewing and manipulation. The product is freely available for download at http://dx.doi.org/10.25901/5ce795d313db8

5.3 Future Work

This study has opened up further areas of research with the MEP performing very well at the field, catchment and continental scales.

The first manuscript of this study identified the effect of advection when the MEP ET is estimated at high temporal resolution. The inclusion of a horizontal advection equation in the MEP model is entirely possible and would be a study that would be useful in improving the performance of the MEP under specific environmental conditions.

Further development of the MEP ET from continental scale to global scale at a higher spatial resolution using data from satellites in orbit as well as the inclusion of the sensible heat fluxes is a priority future study.

Appendix A: MEP Model

The MEP model of evaporation and transpiration was derived from the dissipation function in Equation (A1) in (Wang and Bras (2011)

$$D(E,G,H) \equiv \frac{2E^2}{I_e} + \frac{2G^2}{I_s} + \frac{2H^2}{I_a} \quad \text{(A1)}$$

where $I_e, I_s,$ and I_a are the thermal inertia relative to latent heat, ground heat and sensible heat flux, respectively,

$$I_s = \left(2.1\rho^{\left[1.2-0.02\left(\frac{\rho}{\rho_w}\right)100\theta\right]}e^{\left[-0.007\left(\frac{100\theta\rho}{\rho_w}-20\right)^2\right]} + \rho^{\left[0.8+0.02\left(\frac{\rho}{\rho_w}\right)100\theta\right]}\right)^{0.5} \times \left(\frac{\left(\frac{20\theta}{\rho_w}\right)\rho^2}{0.01}\right) \quad \text{(A2)}$$

I_s is parameterized as a function of soil moisture and water density and bulk density (Cai et al., 2007) where ρ_w is density of water (kg/m^3); θ is the soil moisture content of the soil (m^3/m^3);

$$I_o = C_o\rho_a C_p\sqrt{kz}\left(\frac{kgz}{\rho_a C_p T_r}\right)^{\frac{1}{6}} \quad \text{(A3)}$$

C_o is the empirical constant characterizing the atmospheric stability (Businger et al., 1971): $C_o = 1.7$ Unstable, 1.2 Stable; ρ_a is the density of air (Kgm^{-3}); k = 0.4 the von Kármán constant; z is the distance above the target surface for which the Monin-Obukhov similarity theory is valid (m); $g = 9.8$ m/s^2 the acceleration due to gravity; T_r (~ 300 K) is an atmospheric reference temperature;

$$I_a = I_o|H|^{-\frac{1}{6}},\ I_e = \sigma I_a, \quad \text{(A4)}$$

In the MEP equation over vegetated land surface in Wang and Bras (2011), the reciprocal Bowen ratio; $\beta(\sigma) = 6\left(\sqrt{1+\frac{11}{36}\sigma - 1}\right)$, was introduced to represent the target surface conditions as a function of specific humidity and temperature, where $\sigma = \frac{\lambda^2}{c_p R_v}\frac{q_s}{T_s^2}$;

where q_{sat} (saturated specific humidity in the stomatal cavity) is constrained by the opening and closing of the stomatal cavity defined by the parameter η_s. Where η_s is a value between 0 and 1. When there is complete closure of the stomatal cavity, η_s is 0 and when the stomatal cavity is completely open, 1.

$$q_{sat} = \eta_s(q_s) \quad \text{(A5)}$$

. Hence, the MEP flux equations over vegetated land can be written as,

$$E_v = \frac{R_{n\_v}}{1+\beta(\sigma)_v^{-1}},\ H_v = \frac{R_{n\_v}}{1+\beta(\sigma)_v} \quad \text{(A6)}$$

At regional scales where air specific humidity and air temperature are used as surrogates of canopy surface specific humidity and temperature, $\beta(\sigma)$ in equation A5 is replaced with σ

$$\theta\ @FC = 7.561 + 1.176Clay - 0.009843Clay^2 + 0.2132Silt \quad \text{(A7)}$$

$$\theta\ @PWP = -1.304 + 1.117Clay - 0.009309Clay^2 \quad \text{(A8)}$$

Pedotransfer functions in Equations A6 and A7 are used to determine the soil moisture content at field capacity and permanent wilting point as the inputs into the Hutson and Cass model in Equation. FC is the field capacity (-); Clay and Silt are the clay and silt fraction of the soil; and PWP is permanent wilting point (-).

In calculating the specific humidity, the Clausius-Clapeyron equation is used to determine the saturated vapour pressure;

$$e_{sat} = 0.611 \times \exp\left[\left(\frac{\lambda}{R_v}\right) \times \left(\frac{1}{273} - \frac{1}{T}\right)\right] \quad \text{(A9)}$$

where e_{sat} is the saturated is vapour pressure (kPa); λ is the latent heat of vaporisation 2.5×10^6 JKg^{-1}; R_v is the gas constant for moist air at 461 Jkg^{-1}K^{-1} and T is temperature in Kelvin (K)

$$e_{act} = \text{RH} \times e_{sat} \quad \text{(A10)}$$

Where e_{act} is the actual vapour pressure (kPa) and RH is the relative humidity in fraction

$$r = \varepsilon \times \left(\frac{e_{act}}{P - e_{act}}\right) \quad \text{(A11)}$$

Where r is the mixing ratio in kg/kg, ε is $\varepsilon = \frac{R_d}{R_v}$, the ratio of the specific gas constant for dry air (Jkg^{-1}K^{-1}) to the specific gas constant for water vapour (Jkg^{-1}K^{-1}).

Once the mixing ratio is obtained, we solve for specific humidity (q)

$$q = \frac{r}{r+1} \quad \text{(A12)}$$

The MEP model was validated by the EC using the statistical metrics: RMSE, MAE, R, NSE and PBIAS, where;

$$RMSE = \sqrt{\frac{\sum_{n=1}^{N}(Q_n - \widehat{Q_n})^2}{N}} \quad \text{(A13)}$$

$$MAE = \frac{\sum_{n=1}^{N}|Q_n - \widehat{Q_n}|}{N} \quad \text{(A14)}$$

$$R = \frac{\left(\sum_{n=1}^{N}(Q_n - \overline{Q})(\widehat{Q_n} - \widetilde{Q_n}\right)}{\sqrt{\sum_{n=1}^{N}(Q_n - \overline{Q})^2}\sqrt{\sum_{n=1}^{N}(\widehat{Q_n} - \widetilde{Q_n})^2}} \quad \text{(A15)}$$

$$NSE = 1 - \frac{\sum_{n=1}^{N}(Q_n - \widehat{Q_n})^2}{\sum_{n=1}^{N}(Q_n - \overline{Q})^2} \quad \text{(A16)}$$

$$PBIAS = 100 \times \frac{\sum_{n=1}^{N}(Q_n - \widehat{Q_n})}{\sum_{n=1}^{N} Q_n} \quad \text{(A17)}$$

where x_n and y_n are observed and simulated daily ET values (mm); N is the number of observed or simulated ET values; Q_n (mm) is the measured ET at day n; $\widehat{Q_n}$ (mm) is the simulated ET at day n; $\widetilde{Q_n}$ (mm) is the mean simulated discharge at day n; and $\overline{Q}$ (mm) is the mean ET.

Appendix B: Evapotranspiration in SWAT

SWAT provides the user with three options of modelling ET at the HRU level and at daily temporal resolution (Penman-Monteith, Hargreaves or Priestly-Taylor methods). In this study, the Penman-Monteith method is used. SWAT initially calculates the potential evapotranspiration (PET) for a reference crop (Alfalfa) using the Penman-Monteith equation for well-watered plants (Jensen et al., 1990),

$$\lambda E_0 = \frac{\Delta(H_{net}-G)+\rho.c_p.\frac{e_{sat}-e}{r_a}}{\Delta+\gamma(1+\frac{r_c}{r_a})} \quad \text{(B1)}$$

where λ is the latent heat of vaporization (MJ kg^{-1}); E_0 is the potential evapotranspiration rate (mm/d); Δ is the slope of the saturation vapor pressure vs temperature curve (kPa ^{o}C^{-1}); H_{net} is the net radiation at the surface (MJ m^{-2} d^{-1}); G is the heat flux density to the ground (MJ m^{-2} d^{-1}); ρ is the air density (kg m^{-3}); c_p is the specific heat of dry air at constant pressure (J kg^{-1} K^{-1}); P is the atmospheric pressure (kPa); e_{sat} is saturation vapor pressure of air (kPa); e is water vapor pressure (kPa); r_a is the aerodynamic resistance (s m^{-1}); γ is the psychometric constant (kPa ^{o}C^{-1}) and r_c is the canopy resistance (s m^{-1}).

Total ET (AET) in SWAT is made up of four components: canopy evaporation, transpiration, soil evaporation and groundwater ET (Revap). Revap is the movement of water from the saturated zone into the overlying unsaturated zone to supplement the water need for evapotranspiration. The Revap process may be insignificant in regions where the saturated zone is much deeper than the root zone and as such the result is separately reported from the ET result in the SWAT result database. As SWAT calculates Revap separately, for a calculation of AET in regions where the saturated zone is within the root zone, the user should add the Revap result column to the ET calculations. The AET components are calculated from the PET starting with the canopy evaporation. For this first component the following storage equations are used in determining the volume of water available for evaporation from the wet canopy in SWAT

$$C_{day} = C_{mx}\left(\frac{L_{ai}}{L_{ai\_mx}}\right) \quad \text{(B2)}$$

when $R'_{day} \leq C_{day} - R_{int(i)}$:

$$R_{int(f)} = R_{int(i)} + R'_{day}\,; and\ R_{day} = 0 \quad \text{(B3)}$$

when $R'_{day} > C_{day} - R_{int(i)}$:

$$R_{int(f)} = C_{day};\ R_{day} = R'_{day} - \left(C_{day} - R_{int(i)}\right) \quad \text{(B4)}$$

where C_{day} is the maximum amount of water that can be stored in the canopy on a given day (mm); C_{mx} is the amount of water that can be stored in the canopy when the canopy is fully matured (mm); L_{ai} is the leaf area index on a given day (); L_{ai_mx} is the maximum leaf area index when the plant is fully matured (-); $R_{int(i)}$ is the initial amount of free water available in the canopy at the beginning of the day (mm); $R_{int(f)}$ is the final amount of free water available in the canopy at the end of the day (mm); R'_{day} is the amount of precipitation on a given day before accounting for canopy interception (mm); and R_{day} is the amount of precipitation reaching the soil on a given day (mm).

The SWAT ET algorithm initially evaporates as much water as can be accommodated in the PET from the wet canopy. If the total volume of water in canopy storage equals or exceeds PET for the day, then ET is calculated as

$$E_a = E_{can} = E_0 \tag{B5}$$

where E_a is AET (mm d^{-1}); E_{can} is evaporation from canopy constrained by E_0, i.e. PET (mm d^{-1}). However, if the water in canopy storage is less than the PET for the day, transpiration, soil evaporation and Revap are constrained by E'_0, which is the potential evapotranspiration adjusted for the evaporation of the water on the canopy surface (mm d^{-1}).

$$E'_0 = E_0 - E_{can} \tag{B6}$$

The second AET component (transpiration) of SWAT is calculated using the following equations;

$$\lambda E_{t\_max} = \frac{\Delta(H_{net}-G)+\gamma \mathrm{K}(\frac{0.622.\lambda.\rho}{P})\frac{e_{sat}-e}{r_a}}{\Delta+\gamma(1+\frac{r_c}{r_a})} \tag{B7}$$

$$W_z = \left(\frac{E_{t\_max}}{1-e^{-\tau}}\right) \times \left(1 - e^{(-\tau \times (\frac{z}{zr})}\right) \tag{B8}$$

$$W'_l = W_l + (W_d \times e_{pco}) \tag{B9}$$

$$W"_l = W'_l \times e^{\left(5\times\left(\frac{S_{wl}}{(0.25\times A_{wcl})}-1\right)\right)} \; when \; S_{wl} < 25\% \; of \; A_{wcl} \tag{B10}$$

$$W"_l = W'_l \, when \, S_{wl} > 25\% \; of \; A_{wcl} \tag{B11}$$

$$E_{t,l} = \min[W"_l, (S_{wl} - W_{pl})] \tag{B12}$$

$$E_t = \sum_{l=1}^{n} E_{t,l} \tag{B13}$$

where E_{t_max} is the maximum transpiration rate (mm/d); $K = 8.64 \times 10^4$; P is the atmospheric pressure (kPa); W_z is the potential water taken up by plant from the soil surface to a specific depth (mm/d) z; τ is the plant water consumption distribution function; z is the depth from soil surface (mm); z_r is the plant root depth from soil

surface (mm); W_l is the potential water consumption by plant in the soil layer l (mm); W'_l is the potential water consumption by plant in the layer l adjusted for demand (mm); W_d is the plant water consumption demand deficit from overlying soil layers (mm); e_{pco} is the plant water consumption compensation factor (-); $W"_l$ is the potential plant water consumption adjusted for initial soil water content (mm); S_{wl} is the soil water content of layer l in a day (mm); A_{wcl} is the available water capacity of layer l (mm); W_{pl} is soil water content of layer l at wilting point (mm); $E_{t,l}$ is the actual transpiration water volume from layer l in a given day (mm/d); E_t is the total actual transpiration by plants in a given day (mm/d). Plant transpiration parameters such as stomatal conductance, maximum leaf area index and maximum plant height are retrieved from a SWAT database while climate data required by the Penman-Monteith method are sourced from input data.

The third AET SWAT component, the soil evaporation on a given day, is a function of the transpiration, degree of shading and potential evapotranspiration adjusted for canopy evaporation. The maximum soil evaporation on a given day (E_s) (mm d^{-1}) is calculated as

$$E_s = E'_0 cov_{sol} \quad \text{(B14)}$$

$$cov_{sol} = e^{(-5.0\ 10^{-5} CV)} \quad \text{(B15)}$$

where cov_{sol} is the soil cover index (-) and CV is the aboveground biomass for the day (kg/ha). The maximum possible soil evaporation in a day is then subsequently adjusted for plant water use (E'_s) (mm d^{-1})

$$E'_s = min\left(E_s, \frac{E_s\, E'_0}{E_s + E_t}\right) \quad \text{(B16)}$$

The SWAT ET algorithm then partitions the evaporative demand between the soils layers, with the top 10 mm of soil accounting for 50% of soil water evaporated. Equation 17 and 18 are used to calculate the evaporative demand at specific depths and evaporative demands for soil layers respectively.

$$E_{soil,z} = E''_s \frac{z}{z + e^{(2.374 - (0.00713\ z))}} \quad \text{(B17)}$$

$$E_{soil,l} = E_{soil,zl} - E_{soil,zu} . e_{sco} \quad \text{(B18)}$$

$$E'_{soil,l} = E_{soil,l} \times e^{\left(2.5 \times \left(\frac{S_{wl} - F_{cl}}{(F_{cl} - W_{pl})} - 1\right)\right)} when\ S_{wl} < F_{cl} \quad \text{(B19)}$$

$$E'_{soil,l} = E_{soil,l}\ when\ S_{wl} > F_{cl} \quad \text{(B20)}$$

$$E"_{soil,l} = \min[E'_{soil,l}, 0.8(S_{wl} - W_{pl})] \quad \text{(B21)}$$

$$E_{soil} = \sum_{l=1}^{n} E"_{soil,l} \quad \text{(B22)}$$

where $E_{soil,z}$ is the water demand for evaporation at depth z (mm); E_s'' is the maximum possible water to be evaporated in a day (mm); e_{sco} is the soil evaporation compensation factor; $E_{soil,l}$ is the water demand for evaporation in layer l (mm); $E_{soil,zl}$ is the evaporative demand at the lower boundary of the soil layer (mm); $E_{soil,zu}$ is the evaporative demand at upper boundary of the soil layer (mm); F_{cl} is the water content of the soil layer l at field capacity (mm) and $E"_{soil,l}$ is the volume of water evaporated from soil layer l (mm/d); E_{soil} is the total volume of water evaporated from soil on a given day (mm/d).

The fourth component of the ET calculations in SWAT is referred to as "Revap". Revap in SWAT is the amount of water transferred from the hydraulically connected shallow aquifer to the unsaturated zone in response to water demand for evapotranspiration. The Revap component in SWAT is akin to ET from groundwater. Revap is often a dominant catchment process in a groundwater dependent ecosystem and it is calculated at the HRU scale. Revap is estimated as a fraction of the potential evapotranspiration (PET) and it is dependent on a threshold depth of water in the shallow aquifer which is set by the user.

$$w_{revap,mx} = \beta_{revap} E_0 \quad \text{(B23)}$$

$$w_{revap} = w_{revap,mx} - a_{thr} \quad if$$

$$a_{thr} < a_{sh} < (a_{thr} + w_{revap,mx}) \quad \text{(B24)}$$

$$w_{revap} = 0 \qquad if\, a_{sh} \leq a_{thr} \quad \text{(B25)}$$

$$w_{revap} = w_{revap,mx} \qquad if\, a_{sh} \geq (a_{thr} + w_{revap,mx}) \quad \text{(B26)}$$

where $w_{revap,mx}$ is the maximum volume of water transferred to the unsaturated zone in response to water shortages for the day (mm); β_{revap} is the Revap coefficient (-); w_{revap} is the actual volume of water transferred to the unsaturated zone to supplement water shortage for the day (mm); a_{sh} is the water volume stored in the shallow aquifer at the beginning of the day (mm); and the a_{thr} is the threshold water level in the shallow aquifer required for Revap to occur (mm) (Neitsch et al., 2011).

Appendix C: MODIS Evapotranspiration

ET in the MOD16 is a summation of three components: wet canopy evaporation, plant transpiration and soil evaporation. Wet canopy evaporation (λ_{can}) in MOD16 is calculated using a modified version of the Penman-Monteith equation,

$$\lambda E_{can} = \frac{(\Delta H_{net}\ F_C)+\rho c_p(e_{sat}-e)\frac{F_{par}}{r_a}F_{wet}}{\Delta+\left(\frac{P\ C_p\ r_{vc}}{\lambda\ \varepsilon\ r_a}\right)} \quad \text{(C1)}$$

Where the parameters are as earlier defined, λE_{can} is the latent heat flux (Wm^{-2}); H_{net} is net radiation relative to canopy (Wm^{-2}); F_{par} is the fraction of absorbed photosynthetically active radiation ; F_{wet} is the fraction of the soil covered by water; r_{vc} is the resistance to latent heat transfer (s m^{-1}); and ε is the emissivity.

The plant transpiration (λE_t) is calculated using another variation of the Penman-Monteith equation,

$$\lambda E_t = \frac{(\Delta H_{net}\ F_C)+\rho c_p(e_{sat}-e)\frac{F_C}{r_a}(1-F_{wet})}{\Delta+\gamma\left(1+\frac{r_c}{r_a}\right)} \quad \text{(C2)}$$

The soil evaporation (λE_{soil}) is a summation of the potential soil evaporation (λE_{soil_POT}) limited by the soil moisture constraint function (Fisher et al., 2008) and the evaporation from wet soil (λE_{wet_soil}),

$$\lambda E_{soil} = \lambda E_{wet\_soil} + \lambda E_{soil\_POT}\left(\frac{R_h}{100}\right)^{\frac{V_{PD}}{\phi}} \quad \text{(C3)}$$

$$\lambda E_{wet\_soil} = \frac{(\Delta\ H_{net})+\rho c_p(1.0-F_C)\frac{V_{PD}}{r_a}(F_{wet})}{\Delta+\gamma\left(\frac{r_{tot}}{r_a}\right)} \quad \text{(C4)}$$

$$\lambda E_{soil\_POT} = \frac{(\Delta H_{net})+\rho c_p(1.0-F_C)\frac{V_{PD}}{r_a}(1-F_{wet})}{\Delta+\gamma\left(\frac{r_{tot}}{r_a}\right)} \quad \text{(C5)}$$

where H_{net} and r_a are relative to the soil surface; r_{tot} is the total aerodynamic resistance to vapor transport (s m^{-1}); V_{PD} is the vapor pressure deficit (Pa); R_h is the relative humidity (%); and β is a dimnesionless coefficient defining the relative sensitivity of R_h to V_{PD}. In MOD16 the constant ϕ is set to 200.

Total evapotranspiration (λE) in MOD16 is thus calculated as

$$\lambda E = \lambda E_{can} + \lambda E_t + \lambda E_{soil} \quad \text{(C6)}$$

References

ABBASPOUR, K. 2007. User manual for SWAT-CUP, SWAT calibration and uncertainty analysis programs. *Swiss Federal Institute of Aquatic Science and Technology, Eawag, Duebendorf, Switzerland*.

ABBASPOUR, K. C., YANG, J., MAXIMOV, I., SIBER, R., BOGNER, K., MIELEITNER, J., ZOBRIST, J. & SRINIVASAN, R. 2007. Modelling hydrology and water quality in the pre-alpine/alpine Thur watershed using SWAT. *Journal of hydrology,* 333**,** 413-430.

ABTEW, W. & MELESSE, A. 2013. Climate change and evapotranspiration. *Evaporation and Evapotranspiration*. Springer.

ALLEN, R. G., CLEMMENS, A. J., BURT, C. M., SOLOMON, K. & O'HALLORAN, T. 2005. Prediction accuracy for projectwide evapotranspiration using crop coefficients and reference evapotranspiration. *Journal of Irrigation and Drainage Engineering,* 131**,** 24-36.

ALLEN, R. G., PEREIRA, L. S., HOWELL, T. A. & JENSEN, M. E. 2011. Evapotranspiration information reporting: I. Factors governing measurement accuracy. *Agricultural Water Management,* 98**,** 899-920.

ALLEN, R. G., PRUITT, W. O., WRIGHT, J. L., HOWELL, T. A., VENTURA, F., SNYDER, R., ITENFISU, D., STEDUTO, P., BERENGENA, J. & YRISARRY, J. B. 2006. A recommendation on standardized surface resistance for hourly calculation of reference ET o by the FAO56 Penman-Monteith method. *Agricultural Water Management,* 81**,** 1-22.

ALLEN, R. G., SMITH, M., PERRIER, A. & PEREIRA, L. S. 1994. An update for the definition of reference evapotranspiration. *ICID bulletin,* 43**,** 1-34.

ALLEN, R. G., TASUMI, M. & TREZZA, R. 2007. Satellite-based energy balance for mapping evapotranspiration with internalized calibration (METRIC) - Model. *Journal of Irrigation and Drainage Engineering,* 133**,** 380-394.

AMATYA, D. M., SKAGGS, R. W. & GREGORY, J. D. 1995. Comparison of Methods for Estimating REF-ET. *Journal of Irrigation and Drainage Engineering,* 121**,** 427-435.

ANDERSON, M. C., HAIN, C., WARDLOW, B., PIMSTEIN, A., MECIKALSKI, J. R. & KUSTAS, W. P. 2011. Evaluation of drought indices based on thermal remote sensing of evapotranspiration over the continental United States. *Journal of Climate,* 24**,** 2025-2044.

AUBINET, M., VESALA, T. & PAPALE, D. 2012. *Eddy covariance: a practical guide to measurement and data analysis*, Springer Science & Business Media.

BALDOCCHI, D. D. 2003. Assessing the eddy covariance technique for evaluating carbon dioxide exchange rates of ecosystems: past, present and future. *Global Change Biology,* 9**,** 479-492.

BASTIAANSSEN, W., MENENTI, M., FEDDES, R. & HOLTSLAG, A. 1998a. A remote sensing surface energy balance algorithm for land (SEBAL). 1. Formulation. *Journal of hydrology,* 212**,** 198-212.

BASTIAANSSEN, W. G. M., MENENTI, M., FEDDES, R. A. & HOLTSLAG, A. A. M. 1998b. A remote sensing surface energy balance algorithm for land (SEBAL) - 1. Formulation. *Journal of Hydrology,* 212**,** 198-212.

BASTIAANSSEN, W. G. M., MENENTI, M., FEDDES, R. A. & HOLTSLAG, A. A. M. 1998c. A remote sensing surface energy balance algorithm for land (SEBAL). 1. Formulation. *Journal of hydrology,* 212**,** 198-212.

BENYON, R. G., THEIVEYANATHAN, S. & DOODY, T. M. 2006. Impacts of tree plantations on groundwater in south-eastern Australia. *Australian Journal of Botany,* 54**,** 181-192.

BERINGER, J. 2013a. Fogg Dam OzFlux tower site. OzFlux: Australian and New Zealand Flux Research and Monitoring.

BERINGER, J. 2013b. Red Dirt Melon Farm OzFlux tower site. OzFlux: Australian and New Zealand Flux Research and Monitoring.

BERINGER, J. 2013c. Sturt Plains OzFlux tower site. OzFlux: Australian and New Zealand Flux Research and Monitoring.

BERINGER, J. 2014a. Adelaide River OzFlux tower site. OzFlux: Australian and New Zealand Flux Research and Monitoring.

BERINGER, J. 2014b. Daly Uncleared OzFlux tower site. OzFlux: Australian and New Zealand Flux Research and Monitoring.

BERINGER, J. 2014c. Dry River OzFlux tower site. OzFlux: Australian and New Zealand Flux Research and Monitoring.

BERINGER, J. 2014d. Howard Springs OzFlux tower site. OzFlux: Australian and New Zealand Flux Research and Monitoring.

BERINGER, J. 2014e. Riggs Creek OzFlux tower site. OzFlux: Australian and New Zealand Flux Research and Monitoring.

BERINGER, J. 2014f. Wallaby Creek OzFlux tower site. OzFlux: Australian and New Zealand Flux Research and Monitoring.
BERINGER, J. 2014g. Whroo OzFlux tower site. OzFlux: Australian and New Zealand Flux Research and Monitoring.
BERINGER, J. 2014h. Wombat State Forest OzFlux-tower site. OzFlux: Australian and New Zealand Flux Research and Monitoring.
BHATTARAI, N., SHAW, S. B., QUACKENBUSH, L. J., IM, J. & NIRAULA, R. 2016. Evaluating five remote sensing based single-source surface energy balance models for estimating daily evapotranspiration in a humid subtropical climate. *International Journal of Applied Earth Observation and Geoinformation,* 49**,** 75-86.
BOE, J. & TERRAY, L. 2008. Uncertainties in summer evapotranspiration changes over Europe and implications for regional climate change. *Geophysical Research Letters,* 35.
BROTZGE, J. A. & CRAWFORD, K. C. 2003. Examination of the surface energy budget: A comparison of eddy correlation and Bowen ratio measurement systems. *Journal of Hydrometeorology,* 4**,** 160-178.
BROWN, S. M., PETRONE, R. M., CHASMER, L., MENDOZA, C., LAZERJAN, M. S., LANDHÄUSSER, S. M., SILINS, U., LEACH, J. & DEVITO, K. J. 2014. Atmospheric and soil moisture controls on evapotranspiration from above and within a Western Boreal Plain aspen forest. *Hydrological processes,* 28**,** 4449-4462.
BRUTSAERT, W. & MAWDSLEY, J. A. 1976. The applicability of planetary boundary layer theory to calculate regional evapotranspiration. *Water Resources Research,* 12**,** 852-858.
BUSINGER, J. A., WYNGAARD, J. C., IZUMI, Y. & BRADLEY, E. F. 1971. Flux-Profile Relationships in Atmospheric Surface Layer. *Journal of the Atmospheric Sciences,* 28**,** 181-&.
CAI, G., XUE, Y., HU, Y., WANG, Y., GUO, J., LUO, Y., WU, C., ZHONG, S. & QI, S. 2007. Soil moisture retrieval from MODIS data in Northern China Plain using thermal inertia model. *International Journal of Remote Sensing,* 28**,** 3567-3581.
CARLSON, T. N., CAPEHART, W. J. & GILLIES, R. R. 1995. A New Look at the Simplified Method for Remote-Sensing of Daily Evapotranspiration. *Remote Sensing of Environment,* 54**,** 161-167.
CHAVEZ, J. L., GOWDA, P. H., HOWELL, T. A., NEALE, C. M. U. & COPELAND, K. S. 2009. Estimating hourly crop ET using a two-source energy balance model and multispectral airborne imagery. *Irrigation Science,* 28**,** 79-91.
CHEN, Y., XIA, J., LIANG, S., FENG, J., FISHER, J. B., LI, X., LI, X., LIU, S., MA, Z. & MIYATA, A. 2014. Comparison of satellite-based evapotranspiration models over terrestrial ecosystems in China. *Remote sensing of environment,* 140**,** 279-293.
CHIEW, F., WANG, Q., MCCONACHY, F., JAMES, R., WRIGHT, W. & DEHOEDT, G. Evapotranspiration maps for Australia. Water Challenge: Balancing the Risks: Hydrology and Water Resources Symposium 2002, 2002. Institution of Engineers, Australia, 167.
CHIROUZE, J., BOULET, G., JARLAN, L., FIEUZAL, R., RODRIGUEZ, J. C., EZZAHAR, J., ER-RAKI, S., BIGEARD, G., MERLIN, O., GARATUZA-PAYAN, J., WATTS, C. & CHEHBOUNI, G. 2014. Intercomparison of four remote-sensing-based energy balance methods to retrieve surface evapotranspiration and water stress of irrigated fields in semi-arid climate. *Hydrology and Earth System Sciences,* 18**,** 1165-1188.
CHOI, M., KUSTAS, W. P., ANDERSON, M. C., ALLEN, R. G., LI, F. Q. & KJAERSGAARD, J. H. 2009. An intercomparison of three remote sensing-based surface energy balance algorithms over a corn and soybean production region (Iowa, US) during SMACEX. *Agricultural and Forest Meteorology,* 149**,** 2082-2097.
CHOUDHURY, B. 1999. Evaluation of an empirical equation for annual evaporation using field observations and results from a biophysical model. *Journal of Hydrology,* 216**,** 99-110.
CLEUGH, H. A., LEUNING, R., MU, Q. & RUNNING, S. W. 2007a. Regional evaporation estimates from flux tower and MODIS satellite data. *Remote Sensing of Environment,* 106**,** 285-304.
CLEUGH, H. A., LEUNING, R., MU, Q. Z. & RUNNING, S. W. 2007b. Regional evaporation estimates from flux tower and MODIS satellite data. *Remote Sensing of Environment,* 106**,** 285-304.
COLAIZZI, P. D., KUSTAS, W. P., ANDERSON, M. C., AGAM, N., TOLK, J. A., EVETT, S. R., HOWELL, T. A., GOWDA, P. H. & O'SHAUGHNESSY, S. A. 2012. Two-source energy balance model estimates of evapotranspiration using component and composite surface temperatures. *Advances in Water Resources,* 50**,** 134-151.
COOPER, D. J., SANDERSON, J. S., STANNARD, D. I. & GROENEVELD, D. P. 2006. Effects of long-term water table drawdown on evapotranspiration and vegetation in an arid region phreatophyte community. *Journal of Hydrology,* 325**,** 21-34.
CRAIG, M. 2014. Great Western Woodlands. OzFlux: Australian and New Zealand Flux Research and Monitoring.

CRESSWELL, H. P. & PAYDAR, Z. 1996. Water retention in Australian soils. I. Description and prediction using parametric functions. *Soil Research,* 34**,** 195-212.
CULLEN, N. J., MÖLG, T., KASER, G., STEFFEN, K. & HARDY, D. R. 2017. Energy-balance model validation on the top of Kilimanjaro, Tanzania, using eddy covariance data. *Annals of Glaciology,* 46**,** 227-233.
DE ARRUDA SOUZA, V., ROBERTI, D. R., ZIMMER, T., RUHOFF, A., SANTINI ADAMATTI, D., DE CASSIA MARQUES ALVES, R., BORTOLUZZI DIAZ, M., GONÇALVES DE GONÇALVES, L. G. & LEAL DE MORAES, O. L. What drives evapotranspiration over irrigated cropland? A comparison between flux tower measurements and MODIS remote sensing estimations. EGU General Assembly Conference Abstracts, 2018. 11010.
DE BRUIN, H. Physical aspects of the planetary boundary layer with special reference to regional evapotranspiration. Proceedings of the Workshop on the Estimation of Areal Evapotranspiration, 1989. 9-22.
DEREK, E. & JAMES, C. 2014a. Alice Springs Mulga OzFlux site. OzFlux: Australian and New Zealand Flux Research and Monitoring.
DEREK, E. & JAMES, C. 2014b. Ti Tree East OzFlux Site. OzFlux: Australian and New Zealand Flux Research and Monitoring.
DEWAR, R. 2003. Information theory explanation of the fluctuation theorem, maximum entropy production and self-organized criticality in non-equilibrium stationary states. *Journal of Physics A: Mathematical and General,* 36**,** 631.
DEWAR, R. C. 2005. Maximum entropy production and the fluctuation theorem. *Journal of Physics A: Mathematical and General,* 38**,** L371-L381.
DI, S.-C., LI, Z.-L., TANG, R., WU, H., TANG, B.-H. & LU, J. 2015. Integrating two layers of soil moisture parameters into the MOD16 algorithm to improve evapotranspiration estimations. *International Journal of Remote Sensing,* 36**,** 4953-4971.
DIARRA, A., JARLAN, L., ER-RAKI, S., LE PAGE, M., AOUADE, G., TAVERNIER, A., BOULET, G., EZZAHAR, J., MERLIN, O. & KHABBA, S. 2017. Performance of the two-source energy budget (TSEB) model for the monitoring of evapotranspiration over irrigated annual crops in North Africa. *Agricultural Water Management,* 193**,** 71-88.
DICKINSON, R. E., HENDERSON-SELLERS, A., ROSENZWEIG, C. & SELLERS, P. J. 1991. Evapotranspiration models with canopy resistance for use in climate models, a review. *Agricultural and Forest Meteorology,* 54**,** 373-388.
DOMINGO, F., VILLAGARCıA, L., BOER, M., ALADOS-ARBOLEDAS, L. & PUIGDEFÁBREGAS, J. 2001. Evaluating the long-term water balance of arid zone stream bed vegetation using evapotranspiration modelling and hillslope runoff measurements. *Journal of Hydrology,* 243**,** 17-30.
DONOHUE, R. J., RODERICK, M. L. & MCVICAR, T. R. 2008. Deriving consistent long-term vegetation information from AVHRR reflectance data using a cover-triangle-based framework. *Remote Sensing of Environment,* 112**,** 2938-2949.
DORIGO, W., WAGNER, W., ALBERGEL, C., ALBRECHT, F., BALSAMO, G., BROCCA, L., CHUNG, D., ERTL, M., FORKEL, M., GRUBER, A., HAAS, E., HAMER, P. D., HIRSCHI, M., IKONEN, J., DE JEU, R., KIDD, R., LAHOZ, W., LIU, Y. Y., MIRALLES, D., MISTELBAUER, T., NICOLAI-SHAW, N., PARINUSSA, R., PRATOLA, C., REIMER, C., VAN DER SCHALIE, R., SENEVIRATNE, S. I., SMOLANDER, T. & LECOMTE, P. 2017. ESA CCI Soil Moisture for improved Earth system understanding: State-of-the art and future directions. *Remote Sensing of Environment,* 203**,** 185-215.
DORIGO, W. A., GRUBER, A., DE JEU, R. A. M., WAGNER, W., STACKE, T., LOEW, A., ALBERGEL, C., BROCCA, L., CHUNG, D., PARINUSSA, R. M. & KIDD, R. 2015. Evaluation of the ESA CCI soil moisture product using ground-based observations. *Remote Sensing of Environment,* 162**,** 380-395.
DOWLING, T., BROOKS, M. & READ, A. Continental hydrologic assessment using the 1 second (30m) resolution Shuttle Radar Topographic Mission DEM of Australia. 19th International Congress on Modelling and Simulation. Perth, 2011.
DREXLER, J. Z., SNYDER, R. L., SPANO, D. & PAW U, K. T. 2004a. A review of models and micrometeorological methods used to estimate wetland evapotranspiration. *Hydrological Processes,* 18**,** 2071-2101.
DREXLER, J. Z., SNYDER, R. L., SPANO, D., PAW, U. & THA, K. 2004b. A review of models and micrometeorological methods used to estimate wetland evapotranspiration. *Hydrological Processes,* 18**,** 2071-2101.
DU, J. & SONG, K. 2018. Validation of Global Evapotranspiration Product (MOD16) Using Flux Tower Data from Panjin Coastal Wetland, Northeast China. *Chinese geographical science,* 28**,** 420-429.

DYER, A. J. & HICKS, B. B. 1970. Flux-gradient relationships in the constant flux layer. *Quarterly Journal of the Royal Meteorological Society,* 96**,** 715-721.
DYKE, J. & KLEIDON, A. 2010. The Maximum Entropy Production Principle: Its Theoretical Foundations and Applications to the Earth System. *Entropy,* 12**,** 613-630.
ERSHADI, A., MCCABE, M., EVANS, J. P. & WALKER, J. P. 2013. Effects of spatial aggregation on the multi-scale estimation of evapotranspiration. *Remote Sensing of Environment,* 131**,** 51-62.
ESHONKULOV, R., POYDA, A., INGWERSEN, J., WIZEMANN, H.-D., WEBER, T. K. D., KREMER, P., HÖGY, P., PULATOV, A. & STRECK, T. 2019. Evaluating multi-year, multi-site data on the energy balance closure of eddy-covariance flux measurements at cropland sites in southwestern Germany. *Biogeosciences,* 16**,** 521-540.
EWENZ, C. 2008. Loxton OzFlux tower site. OzFlux: Australian and New Zealand Flux Research and Monitoring.
FEIGENWINTER, C., BERNHOFER, C., EICHELMANN, U., HEINESCH, B., HERTEL, M., JANOUS, D., KOLLE, O., LAGERGREN, F., LINDROTH, A. & MINERBI, S. 2008. Comparison of horizontal and vertical advective CO 2 fluxes at three forest sites. *agricultural and forest meteorology,* 148**,** 12-24.
FERNANDES, L. C., PAIVA, C. M. & ROTUNNO FILHO, O. C. 2012. Evaluation of six empirical evapotranspiration equations-case study: Campos dos Goytacazes/RJ. *Revista Brasileira de Meteorologia,* 27**,** 272-280.
FISHER, J. B., DEBIASE, T. A., QI, Y., XU, M. & GOLDSTEIN, A. H. 2005. Evapotranspiration models compared on a Sierra Nevada forest ecosystem. *Environmental Modelling & Software,* 20**,** 783-796.
FISHER, J. B., TU, K. P. & BALDOCCHI, D. D. 2008. Global estimates of the land–atmosphere water flux based on monthly AVHRR and ISLSCP-II data, validated at 16 FLUXNET sites. *Remote Sensing of Environment,* 112**,** 901-919.
FOKEN, T. 2006. 50 Years of the Monin–Obukhov Similarity Theory. *Boundary-Layer Meteorology,* 119**,** 431-447.
FOKEN, T. & ONCLEY, S. 1995. Workshop on Instrumental and Methodical Problems of Land-Surface Flux Measurements. *Bulletin of the American Meteorological Society,* 76**,** 1191-1193.
FOKEN, T., WIMMER, F., MAUDER, M., THOMAS, C. & LIEBETHAL, C. 2006. Some aspects of the energy balance closure problem. *Atmospheric Chemistry and Physics,* 6**,** 4395-4402.
FRIEDL, M. A., SULLA-MENASHE, D., TAN, B., SCHNEIDER, A., RAMANKUTTY, N., SIBLEY, A. & HUANG, X. 2010. MODIS Collection 5 global land cover: Algorithm refinements and characterization of new datasets. *Remote sensing of Environment,* 114**,** 168-182.
GALLANT, J., DOWLING, T., READ, A., WILSON, N., TICKLE, P. & INSKEEP, C. 2011. 1-Second SRTM-derived Digital Elevation Models user guide.(Geoscience Australia: Canberra).
GALVÁN, L., OLÍAS, M., IZQUIERDO, T., CERÓN, J. & DE VILLARÁN, R. F. 2014. Rainfall estimation in SWAT: An alternative method to simulate orographic precipitation. *Journal of hydrology,* 509**,** 257-265.
GAO, Y. & LONG, D. 2008. Intercomparison of remote sensing-based models for estimation of evapotranspiration and accuracy assessment based on SWAT. *Hydrological processes,* 22**,** 4850-4869.
GAUR, N., MOHANTY, B. P. & KEFAUVER, S. C. 2017. Effect of observation scale on remote sensing based estimates of evapotranspiration in a semi-arid row cropped orchard environment. *Precision Agriculture,* 18**,** 762-778.
GERGES, N. Z. 1999. *The Geology & Hydrogeology of the Adelaide Metropolitan Area.* Flinders University of South Australia.
GHILAIN, N., ARBOLEDA, A. & GELLENS-MEULENBERGHS, F. 2011. Evapotranspiration modelling at large scale using near-real time MSG SEVIRI derived data. *Hydrology and Earth System Sciences,* 15**,** 771-786.
GLENN, E. P., DOODY, T. M., GUERSCHMAN, J. P., HUETE, A. R., KING, E. A., MCVICAR, T. R., VAN DIJK, A. I. J. M., VAN NIEL, T. G., YEBRA, M. & ZHANG, Y. Q. 2011. Actual evapotranspiration estimation by ground and remote sensing methods: the Australian experience. *Hydrological Processes,* 25**,** 4103-4116.
GLENN, E. P., HUETE, A. R., NAGLER, P. L., HIRSCHBOECK, K. K. & BROWN, P. 2007. Integrating remote sensing and ground methods to estimate evapotranspiration. *Critical Reviews in Plant Sciences,* 26**,** 139-168.
GÖCKEDE, M., REBMANN, C. & FOKEN, T. 2004. A combination of quality assessment tools for eddy covariance measurements with footprint modelling for the characterisation of complex sites. *Agricultural and Forest Meteorology,* 127**,** 175-188.
GOVENDER, M. & EVERSON, C. 2005. Modelling streamflow from two small South African experimental catchments using the SWAT model. *Hydrological Processes,* 19**,** 683-692.

GREEN, G. & ZULFIC, D. 2008. *Summary of groundwater recharge estimates for the catchments of the Western Mount Lofty Ranges Prescribed Water Resources Area*, Department of Water, Land and Biodiversity Conservation.
GRUBER, A., DORIGO, W. A., CROW, W. & WAGNER, W. 2017. Triple Collocation-Based Merging of Satellite Soil Moisture Retrievals. *Ieee Transactions on Geoscience and Remote Sensing,* 55**,** 6780-6792.
GRUBER, A., SCANLON, T., VAN DER SCHALIE, R., WAGNER, W. & DORIGO, W. 2019. Evolution of the ESA CCI Soil Moisture climate data records and their underlying merging methodology. *Earth System Science Data,* 11**,** 717-739.
GUERSCHMAN, J. P., VAN DIJK, A. I. J. M., MATTERSDORF, G., BERINGER, J., HUTLEY, L. B., LEUNING, R., PIPUNIC, R. C. & SHERMAN, B. S. 2009. Scaling of potential evapotranspiration with MODIS data reproduces flux observations and catchment water balance observations across Australia. *Journal of Hydrology,* 369**,** 107-119.
GUPTA, H. V., KLING, H., YILMAZ, K. K. & MARTINEZ, G. F. 2009. Decomposition of the mean squared error and NSE performance criteria: Implications for improving hydrological modelling. *Journal of Hydrology,* 377**,** 80-91.
HAJJI, I., NADEAU, D. F., MUSIC, B., ANCTIL, F. & WANG, J. 2018a. Application of the Maximum Entropy Production Model of Evapotranspiration over Partially Vegetated Water-Limited Land Surfaces. *Journal of Hydrometeorology,* 19**,** 989-1005.
HAJJI, I., NADEAU, D. F., MUSIC, B., ANCTIL, F. & WANG, J. F. 2018b. Application of the Maximum Entropy Production Model of Evapotranspiration over Partially Vegetated Water-Limited Land Surfaces. *Journal of Hydrometeorology,* 19**,** 989-1005.
HONG, S.-H., HENDRICKX, J. M. & BORCHERS, B. 2009. Up-scaling of SEBAL derived evapotranspiration maps from Landsat (30m) to MODIS (250m) scale. *Journal of hydrology,* 370**,** 122-138.
HOWELL, T. A., SCHNEIDER, A. D. & JENSEN, M. E. History of lysimeter design and use for evapotranspiration measurements. Lysimeters for evapotranspiration and environmental measurements, 1991. ASCE, 1-9.
HSIEH, C.-I., KATUL, G. & CHI, T.-W. 2000. An approximate analytical model for footprint estimation of scalar fluxes in thermally stratified atmospheric flows. *Advances in water Resources,* 23**,** 765-772.
HU, G., JIA, L. & MENENTI, M. 2015a. Comparison of MOD16 and LSA-SAF MSG evapotranspiration products over Europe for 2011. *Remote Sensing of Environment,* 156**,** 510-526.
HU, G. C., JIA, L. & MENENTI, M. 2015b. Comparison of MOD16 and LSA-SAF MSG evapotranspiration products over Europe for 2011. *Remote Sensing of Environment,* 156**,** 510-526.
HUANG, S. Y., DENG, Y. & WANG, J. F. 2017. Revisiting the global surface energy budgets with maximum-entropy-production model of surface heat fluxes. *Climate Dynamics,* 49**,** 1531-1545.
HUTSON, J. & CASS, A. 1987. A retentivity function for use in soil–water simulation models. *Journal of Soil Science,* 38**,** 105-113.
JAYNES, E. T. 1957. Information theory and statistical mechanics. *Physical review,* 106**,** 620.
JEFFREY, S. J., CARTER, J. O., MOODIE, K. B. & BESWICK, A. R. 2001. Using spatial interpolation to construct a comprehensive archive of Australian climate data. *Environmental Modelling & Software,* 16**,** 309-330.
JEFFREYS, H. 1918. XXX. Some problems of evaporation. *The London, Edinburgh, and Dublin Philosophical Magazine and Journal of Science,* 35**,** 270-280.
JENSEN, M. E., BURMAN, R. D. & ALLEN, R. G. 1990. Evapotranspiration and irrigation water requirements: a manual. *ASCE manuals and reports on engineering practice (USA). no. 70.*
JIA, Z. Z., LIU, S. M., XU, Z. W., CHEN, Y. J. & ZHU, M. J. 2012. Validation of remotely sensed evapotranspiration over the Hai River Basin, China. *Journal of Geophysical Research-Atmospheres,* 117**,** D13113.
JOHNSTON, R., BARRY, S., BLEYS, E., BUI, E. N., MORAN, C., SIMON, D., CARLILE, P., MCKENZIE, N., HENDERSON, B. & CHAPMAN, G. 2003a. ASRIS: the database. *Soil Research,* 41**,** 1021-1036.
JOHNSTON, R. M., BARRY, S. J., BLEYS, E., BUI, E. N., MORAN, C. J., SIMON, D. A. P., CARLILE, P., MCKENZIE, N. J., HENDERSON, B. L., CHAPMAN, G., IMHOFF, M., MASCHMEDT, D., HOWE, D., GROSE, C., SCHOKNECHT, N., POWELL, B. & GRUNDYJ, M. 2003b. ASRIS: the database. *Australian Journal of Soil Research,* 41**,** 1021-1036.
JUNG, M., REICHSTEIN, M., CIAIS, P., SENEVIRATNE, S. I., SHEFFIELD, J., GOULDEN, M. L., BONAN, G., CESCATTI, A., CHEN, J. Q., DE JEU, R., DOLMAN, A. J., EUGSTER, W., GERTEN, D., GIANELLE, D., GOBRON, N., HEINKE, J., KIMBALL, J., LAW, B. E., MONTAGNANI, L., MU, Q. Z., MUELLER, B., OLESON, K., PAPALE, D., RICHARDSON, A. D., ROUPSARD, O., RUNNING, S., TOMELLERI, E., VIOVY, N., WEBER, U., WILLIAMS, C., WOOD, E., ZAEHLE,

S. & ZHANG, K. 2010. Recent decline in the global land evapotranspiration trend due to limited moisture supply. *Nature,* 467**,** 951-954.
JURETIĆ, D. & ŽUPANOVIĆ, P. 2003. Photosynthetic models with maximum entropy production in irreversible charge transfer steps. *Computational biology and chemistry,* 27**,** 541-553.
KALMA, J. D., MCVICAR, T. R. & MCCABE, M. F. 2008. Estimating land surface evaporation: A review of methods using remotely sensed surface temperature data. *Surveys in Geophysics,* 29**,** 421-469.
KHAN, M. S., LIAQAT, U. W., BAIK, J. & CHOI, M. 2018. Stand-alone uncertainty characterization of GLEAM, GLDAS and MOD16 evapotranspiration products using an extended triple collocation approach. *Agricultural and Forest Meteorology,* 252**,** 256-268.
KIM, H., HWANG, K., MU, Q., LEE, S. & CHOI, M. 2012a. Validation of MODIS 16 global terrestrial evapotranspiration products in various climates and land cover types in Asia. *KSCE Journal of Civil Engineering,* 16**,** 229-238.
KIM, H. W., HWANG, K., MU, Q., LEE, S. O. & CHOI, M. 2012b. Validation of MODIS 16 global terrestrial evapotranspiration products in various climates and land cover types in Asia. *KSCE Journal of Civil Engineering,* 16**,** 229-238.
KLEIDON, A. & FRAEDRICH, K. 2004. 14 Biotic Entropy Production and Global Atmosphere-Biosphere Interactions. *Non-equilibrium Thermodynamics and the Production of Entropy.* Springer.
KLEIDON, A. & LORENZ, R. 2005. 1 entropy production by earth system processes. *Non-equilibrium Thermodynamics and the Production of Entropy.* Springer.
KLEIDON, A., MALHI, Y. & COX, P. M. 2010. Maximum entropy production in environmental and ecological systems. *Philos Trans R Soc Lond B Biol Sci,* 365**,** 1297-302.
KLEIDON, A. & SCHYMANSKI, S. 2008. Thermodynamics and optimality of the water budget on land: A review. *Geophysical Research Letters,* 35.
KLJUN, N., CALANCA, P., ROTACH, M. W. & SCHMID, H. P. 2004. A Simple Parameterisation for Flux Footprint Predictions. *Boundary-Layer Meteorology,* 112**,** 503-523.
KOERBER, G. 2014. Calperum Chowilla OzFlux tower site. OzFlux: Australian and New Zealand Flux Research and Monitoring.
KOLOSKOV, G., MUKHAMEJANOV, K. & TANTON, T. W. 2007. Monin–Obukhov length as a cornerstone of the SEBAL calculations of evapotranspiration. *Journal of hydrology,* 335**,** 170-179.
KORMANN, R. & MEIXNER, F. X. 2001. An Analytical Footprint Model For Non-Neutral Stratification. *Boundary-Layer Meteorology,* 99**,** 207-224.
KOTTEK, M., GRIESER, J., BECK, C., RUDOLF, B. & RUBEL, F. 2006. World map of the Köppen-Geiger climate classification updated. *Meteorologische Zeitschrift,* 15**,** 259-263.
KUSTAS, W. P. & NORMAN, J. M. 1999. Evaluation of soil and vegetation heat flux predictions using a simple two-source model with radiometric temperatures for partial canopy cover. *Agricultural and Forest Meteorology,* 94**,** 13-29.
LARSEN, M. A., REFSGAARD, J. C., JENSEN, K. H., BUTTS, M. B., STISEN, S. & MOLLERUP, M. 2016. Calibration of a distributed hydrology and land surface model using energy flux measurements. *Agricultural and Forest Meteorology,* 217**,** 74-88.
LATHAM, J. 2009. FAO land cover mapping initiatives. *North America Land Cover Summit***,** 75-95.
LEE, X. 1998. On micrometeorological observations of surface-air exchange over tall vegetation. *Agricultural and Forest Meteorology,* 91**,** 39-49.
LHOMME, J. P. & CHEHBOUNI, A. 1999. Comments on dual-source vegetation–atmosphere transfer models. *Agricultural and Forest Meteorology,* 94**,** 269-273.
LIAQAT, U. W. & CHOI, M. 2017. Accuracy comparison of remotely sensed evapotranspiration products and their associated water stress footprints under different land cover types in Korean peninsula. *Journal of Cleaner Production,* 155**,** 93-104.
LIU, S., XU, Z., SONG, L., ZHAO, Q., GE, Y., XU, T., MA, Y., ZHU, Z., JIA, Z. & ZHANG, F. 2016. Upscaling evapotranspiration measurements from multi-site to the satellite pixel scale over heterogeneous land surfaces. *Agricultural and Forest Meteorology,* 230**,** 97-113.
LIU, S. M., XU, Z. W., ZHU, Z. L., JIA, Z. Z. & ZHU, M. J. 2013. Measurements of evapotranspiration from eddy-covariance systems and large aperture scintillometers in the Hai River Basin, China. *Journal of Hydrology,* 487**,** 24-38.
LIU, T., LIU, L., LUO, Y. & LAI, J. 2015. Simulation of groundwater evaporation and groundwater depth using SWAT in the irrigation district with shallow water table. *Environmental Earth Sciences,* 74**,** 315-324.
LIU, Y. Y., DORIGO, W. A., PARINUSSA, R. M., DE JEU, R. A. M., WAGNER, W., MCCABE, M. F., EVANS, J. P. & VAN DIJK, A. I. J. M. 2012. Trend-preserving blending of passive and active microwave soil moisture retrievals. *Remote Sensing of Environment,* 123**,** 280-297.

LOESCHER, H. W., LAW, B. E., MAHRT, L., HOLLINGER, D. Y., CAMPBELL, J. & WOFSY, S. C. 2006. Uncertainties in, and interpretation of, carbon flux estimates using the eddy covariance technique. *Journal of Geophysical Research-Atmospheres,* 111.

LONG, D., LONGUEVERGNE, L. & SCANLON, B. R. 2014. Uncertainty in evapotranspiration from land surface modeling, remote sensing, and GRACE satellites. *Water Resources Research,* 50**,** 1131-1151.

LÓPEZ LÓPEZ, P., STROHMEIER, S., HADDAD, M., SUTANUDJAJA, E., KARROU, M., STERK, G., SCHELLEKENS, J. & BIERKENS, M. Application of earth observation products for hydrological modeling of the Oum Er Rbia river basin. EGU General Assembly Conference Abstracts, 2016. 12117.

LYMBURNER, L., TAN, P., MUELLER, N., THACKWAY, R., LEWIS, A., THANKAPPAN, M., RANDALL, L., ISLAM, A. & SENARATH, U. 2010. 250 metre dynamic land cover dataset of Australia. *Geoscience Australia, Canberra*.

MARK, F. & DAMIEN, S.-M. 2015. MCD12C1 MODIS/Terra+Aqua Land Cover Type Yearly L3 Global 0.05Deg CMG V006 [Data set]. *NASA EOSDIS Land Processes DAAC*.

MAUDER, M., GENZEL, S., FU, J., KIESE, R., SOLTANI, M., STEINBRECHER, R., ZEEMAN, M., BANERJEE, T., DE ROO, F. & KUNSTMANN, H. 2018. Evaluation of energy balance closure adjustment methods by independent evapotranspiration estimates from lysimeters and hydrological simulations. *Hydrological processes,* 32**,** 39-50.

MCBEAN, G. A. 1972. Instrument requirements for eddy correlation measurements. *Journal of Applied Meteorology,* 11**,** 1078-1084.

MCMAHON, T., PEEL, M., LOWE, L., SRIKANTHAN, R., MCVICAR, T. J. H. & SCIENCES, E. S. 2013. Estimating actual, potential, reference crop and pan evaporation using standard meteorological data: a pragmatic synthesis. 17**,** 1331-1363.

MCVICAR, T. R., VAN NIEL, T. G., LI, L. T., RODERICK, M. L., RAYNER, D. P., RICCIARDULLI, L. & DONOHUE, R. J. 2008. Wind speed climatology and trends for Australia, 1975–2006: Capturing the stilling phenomenon and comparison with near-surface reanalysis output. *Geophysical Research Letters,* 35**,** L20403.

MELESSE, A. M., ABTEW, W. & DESSALEGNE, T. 2009. Evaporation estimation of rift valley lakes: comparison of models. *Sensors* 9**,** 9603-15.

MINASNY, B. & MCBRATNEY, A. B. 2002. The neuro-m method for fitting neural network parametric pedotransfer functions *Soil Science Society of America Journal,* 66**,** 1407-1407.

MINASNY, B., MCBRATNEY, A. B. & BRISTOW, K. L. 1999. Comparison of different approaches to the development of pedotransfer functions for water-retention curves. *Geoderma,* 93**,** 225-253.

MIRALLES, D. G., JIMENEZ, C., JUNG, M., MICHEL, D., ERSHADI, A., MCCABE, M. F., HIRSCHI, M., MARTENS, B., DOLMAN, A. J., FISHER, J. B., MU, Q., SENEVIRATNE, S. I., WOOD, E. F. & FERNANDEZ-PRIETO, D. 2016. The WACMOS-ET project - Part 2: Evaluation of global terrestrial evaporation data sets. *Hydrology and Earth System Sciences,* 20**,** 823-842.

MONIN, A. S. & OBUKHOV, A. M. 1954. Basic laws of turbulent mixing in the surface layer of the atmosphere. *Contrib. Geophys. Inst. Acad. Sci. USSR,* 151**,** e187.

MONTGOMERY, R. B. 1948. Vertical Eddy Flux of Heat in the Atmosphere. *Journal of Meteorology,* 5**,** 265-274.

MORAN, M. S. & JACKSON, R. D. 1991. Assessing the spatial distribution of evapotranspiration using remotely sensed inputs. *Journal of Environmental Quality,* 20**,** 725-737.

MORIASI, D. N., ARNOLD, J. G., VAN LIEW, M. W., BINGNER, R. L., HARMEL, R. D. & VEITH, T. L. 2007. Model evaluation guidelines for systematic quantification of accuracy in watershed simulations. *Transactions of the Asabe,* 50**,** 885-900.

MU, Q., HEINSCH, F. A., ZHAO, M. & RUNNING, S. W. 2007. Development of a global evapotranspiration algorithm based on MODIS and global meteorology data. *Remote Sensing of Environment,* 111**,** 519-536.

MU, Q., ZHAO, M. & RUNNING, S. W. 2011a. Improvements to a MODIS global terrestrial evapotranspiration algorithm. *Remote Sensing of Environment,* 115**,** 1781-1800.

MU, Q., ZHAO, M. & RUNNING, S. W. 2013. Algorithm theoretical basis document: MODIS global terrestrial evapotranspiration (ET) product (NASA MOD16A2/A3) collection 5. *Nasa Headquarters*.

MU, Q. Z., ZHAO, M. S. & RUNNING, S. W. 2011b. Improvements to a MODIS global terrestrial evapotranspiration algorithm. *Remote Sensing of Environment,* 115**,** 1781-1800.

MYNENI, R., KNYAZIKHIN, Y. & PARK, T. 2015. MOD15A2H MODIS/terra leaf area index/FPAR 8-day L4 global 500 m SIN grid V006. *NASA EOSDIS Land Processes DAAC*.

NACHABE, M., SHAH, N., ROSS, M. & VOMACKA, J. 2005. Evapotranspiration of two vegetation covers in a shallow water table environment. *Soil Science Society of America Journal,* 69**,** 492-499.

NAJMADDIN, P. M., WHELAN, M. J. & BALZTER, H. 2017. Estimating Daily Reference Evapotranspiration in a Semi-Arid Region Using Remote Sensing Data. *Remote Sensing,* 9**,** 779.

NASH, J. E. & SUTCLIFFE, J. V. 1970. River flow forecasting through conceptual models part I—A discussion of principles. *Journal of hydrology,* 10**,** 282-290.
NEARING, G. S., MORAN, M. S., SCOTT, R. L. & PONCE-CAMPOS, G. 2012. Coupling diffusion and maximum entropy models to estimate thermal inertia. *Remote Sensing of Environment,* 119**,** 222-231.
NEITSCH, S. L., ARNOLD, J. G., KINIRY, J. R. & WILLIAMS, J. R. 2011. Soil and water assessment tool theoretical documentation version 2009. Texas Water Resources Institute.
NISHIDA, K., NEMANI, R. R., GLASSY, J. M. & RUNNING, S. W. 2003. Development of an evapotranspiration index from Aqua/MODIS for monitoring surface moisture status. *IEEE Transactions on Geoscience and Remote Sensing,* 41**,** 493-501.
NORMAN, J., KUSTAS, W., PRUEGER, J. & DIAK, G. 2000. Surface flux estimation using radiometric temperature: A dual-temperature-difference method to minimize measurement errors. *Water Resources Research,* 36**,** 2263-2274.
NORMAN, J. M., ANDERSON, M. C., KUSTAS, W. P., FRENCH, A. N., MECIKALSKI, J., TORN, R., DIAK, G. R., SCHMUGGE, T. J. & TANNER, B. C. W. 2003. Remote sensing of surface energy fluxes at 10(1)-m pixel resolutions. *Water Resources Research,* 39**,** 18.
NORMAN, J. M., KUSTAS, W. P. & HUMES, K. S. 1995. Source Approach for Estimating Soil and Vegetation Energy Fluxes in Observations of Directional Radiometric Surface-Temperature. *Agricultural and Forest Meteorology,* 77**,** 263-293.
OBUKHOV, A. M. 1951. Charakteristiki mikrostruktury vetra v prizemnom sloje atmosfery (Characteristics of the micro-structure of the wind in the surface layer of the atmosphere). *Izv AN SSSR, Ser Geofiz,* 3**,** 49-68.
OHTAKI, E. & MATSUI, T. 1982. Infrared device for simultaneous measurement of fluctuations of atmospheric carbon dioxide and water vapor. *Boundary-Layer Meteorology,* 24**,** 109-119.
PENMAN, H. L. 1948. Natural evaporation from open water, bare soil and grass. *Proc. R. Soc. Lond. A,* 193**,** 120-145.
PRADHANANG, S. M., ANANDHI, A., MUKUNDAN, R., ZION, M. S., PIERSON, D. C., SCHNEIDERMAN, E. M., MATONSE, A. & FREI, A. 2011. Application of SWAT model to assess snowpack development and streamflow in the Cannonsville watershed, New York, USA. *Hydrological Processes,* 25**,** 3268-3277.
PRICE, J. C. 1990. Using Spatial Context in Satellite Data to Infer Regional Scale Evapotranspiration. *Ieee Transactions on Geoscience and Remote Sensing,* 28**,** 940-948.
PROSSER, I. P. 2011. *Water: science and solutions for Australia*, CSIRO.
QIAO, L., HERRMANN, R. B. & PAN, Z. 2013. Parameter uncertainty reduction for SWAT using GRACE, streamflow, and groundwater table data for Lower Missouri River Basin. *JAWRA Journal of the American Water Resources Association,* 49**,** 343-358.
RAB, M. A., CHANDRA, S., FISHER, P. D., ROBINSON, N. J., KITCHING, M., AUMANN, C. D. & IMHOF, M. 2011. Modelling and prediction of soil water contents at field capacity and permanent wilting point of dryland cropping soils. *Soil Research,* 49**,** 389-407.
RAMOELO, A., MAJOZI, N., MATHIEU, R., JOVANOVIC, N., NICKLESS, A. & DZIKITI, S. 2014. Validation of global evapotranspiration product (MOD16) using flux tower data in the African savanna, South Africa. *Remote Sensing,* 6**,** 7406-7423.
RANA, G. & KATERJI, N. 2000. Measurement and estimation of actual evapotranspiration in the field under Mediterranean climate: a review. *European Journal of agronomy,* 13**,** 125-153.
RAZ-YASEEF, N., YAKIR, D., SCHILLER, G. & COHEN, S. 2012. Dynamics of evapotranspiration partitioning in a semi-arid forest as affected by temporal rainfall patterns. *Agricultural and Forest Meteorology,* 157**,** 77-85.
ROERINK, G. J., SU, Z. & MENENTI, M. 2000. S-SEBI: A simple remote sensing algorithm to estimate the surface energy balance. *Physics and Chemistry of the Earth Part B-Hydrology Oceans and Atmosphere,* 25**,** 147-157.
RUHOFF, A. L., PAZ, A. R., ARAGAO, L. E. O. C., MU, Q., MALHI, Y., COLLISCHONN, W., ROCHA, H. R. & RUNNING, S. W. 2013. Assessment of the MODIS global evapotranspiration algorithm using eddy covariance measurements and hydrological modelling in the Rio Grande basin. *Hydrological Sciences Journal,* 58**,** 1658-1676.
RUNNING, S. W., BALDOCCHI, D. D., TURNER, D. P., GOWER, S. T., BAKWIN, P. S. & HIBBARD, K. A. 1999. A Global Terrestrial Monitoring Network Integrating Tower Fluxes, Flask Sampling, Ecosystem Modeling and EOS Satellite Data. *Remote Sensing of Environment,* 70**,** 108-127.
SAVAGE, M. J. 2017. Estimation of grass reference evaporation and sensible heat flux using surface renewal and Monin-Obukhov similarity theory: A simple implementation of an iterative method. *Journal of Hydrology,* 547**,** 742-754.

SCHMID, H. P. 2002. Footprint modeling for vegetation atmosphere exchange studies: a review and perspective. *Agricultural and Forest Meteorology,* 113**,** 159-183.
SCHRODER, I. 2014. Arcturus Emerald OzFlux tower site. OzFlux: Australian and New Zealand Flux Research and Monitoring.
SCHUOL, J., ABBASPOUR, K. C., SRINIVASAN, R. & YANG, H. 2008. Estimation of freshwater availability in the West African sub-continent using the SWAT hydrologic model. *Journal of Hydrology,* 352**,** 30-49.
SCOTT, R. L., CABLE, W. L., HUXMAN, T. E., NAGLER, P. L., HERNANDEZ, M. & GOODRICH, D. C. 2008. Multiyear riparian evapotranspiration and groundwater use for a semiarid watershed. *Journal of Arid Environments,* 72**,** 1232-1246.
SENAY, G. B., BOHMS, S., SINGH, R. K., GOWDA, P. H., VELPURI, N. M., ALEMU, H. & VERDIN, J. P. 2013. Operational Evapotranspiration Mapping Using Remote Sensing and Weather Datasets: A New Parameterization for the SSEB Approach. *Journal of the American Water Resources Association,* 49**,** 577-591.
SHANAFIELD, M., COOK, P. G., GUTIERREZ-JURADO, H. A., FAUX, R., CLEVERLY, J. & EAMUS, D. 2015. Field comparison of methods for estimating groundwater discharge by evaporation and evapotranspiration in an arid-zone playa. *Journal of Hydrology,* 527**,** 1073-1083.
SHANNON, C. E. 1948. A mathematical theory of communication. *Bell system technical journal,* 27**,** 379-423.
SHIPLEY, B. 2010. Inferential permutation tests for maximum entropy models in ecology. *Ecology,* 91**,** 2794-805.
SILBERSTEIN, R. 2015. Gingin OzFlux tower site. OzFlux: Australian and New Zealand Flux Research and Monitoring. *Gingin OzFlux tower site.* . Gingin OzFlux tower site.
SONG, L. S., LIU, S. M., KUSTAS, W. P., ZHOU, J., XU, Z. W., XIA, T. & LI, M. S. 2016. Application of remote sensing-based two-source energy balance model for mapping field surface fluxes with composite and component surface temperatures. *Agricultural and Forest Meteorology,* 230**,** 8-19.
SULEIMAN, A. & CRAGO, R. 2004. Hourly and Daytime Evapotranspiration from Grassland Using Radiometric Surface Temperatures. *Agronomy Journal,* 96**,** 384-390.
SUN, F. B., RODERICK, M. L., FARQUHAR, G. D., LIM, W. H., ZHANG, Y. Q., BENNETT, N. & ROXBURGH, S. H. 2010. Partitioning the variance between space and time. *Geophysical Research Letters,* 37.
SUN, Z. G., WANG, Q. X., MATSUSHITA, B., FUKUSHIMA, T., OUYANG, Z. & WATANABE, M. 2009. Development of a Simple Remote Sensing EvapoTranspiration model (Sim-ReSET): Algorithm and model test. *Journal of Hydrology,* 376**,** 476-485.
SWINBANK, W. C. 1951. The Measurement of Vertical Transfer of Heat and Water Vapor by Eddies in the Lower Atmosphere. *Journal of Meteorology,* 8**,** 135-145.
SYED, K. H., GOODRICH, D. C., MYERS, D. E. & SOROOSHIAN, S. 2003. Spatial characteristics of thunderstorm rainfall fields and their relation to runoff. *Journal of Hydrology,* 271**,** 1-21.
TABARI, H., GRISMER, M. E. & TRAJKOVIC, S. 2013. Comparative analysis of 31 reference evapotranspiration methods under humid conditions. *Irrigation Science,* 31**,** 107-117.
TANG, Q., PETERSON, S., CUENCA, R. H., HAGIMOTO, Y. & LETTENMAIER, D. P. 2009. Satellite-based near-real-time estimation of irrigated crop water consumption. *Journal of Geophysical Research: Atmospheres,* 114.
TANG, R. L., SHAO, K., LI, Z. L., WU, H., TANG, B. H., ZHOU, G. Q. & ZHANG, L. 2015. Multiscale Validation of the 8-day MOD16 Evapotranspiration Product Using Flux Data Collected in China. *Ieee Journal of Selected Topics in Applied Earth Observations and Remote Sensing,* 8**,** 1478-1486.
TANNER, C. B. 1960. Energy Balance Approach to Evapotranspiration from Crops1. *Soil Science Society of America Journal,* 24**,** 1-9.
THORNTON, P. E. 1998. Regional ecosystem simulation: Combining surfaceand satellite-based observations to study linkages between terrestrial energy and mass budgets. *School of Forestry***,** 280.
TIMMERMANS, W. J., KUSTAS, W. P., ANDERSON, M. C. & FRENCH, A. N. 2007. An intercomparison of the surface energy balance algorithm for land (SEBAL) and the two-source energy balance (TSEB) modeling schemes. *Remote Sensing of Environment,* 108**,** 369-384.
TOBIN, K. J. & BENNETT, M. E. 2017. Constraining SWAT Calibration with Remotely Sensed Evapotranspiration Data. *JAWRA Journal of the American Water Resources Association,* 53**,** 593-604.
TRAMBAUER, P., DUTRA, E., MASKEY, S., WERNER, M., PAPPENBERGER, F., VAN BEEK, L. & UHLENBROOK, S. 2014. Comparison of different evaporation estimates over the African continent. *Hydrology and Earth System Sciences,* 18**,** 193.
TYAGI, N. K., SHARMA, D. K. & LUTHRA, S. K. 2000. Determination of evapotranspiration and crop coefficients of rice and sunflower with lysimeter. *Agricultural water management,* 45**,** 41-54.

VALIPOUR, M. 2014. Application of new mass transfer formulae for computation of evapotranspiration. *Journal of Applied Water Engineering and Research,* 2**,** 33-46.
VELPURI, N. M., SENAY, G. B., SINGH, R. K., BOHMS, S. & VERDIN, J. P. 2013. A comprehensive evaluation of two MODIS evapotranspiration products over the conterminous United States: Using point and gridded FLUXNET and water balance ET. *Remote Sensing of Environment,* 139**,** 35-49.
VERSTRAETEN, W. W., VEROUSTRAETE, F. & FEYEN, J. 2008. Assessment of Evapotranspiration and Soil Moisture Content Across Different Scales of Observation. *Sensors,* 8**,** 70-117.
VINEY, N., VAZE, J., CROSBIE, R., WANG, B., DAWES, W. & FROST, A. 2014. AWRA-L v4. 5: technical description of model algorithms and inputs. CSIRO, Australia.
VINUKOLLU, R. K., WOOD, E. F., FERGUSON, C. R. & FISHER, J. B. 2011. Global estimates of evapotranspiration for climate studies using multi-sensor remote sensing data: Evaluation of three process-based approaches. *Remote Sensing of Environment,* 115**,** 801-823.
WAN, Z. M. 2014. New refinements and validation of the collection-6 MODIS land-surface temperature/emissivity product. *Remote Sensing of Environment,* 140**,** 36-45.
WAN, Z. M., ZHANG, Y. L., ZHANG, Q. C. & LI, Z. L. 2002. Validation of the land-surface temperature products retrieved from Terra Moderate Resolution Imaging Spectroradiometer data. *Remote Sensing of Environment,* 83**,** 163-180.
WANG, H., TETZLAFF, D. & SOULSBY, C. 2017. Testing the maximum entropy production approach for estimating evapotranspiration from closed canopy shrubland in a low-energy humid environment. *Hydrological Processes,* 31**,** 4613-4621.
WANG, J. & BRAS, R. L. 2009. A model of surface heat fluxes based on the theory of maximum entropy production. *Water Resources Research,* 45.
WANG, J. F. & BRAS, R. L. 2011. A model of evapotranspiration based on the theory of maximum entropy production. *Water Resources Research,* 47.
WANG, J. F., BRAS, R. L., NIEVES, V. & DENG, Y. 2014. A model of energy budgets over water, snow, and ice surfaces. *Journal of Geophysical Research-Atmospheres,* 119**,** 6034-6051.
WANG, K. C. & DICKINSON, R. E. 2012. A Review of Global Terrestrial Evapotranspiration: Observation, Modeling, Climatology, and Climatic Variability. *Reviews of Geophysics,* 50.
WANG, Y. Q., XIONG, Y. J., QIU, G. Y. & ZHANG, Q. T. 2016. Is scale really a challenge in evapotranspiration estimation? A multi-scale study in the Heihe oasis using thermal remote sensing and the three-temperature model. *Agricultural and Forest Meteorology,* 230-231**,** 128-141.
WEBB, E. K., PEARMAN, G. I. & LEUNING, R. 1980. Correction of flux measurements for density effects due to heat and water vapour transfer. *Quarterly Journal of the Royal Meteorological Society,* 106**,** 85-100.
WEBSTER, E., RAMP, D. & KINGSFORD, R. T. 2017. Incorporating an iterative energy restraint for the Surface Energy Balance System (SEBS). *Remote Sensing of Environment,* 198**,** 267-285.
WIDMOSER, P. & WOHLFAHRT, G. 2018. Attributing the energy imbalance by concurrent lysimeter and eddy covariance evapotranspiration measurements. *Agricultural and Forest Meteorology,* 263**,** 287-291.
WILLIAMS, J., ROSS, P. & BRISTOW, K. Prediction of the Campbell water retention function from texture, structure, and organic matter. p. 427–442. M. Th. van Genuchten et al.(ed.) Proc. Int. Worksh. on Indirect Methods for Estimating the Hydraulic Properties of Unsaturated Soils, Riverside, CA. 11–13 Oct. 1989. US Salinity Lab., Riverside, CA. 1992. -.
WILSON, J. L. & GUAN, H. 2004. Mountain-block hydrology and mountain-front recharge. *Groundwater Recharge in a Desert Environment: The Southwestern United States.* American Geophysical Union.
WILSON, K., GOLDSTEIN, A., FALGE, E., AUBINET, M., BALDOCCHI, D., BERBIGIER, P., BERNHOFER, C., CEULEMANS, R., DOLMAN, H. & FIELD, C. 2002. Energy balance closure at FLUXNET sites. *Agricultural and Forest Meteorology,* 113**,** 223-243.
WILSON, K. B., HANSON, P. J., MULHOLLAND, P. J., BALDOCCHI, D. D. & WULLSCHLEGER, S. D. 2001. A comparison of methods for determining forest evapotranspiration and its components: sap-flow, soil water budget, eddy covariance and catchment water balance. *Agricultural and Forest Meteorology,* 106**,** 153-168.
WOODGATE, W. 2014. Tumbarumba OzFlux tower site. OzFlux: Australian and New Zealand Flux Research and Monitoring
XIONG, Y. J., QIU, G. Y., ZHAO, S. H. & TIAN, F. 2014. Estimating regional evapotranspiration using a three-temperature model and MODIS products. *Remote Sensing of the Terrestrial Water Cycle,* 206**,** 83.
XU, D., AGEE, E., WANG, J. & IVANOV, V. Y. 2019. Estimation of Evapotranspiration of Amazon Rainforest Using the Maximum Entropy Production Method. *Geophysical Research Letters,* 46**,** 1402-1412.

YANG, J. C. & WANG, Z. H. 2014. Land surface energy partitioning revisited: A novel approach based on single depth soil measurement. *Geophysical Research Letters,* 41**,** 8348-8358.
YANG, J. C., WANG, Z. H. & LEE, T. W. 2013. Relative efficiency of surface energy partitioning over different land covers. *British Journal of Environment and Climate Change,* 3**,** 86-102.
YANG, X. Y., LIU, Q., HE, Y., LUO, X. Z. & ZHANG, X. X. 2016. Comparison of daily and sub-daily SWAT models for daily streamflow simulation in the Upper Huai River Basin of China. *Stochastic Environmental Research and Risk Assessment,* 30**,** 959-972.
YANG, Y., LONG, D., GUAN, H., LIANG, W., SIMMONS, C. & BATELAAN, O. 2015. Comparison of three dual-source remote sensing evapotranspiration models during the MUSOEXE-12 campaign: Revisit of model physics. *Water Resources Research,* 51**,** 3145-3165.
YANG, Y. M., QIU, J. X., ZHANG, R. H., HUANG, S. F., CHEN, S., WANG, H., LUO, J. S. & FAN, Y. 2018. Intercomparison of Three Two-Source Energy Balance Models for Partitioning Evaporation and Transpiration in Semiarid Climates. *Remote Sensing,* 10**,** 1149.
ZHANG, B., KANG, S., LI, F. & ZHANG, L. 2008a. Comparison of three evapotranspiration models to Bowen ratio-energy balance method for a vineyard in an arid desert region of northwest China. *Agricultural and Forest Meteorology,* 148**,** 1629-1640.
ZHANG, K., KIMBALL, J. S. & RUNNING, S. W. 2016. A review of remote sensing based actual evapotranspiration estimation. *Wiley Interdisciplinary Reviews: Water,* 3**,** 834-853.
ZHANG, R. H., SUN, X. M., WANG, W. M., XU, J. P., ZHU, Z. L. & TIAN, J. 2005. An operational two-layer remote sensing model to estimate surface flux in regional scale: Physical background. *Sci. China Ser. D,* 48**,** 225-244.
ZHANG, X., SRINIVASAN, R., DEBELE, B. & HAO, F. 2008b. Runoff simulation of the headwaters of the Yellow River using the SWAT model with three snowmelt algorithms. *JAWRA Journal of the American Water Resources Association,* 44**,** 48-61.
ZHAO, L., XIA, J., XU, C.-Y., WANG, Z., SOBKOWIAK, L. & LONG, C. 2013. Evapotranspiration estimation methods in hydrological models. *J. Geogr. Sci,* 23**,** 359-369.